

National University of Science and Technology POLITEHNICA Bucharest



Faculty of Electrical Engineering

FINAL PROJECT

Multiphysics Simulation of Microwave and RF Exposure

Graduate student: Álvaro MELÉNDEZ

Scientific Advisors: Prof. Dr. Eng. Alexandru MOREGA

S.l. Dr. Eng. Alin DOBRE

2025

Table of Contents

Introduction	3
0.1. General Introduction	3
0.2. Frequency Bands Explanation	4
0.3. Differents Aplications	5
0.4. Associated Risks and Challenges	7
0.5. Types of Antennas in Biomedical and Telecommunication Applications	11
Chapter 1 – Microwave Cancer Therapy	13
1.1. Introduction	13
1.2. Theorical Basis	14
1.3 Problem Modeling	15
1.4. Results	22
1.5. Conclusion	33
Chapter 2 – SAR of a Human Head Next to a Wi-Fi Antenna	34
2.1. Introduction	34
2.2.Theorical basis	35
2.3 Problem Modeling	36
2.4. Results	42
2.4. Conclusion.	51
Chapter 3 – SAR in Human Head	52
3.1. Introduction	52
3.2. Theorical Basis	53
3.4. Results	62
3.5. Conclusion.	77
Bibliography	78

Introduction

0.1. General Introduction

Microwave and radiofrequency (RF) technologies represent a key of modern science and engineering, underpinning a wide array of advances in medicine, telecommunications, industry, and daily life. The ability of electromagnetic waves in these frequency ranges to interact with matter in precise and controllable ways has enabled the emergence of innovative applications, from wireless communication networks to advanced diagnostic and therapeutic medical procedures.

In recent decades, the integration of microwave and RF systems has accelerated the digital transformation of society, making wireless connectivity ubiquitous and facilitating the development of smart devices, the Internet of Things (IoT), and telemedicine. At the same time, these technologies have revolutionized the medical field, providing new tools for non-invasive diagnosis, targeted therapy, and real-time monitoring of physiological parameters. Techniques such as microwave ablation harness the capacity of electromagnetic fields to deliver energy selectively to biological tissues, offering minimally invasive alternatives to conventional surgery and improving patient outcomes.

However, the widespread use of microwave and RF sources has also raised important questions regarding safety and public health. The omnipresence of electromagnetic fields in everyday environments, due to mobile phones, Wi-Fi routers, and other wireless devices, has intensified the need to understand the mechanisms of energy absorption in the human body, particularly in sensitive organs like the brain. This has led to the establishment of international exposure standards and the adoption of computational modeling as a key tool for risk assessment and device optimization.

This context underscores the importance of multidisciplinary research that bridges technological innovation and health protection. By leveraging advanced simulation platforms such as COMSOL Multiphysics, it is possible to anticipate the real-world behavior of electromagnetic systems, evaluate their impact under various operating conditions, and guide the design of safer and more effective protocols and devices.

The present work is situated at this intersection of technology and health, aiming to provide a comprehensive analysis of how frequency and power variations in microwave and RF fields affect energy absorption, temperature distribution, and biological safety in scenarios of medical therapy and daily exposure. Through rigorous multiphysics simulations and a focus on practical applications, this project aspires to contribute both to scientific understanding and to the responsible advancement of electromagnetic technologies in society.

0.2. Frequency Bands Explanation

Radio waves and microwaves are part of the electromagnetic spectrum and are classified into different frequency bands, ranging from approximately 30 MHz to beyond 100 GHz, each with specific physical properties and applications. This classification is based not only on technical criteria, but also on historical evolution and the needs of society in diverse fields such as telecommunications, medicine, industry, and defense.

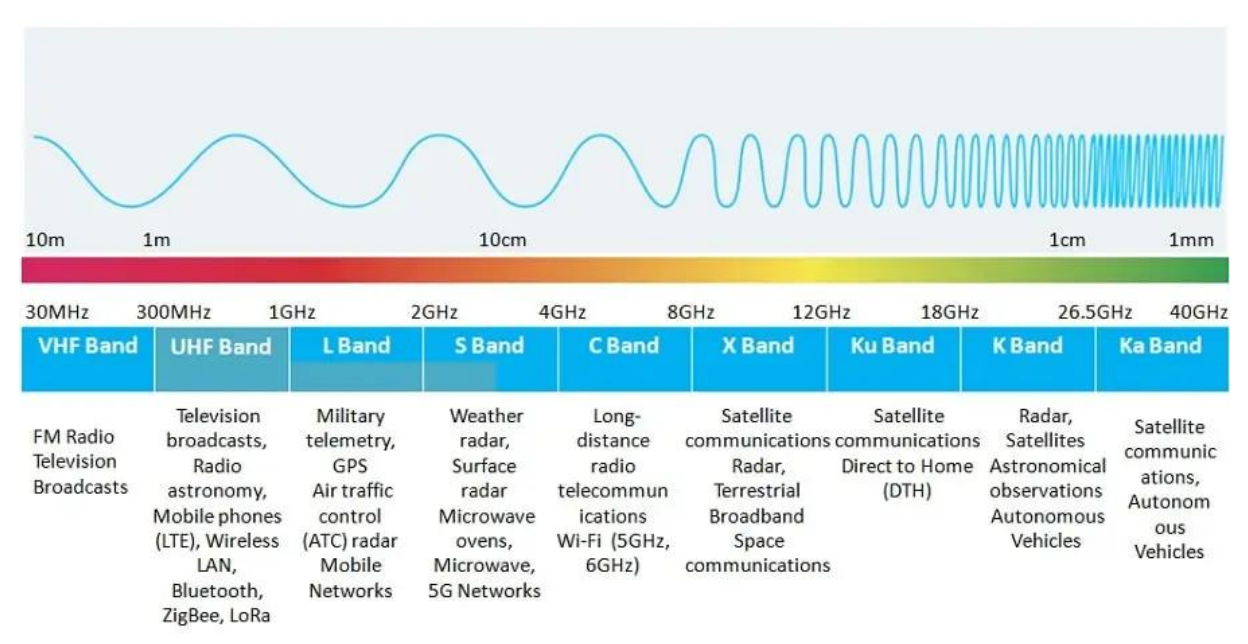


Fig. 0.1 | Types of waves according to their frequency [1]

At lower frequencies, such as the VHF (Very High Frequency, 30–300 MHz) and UHF (Ultra High Frequency, 300–3000 MHz) bands, we find everyday applications like FM radio, digital television, and the first generations of mobile telephony. As we move towards higher frequencies in the gigahertz range, microwaves appear, which have revolutionized wireless data transmission and enabled the development of technologies such as Wi-Fi, Bluetooth, and fourth- and fifth-generation mobile networks.

Within UHF, the L-band (1–2 GHz) is key for GPS, air traffic control radars, and mobile communications, while the S-band (2–4 GHz) is used in weather radars, household microwave ovens, Wi-Fi, and 5G networks.

The 2.45 GHz band, for example, is emblematic because it has been adopted both for domestic use, such as in microwave ovens and Wi-Fi routers, and for medical applications, such as microwave ablation in oncology. Its popularity is due to a balance between penetration capacity in materials and energy efficiency, making it suitable for contexts as diverse as cooking and tumor therapy.

At higher frequencies, the C-band (4–8 GHz) is widely used, especially frequencies like 5 GHz and 6 GHz, which have opened new possibilities in data transmission, enabling higher speeds and less interference in environments saturated with devices. These bands are essential for the latest generations of Wi-Fi (Wi-Fi 5 and Wi-Fi 6/6E), which aim to meet the growing demand for connectivity in homes, businesses, and public spaces.

The X-band, spanning frequencies from 8 to 12 GHz, and the Ku, K, and Ka bands, which range approximately from 12 to 40 GHz, are mainly employed in systems that require high resolution and large data transmission capacity. These bands are fundamental in applications such as precision radars used in advanced meteorology, air traffic control, maritime navigation, and defense systems, as well as in military communications and satellite links for television and high-speed data transmission.

On the other hand, the V and W bands, covering from 40 to 110 GHz, are at the forefront of the most innovative technologies. These frequencies are used for the development of next-generation wireless communication networks such as 5G and 6G, as well as for automotive radars, ultra-high-speed data links, and millimeter-wave imaging systems, which enable high-resolution imaging even under adverse conditions. The ability of these bands to transmit large volumes of information in short periods of time and their use in emerging applications make them a key element in current and future technological evolution.

Each frequency band has its own advantages and limitations: lower frequencies offer greater range and penetration but lower data transmission capacity; higher frequencies, on the other hand, allow for greater bandwidth and precision, although they are more sensitive to obstacles and atmospheric attenuation. Therefore, selecting the appropriate band is always a compromise between the application's requirements, the operating environment, and regulatory constraints.

0.3. Different Applications

0.3.1. Industrial Applications

Microwaves and radiofrequency have become key tools in optimizing industrial processes, mainly due to their ability to transfer energy without direct contact and their selectivity in interacting with materials. In industrial heating, these technologies allow the temperature of food products, textiles, ceramics, or polymers to be raised quickly and uniformly, thanks to the excitation of molecular dipoles (mainly water) and the generation of volumetric heat. This results in higher energy efficiency and a significant reduction in processing times compared to conventional methods based on conduction or convection.

Microwave and RF drying is especially relevant in the food and pharmaceutical industries, where it is necessary to preserve the organoleptic properties and biological activity of products. The ability to control frequency and power makes it possible to adapt the process to the geometry and composition of the material, minimizing thermal degradation and improving final quality. In the materials industry, microwave welding and curing of polymers enables clean and strong joints, with spatial precision that facilitates automation and integration into advanced production lines.

Additionally, the vulcanization of rubber, asphalt recycling, and the decontamination of hazardous waste benefit from the controlled penetration of electromagnetic energy, which allows large volumes or specific areas to be treated without affecting the environment.

0.3.2. Medical Applications

In the medical field, microwave technology has led to significant advances in the treatment and diagnosis of diseases. Microwave ablation is a localized hyperthermia technique used to destroy solid tumors in organs such as the liver, lungs, kidneys, and breast. The process consists of inserting a coaxial antenna into the target tissue and supplying energy, generating an electromagnetic field that induces resistive heating and cellular necrosis. The precision in energy dosing and field focusing allows for maximum tumor destruction while preserving surrounding healthy tissue, being especially useful in unresectable lesions or those difficult to access surgically.

Diathermy uses RF and microwave frequencies to generate heat in deep tissues, facilitating muscle rehabilitation, analgesia, and the treatment of chronic inflammatory processes. In medical sterilization, microwaves enable the rapid and efficient elimination of microorganisms on surgical instruments and hospital materials, without chemical residues or material deterioration.

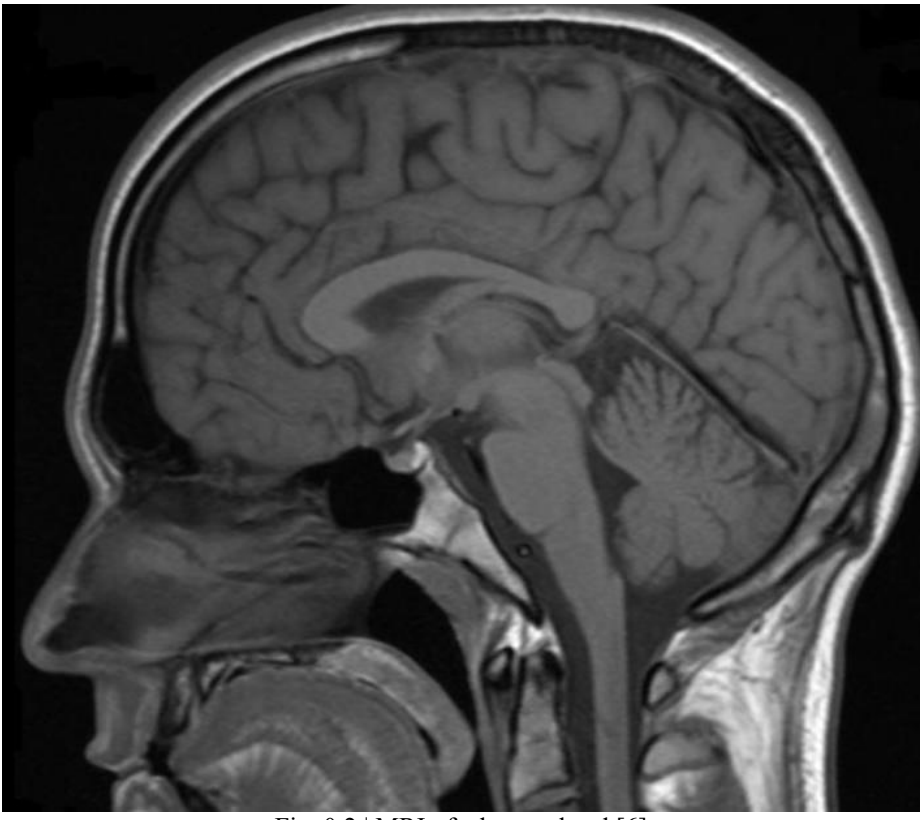


Fig. 0.2 | MRI of a human head [6]

For diagnosis, magnetic resonance imaging (MRI) uses radiofrequency waves to excite atomic nuclei and obtain high-resolution images of the body's interior. Additionally, microwave imaging is an emerging field exploring the detection of tumors and cerebral hemorrhages through differences in the dielectric properties of tissues, opening new possibilities for non-invasive diagnosis and real-time monitoring.

0.3.3. Military Applications

The military sector has historically driven the development of microwave and radiofrequency technologies, especially in radar systems and secure communications. Microwave radars, operating in bands such as X, Ku, and Ka, enable the detection, localization, and tracking of aerial, naval, and ground targets with high resolution and under any weather conditions. The ability to penetrate fog, rain, and vegetation, as well as to obtain three-dimensional images of the environment, are critical advantages in tactical and surveillance operations.

Military communications employ specific bands and advanced modulation techniques to ensure confidentiality, resistance to interference, and robustness against interception or sabotage attempts. Electronic warfare uses microwaves both to jam (jamming) and to deceive (spoofing) enemy systems, as well as to protect friendly systems through electronic countermeasures.

Missile guidance and detection systems, radar navigation, and proximity sensors are based on the propagation and reflection of microwaves, taking advantage of their temporal and spatial precision. Electromagnetic modeling and multiphysics simulation are essential tools in the design and validation of these systems, allowing the prediction of behavior in complex scenarios and optimizing integration into mobile or fixed platforms.

0.4. Associated Risks and Challenges

0.4.1. Biological Effects and Health Risks

Exposure to electromagnetic fields from microwaves and radiofrequency generates legitimate concerns about their possible effects on human health, especially when it comes to prolonged exposures or those close to sensitive organs such as the brain. Although radiation in these bands is non-ionizing and, therefore, does not have enough energy to break molecular bonds or directly damage DNA, it can induce significant biological effects through thermal mechanisms and, to a lesser extent, non-thermal mechanisms.

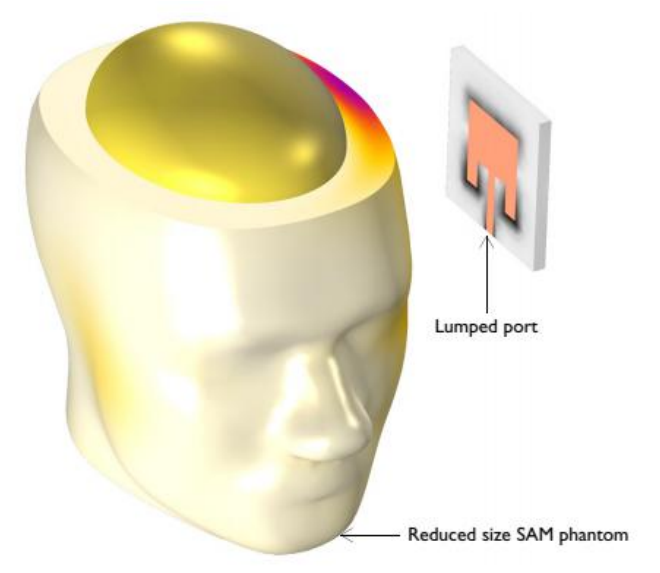


Fig. 0.3 | Influence of an antenna next to a human head [COMSOL2]

The main mechanism of interaction is tissue heating, resulting from the absorption of electromagnetic energy by water molecules and other dipoles present in biological tissues. This phenomenon is quantifiable through the parameter SAR (Specific Absorption Rate). When the SAR exceeds certain thresholds, a local increase in temperature may occur, sufficient to alter cellular function, induce necrosis, or damage sensitive structures. For this reason, international organizations such as ICNIRP and IEEE have established strict exposure limits, especially for devices close to the head and torso, such as mobile phones, Wi-Fi routers, and telecommunications antennas.

In the clinical field, as detailed later in Chapter 1, this thermal effect is precisely what is sought in therapies such as microwave ablation, where the objective is to destroy tumor tissue through controlled heating. However, outside the medical environment, unintentional heating can be harmful, especially in tissues with low thermal dissipation capacity or in situations of continuous exposure.

In addition to thermal effects, there is an ongoing debate about possible non-thermal biological effects, that is, those that could occur at SAR levels below appreciable heating thresholds. Although some studies have suggested possible alterations in neuronal activity, membrane permeability, or gene expression, the scientific evidence available is not conclusive, and these effects remain the subject of research and controversy in the scientific community.

0.4.2 Electromagnetic Interference and Compatibility (EMI/EMC)

electromagnetic interference (EMI) is one of the most relevant challenges in the development and deployment of systems based on microwaves and radiofrequency, both in industrial, medical, and telecommunications environments. EMI occurs when a device or system emits electromagnetic energy that negatively affects the operation of other nearby equipment, whether by inductive, capacitive, or radiative coupling. This interference can manifest as data loss, malfunction, measurement errors, signal degradation, or even critical failures in control, communications, or medical monitoring systems.

The proliferation of electronic devices and the densification of wireless networks have increased the likelihood of EMI phenomena, especially in environments where equipment of different technologies and sensitivities coexist. For example, in hospitals, the presence of imaging equipment, cardiac monitors, infusion pumps, and wireless communication systems requires strict management of electromagnetic compatibility (EMC) to avoid risks to patient safety and the integrity of clinical data.

EMC is the engineering field that studies and regulates the ability of devices to operate correctly in their electromagnetic environment without causing or suffering unacceptable interference. To achieve this, design strategies such as electromagnetic shielding, the use of filters, proper arrangement of cables and components, physical separation of sources and receivers, and the adoption of robust modulation and coding protocols are applied. Additionally, equipment must comply with international standards such as CE, FCC, IEC 60601-1-2 (for medical equipment), ISO, and CISPR, which set maximum emission limits and minimum immunity levels against external disturbances.

0.4.3 Industrial Safety, Electrical Hazards, and Emission Control

The use of microwaves and radiofrequency in industrial and medical environments involves critical safety challenges, both for operators and for the surroundings. The high power density and penetration capacity of these waves can induce significant electrical and thermal risks if not properly managed.

One of the main risks is the generation of induced currents in conductive materials, metallic structures, or even in the human body, which can lead to anything from electric shocks to localized overheating, burns, or, in extreme cases, fires if flammable atmospheres are present. For this reason, the installation and operation of microwave equipment require careful design of electrical systems and the implementation of protective devices.

Electromagnetic shielding is another fundamental aspect to ensure the safety and proper functioning of the equipment. Since microwaves can pass through non-conductive materials and reflect off metallic surfaces, the use of Faraday cages, metallic coatings, and special seals on doors and joints of the equipment is essential. These shielding systems aim to confine radiation to the treatment or processing area, preventing leaks that could affect people or other nearby electronic devices.

0.4.4. Challenges in Modeling and Numerical Simulation

Modeling and numerical simulation are fundamental tools for the design, analysis, and optimization of systems that use microwaves and radiofrequency, especially in biomedical and telecommunications applications. However, their use presents a series of technical and methodological challenges that must be addressed to ensure the reliability and usefulness of the results.

One of the main challenges lies in the physical complexity of the phenomena involved. The interaction between electromagnetic fields and biological or industrial materials involves not only the propagation and absorption of waves, but also coupled processes such as heat generation (Joule effect), thermal transfer, blood perfusion, and, in some cases, the mechanical response of tissues. This multiphysics nature requires the use of advanced platforms such as COMSOL Multiphysics, which allow for the simultaneous solving of Maxwell's equations, heat transfer equations (such as Pennes' bioheat equation), and models of mass transport or fluid dynamics, depending on the case.

Another relevant challenge is the realistic representation of geometry and material properties. In biomedical simulations, for example, it is essential to incorporate the spatial heterogeneity of tissues, their dielectric (permittivity and conductivity), thermal, and anatomical properties, as well as their interindividual variability. For this, interpolation of data obtained from magnetic resonance imaging or tomography is used, along with the definition of spatial functions that assign local properties to each point of the model. This approach, although more realistic, increases computational complexity and requires careful management of hardware and software resources.

Spatial and temporal discretization is another critical aspect. The need to resolve fields with very steep gradients near sources (antennas, electrodes) or at interfaces between materials imposes the use of very fine meshes in critical areas, which can exponentially increase the number of elements and computation time. The choice of meshing strategy (tetrahedral, swept, adaptive) and the optimization of element density are key decisions for balancing accuracy and computational efficiency.

The treatment of boundary conditions, such as the implementation of perfectly matched layers (PML) to simulate free space and avoid artificial reflections, or the correct definition of sources and loads, also directly impacts the quality of the simulation. Additionally, the validation of numerical results against experimental data or analytical models is essential to guarantee the reliability of predictions, especially in clinical or safety applications.

0.4.5. Trends and Future of Technology

Microwave and radiofrequency technology is undergoing rapid transformation driven by the demand for greater capacity, speed, and efficiency in communications and industrial, medical, and scientific applications. This evolution is characterized by several key trends that define the sector's future and highlight the importance of research and multiphysics simulation as strategic tools to address new challenges.

The deployment of 5G networks has led to the massive adoption of millimeter-wave bands (mmWave, 24–100 GHz), which enable much higher transmission speeds and network capacities than previous technologies. The leap toward 6G is already on the horizon, with research focused on the use of terahertz (THz) bands, which promise even higher data rates and the integration of sensing and communication capabilities within a single infrastructure. These technologies open the door to applications such as smart cities, autonomous vehicles, augmented reality, and massive communications for connected devices.

The development of increasingly compact and multifunctional devices is a dominant trend. The miniaturization of RF and microwave components, facilitated by new materials such as liquid crystal polymers (LCP) and advanced manufacturing techniques (including 3D printing), allows antennas, filters, and circuits to be integrated into small spaces, improving efficiency and reducing costs and energy consumption. The use of advanced materials, such as substrates with low permittivity and high thermal stability, and the adoption of additive manufacturing techniques, are revolutionizing the production of RF circuits and devices, enabling more complex, lightweight, and customized designs for specific applications.

In this context of accelerated innovation, multiphysics simulation has become an essential tool for the safe and efficient development of new technologies. Advanced modeling allows for the prediction of the real behavior of complex systems before fabrication, the optimization of component and device design, and the assurance of electromagnetic compatibility, energy efficiency, and compliance with international regulations. Simulation is also key for validating the integration of new materials, exploring multiphysics effects (such as electromagnetic-thermal-mechanical coupling), and anticipating safety or performance issues under extreme conditions.

0.5. Types of Antennas in Biomedical and Telecommunication Applications

Antennas are essential components in the transmission and reception of electromagnetic waves in microwave and radiofrequency systems. Their design and selection depend on the specific application, the operating environment, and the requirements for integration and safety. In the biomedical and telecommunications context, the most prominent are slotted coaxial antennas, patch (microstrip) antennas, and flexible and miniaturized variants for implantable or wearable devices.

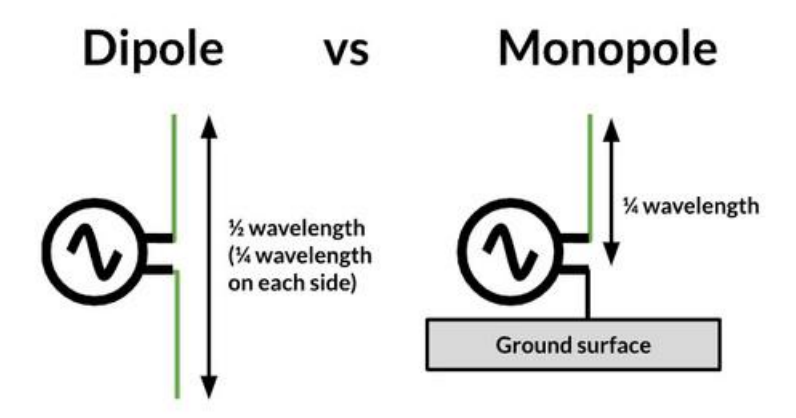


Fig. 0.4 | Dipole and monopole antenna scheme [7]

Dipole and monopole antennas are the most basic and fundamental configurations, often serving as building blocks for more complex designs. A dipole antenna consists of two linear conductors of specific length, fed at its center. Monopoles, on the other hand, are essentially half a dipole mounted perpendicularly on a conductive ground plane, reducing their physical size by half. Both are omnidirectional antennas in the plane perpendicular to their axis and are widely used in broadcasting, two-way communications, and as elements in antenna arrays. Their simple design and ease of fabrication make them ideal for a wide variety of RF applications, although their size can be a limitation at low frequencies.

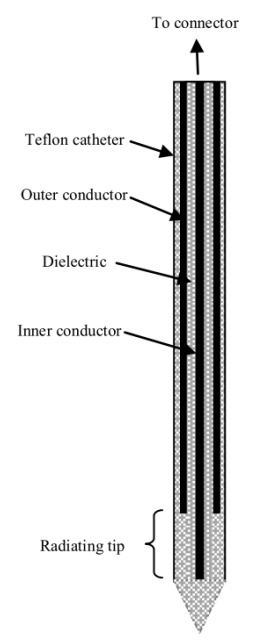


Fig. 0.5 | Slotted coaxial antenna scheme [8]

The slotted coaxial antenna is widely used in microwave ablation therapies, where precise and localized deposition of energy in biological tissue is required. This type of antenna consists of a central conductor surrounded by a dielectric and an external conductor, with one or more slots strategically located near the tip. These slots allow electromagnetic radiation to efficiently couple to the surrounding tissue, generating a symmetric and controlled heating pattern. The typical operating frequency is 2.45 GHz, which offers a balance between penetration and thermal efficiency. The design of the slot and the geometry of the antenna are optimized to maximize tumor destruction and minimize damage to healthy tissues.

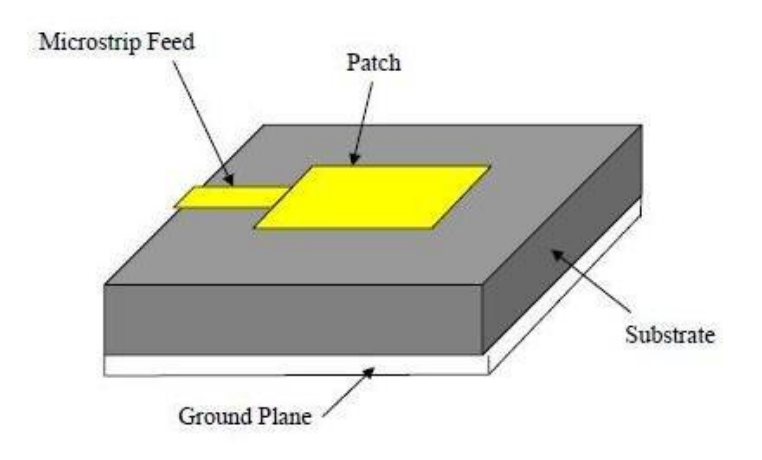


Fig. 0.6 | Patch antenna scheme [9]

Patch antennas, also known as microstrip antennas, are especially valued in telecommunications and portable or implantable biomedical systems. These antennas have a flat and compact structure, formed by a metallic patch on a dielectric substrate and a ground plane. Their low profile and ease of integration make them ideal for devices such as mobile phones, Wi-Fi routers, medical sensors, and body monitoring systems. Patch antennas can be designed to operate in specific bands (such as 2.45 GHz, 5 GHz, or 6 GHz), and their radiation pattern can be adjusted by modifying the patch geometry and substrate properties. In biomedical applications, they are used both in external monitoring and in implants, where SAR control and biocompatibility are fundamental.

Chapter 1 – Microwave Cancer Therapy

1.1. Introduction

Microwave therapy is emerging as an innovative technique in cancer treatment, standing out in the field of oncological hyperthermia due to its ability to destroy tumor cells through the localized application of heat. This method is based on the insertion of a small-diameter coaxial antenna directly into the affected tissue, which, when operating at high frequencies such as 2.45 GHz, generates an electromagnetic field that induces resistive heating. This phenomenon leads to the coagulation and necrosis of cancer cells, offering a minimally invasive alternative compared to conventional surgical approaches.

One of the critical challenges of this technology lies in the precise control of the supplied power and the spatial distribution of heat factors that determine both the efficacy of tumor ablation and the protection of the surrounding healthy tissue. To address these challenges, it is essential to model the interaction between electromagnetic fields and heat transfer processes in biological tissue. In this context, multiphysics modeling emerges as an essential tool, enabling the coupled analysis of electromagnetic and thermal behavior through equations such as the bioheat equation and the calculation of the specific absorption rate (SAR).

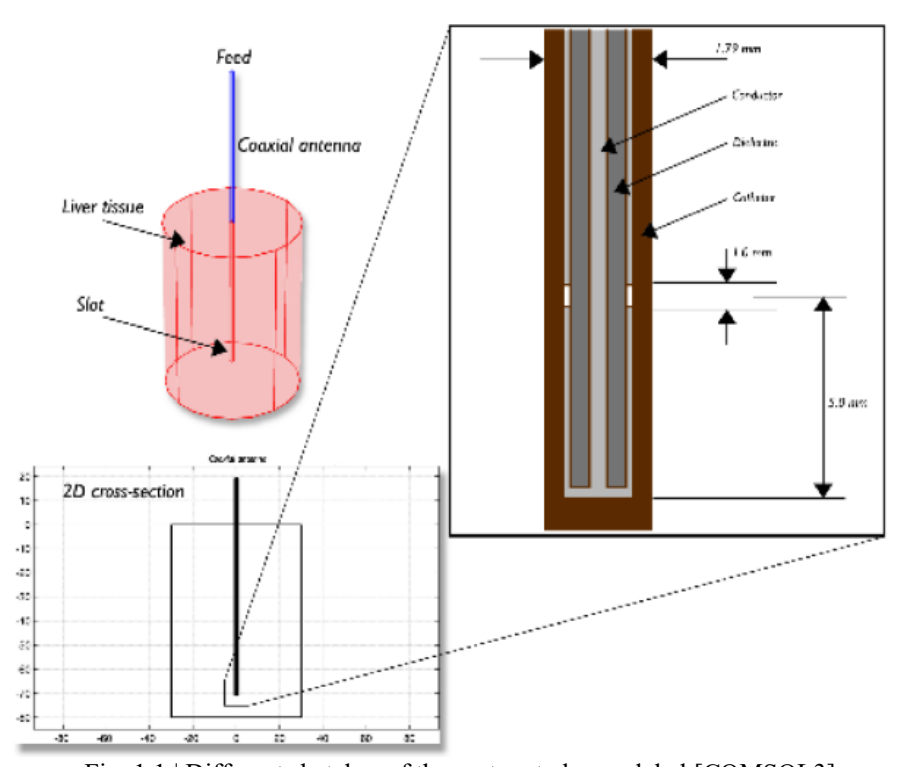


Fig. 1.1 | Different sketches of the system to be modeled [COMSOL3]

The present work focuses on the simulation of microwave therapy applied to hepatic tissue, using a slotted coaxial antenna modeled in COMSOL Multiphysics. Starting from a baseline configuration at 2.45 GHz and 10 W, the study explores how strategic variations in power (8, 10, 12, 15 W) and frequency (2, 2.45, 3, 3.5 GHz) modify the temperature distribution, SAR, and necrosis volume. These parameters are analyzed with the objective of optimizing therapeutic efficacy while ensuring compliance with safety standards such as those established by the ICNIRP (SAR \leq 2 W/kg in 10 g of tissue).

The clinical relevance of this analysis lies in its potential to improve hepatic ablation protocols, particularly in hepatocarcinomas and metastases, where precision in energy targeting and preservation of healthy parenchyma are critical. Through simulations that integrate the dielectric properties of tissue, blood perfusion, and thermal dynamics, this work aims to provide quantitative data linking operational adjustments to clinical outcomes, establishing a bridge between computational modeling and practical application in interventional oncology.

1.2. Theorical Basis

The physical basis of this technique lies in the interaction of microwaves with water molecules present in biological tissues. Microwaves, being high-frequency electromagnetic waves, cause the vibration and rotation of water dipoles, generating heat through molecular friction. This mechanism allows temperatures above 60 °C to be reached in the treated area, producing coagulative necrosis and cell death, thus achieving tumor ablation and a safety margin without damaging the surrounding healthy tissue.

The procedure is carried out by inserting a thin antenna, generally of coaxial type with an annular slot, directly into the tumor. The antenna is connected to a microwave generator that supplies energy, which is then radiated and locally absorbed in the target tissue. The design of the antenna and the operating frequency are optimized to maximize energy deposition in the tumor and minimize dispersion to adjacent tissues.

From a physical-mathematical perspective, the distribution of electromagnetic energy and the resulting heating in the tissue are described by two coupled phenomena.

1.2.1. Electromagnetic Propagation

In the tissue, the antenna generates an electromagnetic field whose distribution depends on the dielectric and conductive properties of the tissue and the geometry of the antenna. The absorption of energy is quantified by the specific absorption rate (SAR), which expresses the power absorbed per unit mass of tissue. In this context, the electromagnetic field is modeled using a transverse magnetic (TM) wave formulation, where the main component is the azimuthal magnetic field.

The electromagnetic modeling is performed in 2D, taking advantage of the axial symmetry of the problem. The scalar wave equation for the azimuthal component of the magnetic field $(H\phi)$ is used:

$$\nabla \times \left(\left(\varepsilon_r - \frac{j\sigma}{\omega \varepsilon_0} \right)^{-1} \nabla \times H_\varphi \right) - \mu_r k_0^2 H_\varphi = 0$$

where ε_r is the relative permittivity, σ the electrical conductivity, ω the angular frequency, ε_0 the vacuum permittivity, μ_r the relative permeability, and k_0 the wave number in vacuum.

The boundary conditions for the metallic surfaces of the antenna impose that the tangential electric field is zero ($n\times E=0$). The input port is modeled as a port condition with a specific input power (10 W). The external limits of the domain are truncated with absorbing conditions to simulate the propagation and dissipation of the wave in the tissue, and a symmetry condition is used on the axis (r=0).

This approach allows for the calculation of the spatial distribution of the electromagnetic field, the SAR, and the power absorbed in the surrounding tissue.

1.2.2. Biological heat transfer

The induced heating is modeled using the Pennes bioheat equation, which describes heat transfer in tissues by considering thermal conduction, blood perfusion, and the external heat source generated by electromagnetic absorption:

$$\nabla \cdot (-k\nabla T) = \rho_h C_h \omega_h (T_h - T) + Q_{ext}$$

where k is the thermal conductivity of the tissue, ρ_b is the blood density, C_b is the specific heat of blood, ω_b is the blood perfusion rate, T_b is the blood temperature, and Q_{ext} is the heat source due to electromagnetic absorption. The metabolic term is usually neglected in this context.

The clinical objective is to achieve complete necrosis of the tumor, also covering a safety margin of 5–10 mm around the lesion, without affecting healthy structures or neighboring organs. The effectiveness of the treatment depends on achieving sufficient and homogeneous heating throughout the entire tumor volume, as temperatures above 60 °C for several minutes ensure irreversible cell death.

1.3 Problem Modeling

1.3.1. Definitions and Geometry

The first step in modeling the problem is to define the fundamental constants of the system, as these parameters determine the physical and operational properties that will be used throughout the simulation. According to the guidelines and the official COMSOL model, these constants are loaded from an external file in the Parameters section, which ensures consistency and facilitates parametric analyses.

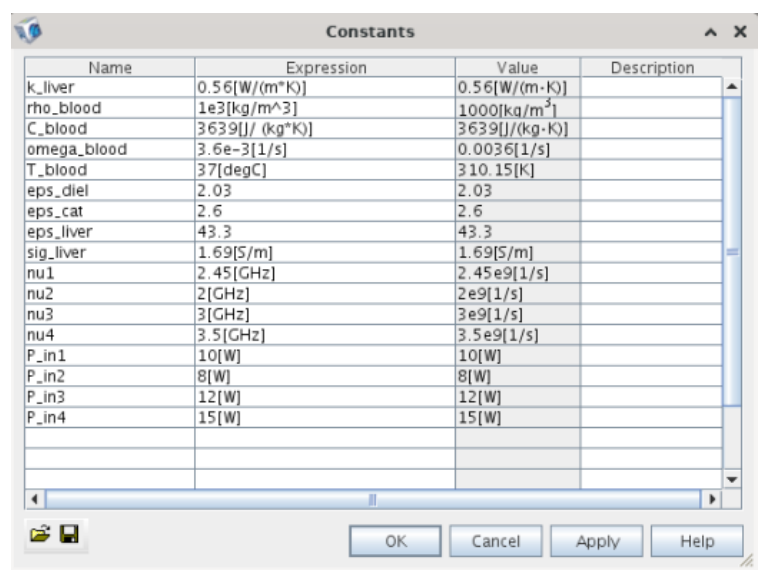


Fig. 1.2 | Definition of Constants

in the original model, the operating frequency is set at 2.45 GHz, a standard frequency for microwave coagulation therapy due to its penetration capability and thermal efficiency in hepatic tissue. In this study, in addition to the base frequency, additional frequencies of 2.0, 3.0, and 3.5 GHz have been incorporated to analyze how energy distribution and tissue heating vary as a function of frequency. This allows for a comparison of thermal efficacy and selectivity in different clinical scenarios. Similarly, the input power, which in the original model is 10 W, is parameterized to explore values of 8, 12, and 15 W, thus enabling the evaluation of the impact of supplied power on the volume of necrosed tissue and the safety of the procedure.

The geometric properties of the antenna, such as the diameter of the central conductor (0.29 mm), the inner and outer diameters of the outer conductor (0.94 mm and 1.19 mm, respectively), the diameter of the PTFE catheter (1.79 mm), and the position and length of the slot (1 mm wide, located 5 mm from the tip), are maintained according to the original design, as they are essential for constructing a realistic geometry of the slotted coaxial antenna.

Regarding material properties, the relative permittivity and electrical conductivity are defined for each relevant material: the antenna's inner dielectric has a permittivity of 2.03, the catheter 2.60, and hepatic tissue exhibits a permittivity of 43.03 and a conductivity of 1.69 S/m. These values determine how electromagnetic energy propagates and is absorbed in each region of the model.

For the thermal and physiological aspects, constants such as the thermal conductivity of the liver, the density and specific heat of blood (1050 kg/m³ and 3639 J/(kg·K)), the blood perfusion rate (0.0036 s $^{-1}$), and the arterial inlet temperature (37 °C) are established. All these parameters are necessary to solve the bioheat equation and model heat transport and dissipation due to blood circulation.

The system geometry is based on the representation of a microwave antenna specifically designed for tumor ablation applications in the liver. This antenna is modeled as a thin coaxial cable, with an annular slot 1 mm wide located exactly 5 mm from the tip, which is short-circuited. The entire antenna structure is covered by a PTFE catheter, ensuring biocompatibility and electrical insulation during insertion into hepatic tissue.

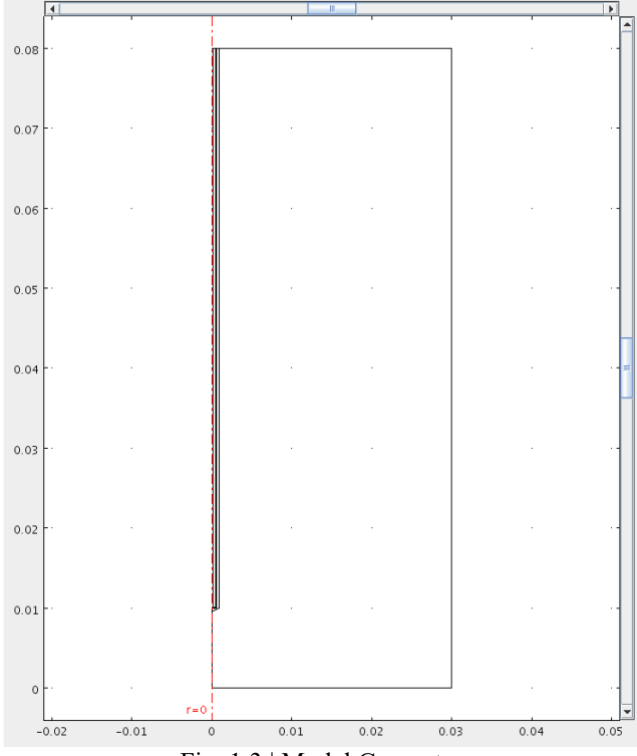


Fig. 1.3 | Model Geometry

To simulate a realistic physiological environment, the antenna is inserted into a domain representing the surrounding hepatic tissue. Taking advantage of the axial symmetry of the configuration, a two-dimensional model in cylindrical coordinates (r, z) is used. This approach not only simplifies the geometric construction and numerical resolution, but also significantly reduces computational cost, allowing for a finer mesh and accurate results within reasonable computation times.

The detailed construction of the geometry follows a precise sequence: first, a large rectangular domain (30 mm wide by 80 mm high) is defined to represent the hepatic tissue. Within this domain, the different coaxial components of the antenna are inserted: the central conductor (0.29 mm in diameter), the inner dielectric, the outer conductor (with inner and outer diameters of 0.94 mm and 1.19 mm, respectively), and the PTFE catheter (1.79 mm in diameter). The annular slot is modeled as an interruption in the outer conductor, located 5 mm from the tip of the antenna and with an axial length of 1 mm. The rest of the antenna tip remains short-circuited, which contributes to the focusing of the electromagnetic field in the region near the slot.

1.3.2. Bioheat Configuration

The bioheat equation is applied exclusively to the domain representing hepatic tissue, selecting this domain in the configuration. The characteristic physiological and thermal parameters are introduced: the thermal conductivity of the liver is defined as 0.56 W/(m·K), the density of blood as 1000 kg/m^3 , the specific heat of blood as 3639 J/(kg·K), and the blood perfusion rate as $3.6 \times 10^{-3} \text{ s}^{-1}$. The inlet blood temperature is set at 37 °C, reflecting the basal body temperature. The model disregards metabolic heat generation (Qmet = 0), as its contribution is negligible compared to the external source.

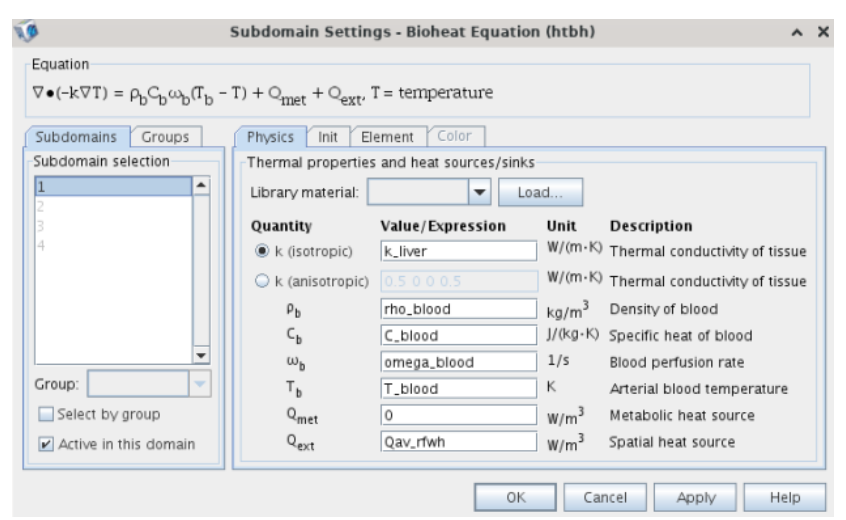


Fig. 1.4 | Example of the subdomain settings of the Bioheta Equation part

The external heat source, Qext, corresponds to the resistive power generated by the electromagnetic field, which is automatically calculated from the solution of the TM Waves module. This transfer of energy from the electromagnetic field to the tissue is responsible for the localized heating that characterizes ablation therapy.

At the outer boundaries of the hepatic domain, thermal insulation conditions are imposed, meaning there is no heat flux across the external borders of the model. This simplification is valid because the domain has been sized sufficiently large so that the temperature at the edges remains close to the basal temperature, and blood perfusion contributes to deep heat dissipation.

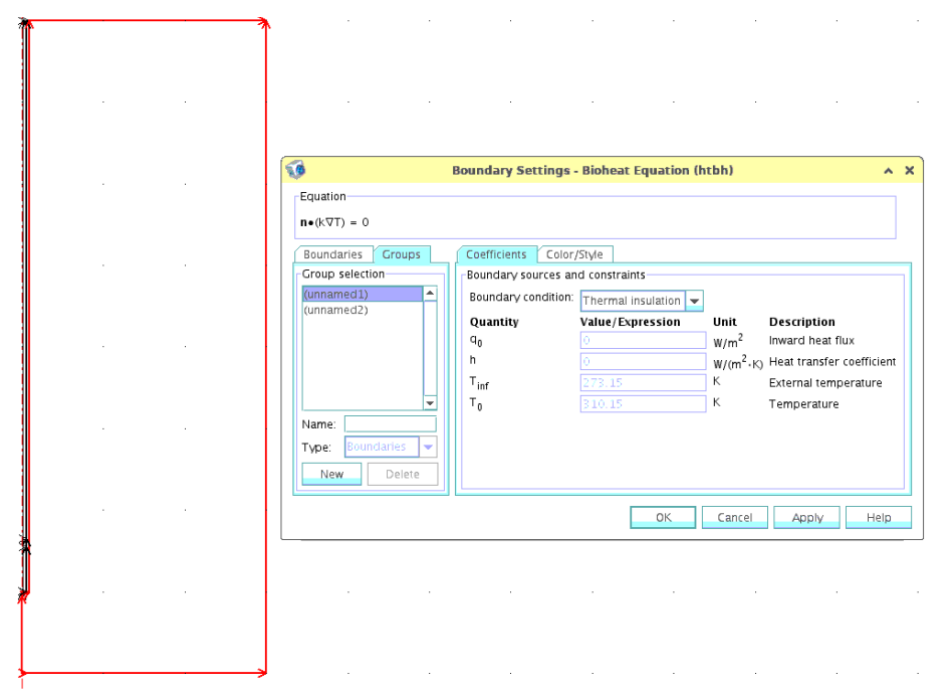


Fig. 1.5 | Boundary Settings for the liver

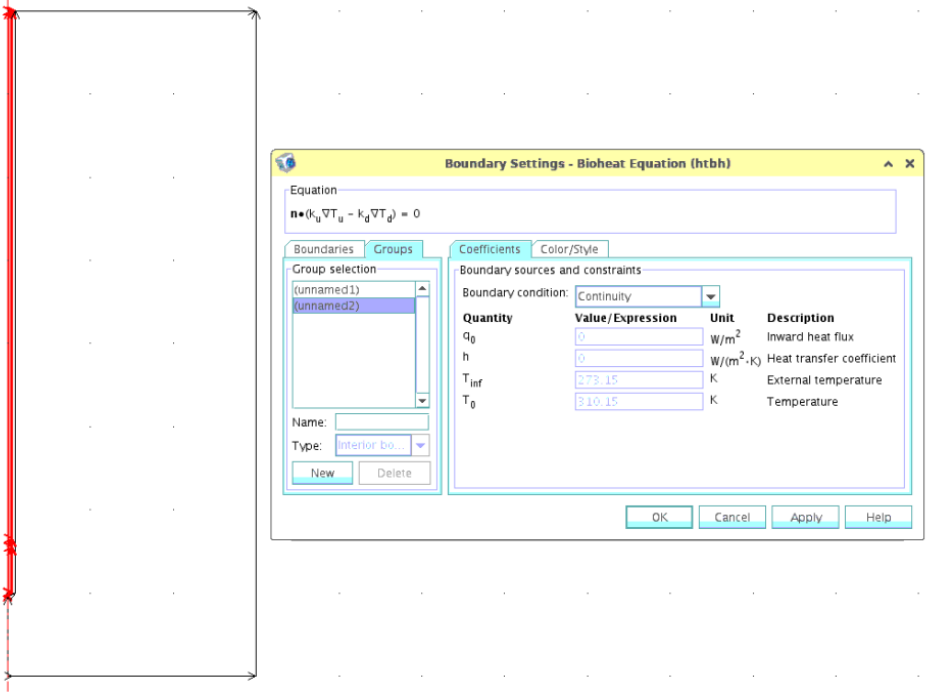


Fig. 1.6 | Boundary Settings for the antenna

The initial temperature field is set equal to the inlet blood temperature (37 °C) throughout the entire domain, ensuring realistic physiological conditions at the start of the simulation. In this way, the bioheat equation solves for the steady-state temperature distribution, allowing for analysis of both the extent of the ablated zone and the efficacy and safety of the treatment.

1.3.3. TM Waves Configuratios

In the configuration of the TM Waves module for the microwave therapy model in the liver, the transverse magnetic wave formulation is used in the harmonic regime, where the main unknown is the azimuthal component of the magnetic field, $H\phi$. This formulation is particularly suitable for geometries with axial symmetry, such as the coaxial antenna and the hepatic tissue domain, allowing the problem to be solved in two dimensions (r, z) and optimizing computational resources without sacrificing physical accuracy.

Within the domain, the scalar wave equation for H ϕ is solved, considering the dielectric and conductive properties of each material. The inner dielectric of the antenna is assigned a relative permittivity of 2.03, the PTFE catheter a relative permittivity of 2.60, and the hepatic tissue a relative permittivity of 43.03 and an electrical conductivity of 1.69 S/m. The remaining materials are considered non-conductive for the electromagnetic simulation.

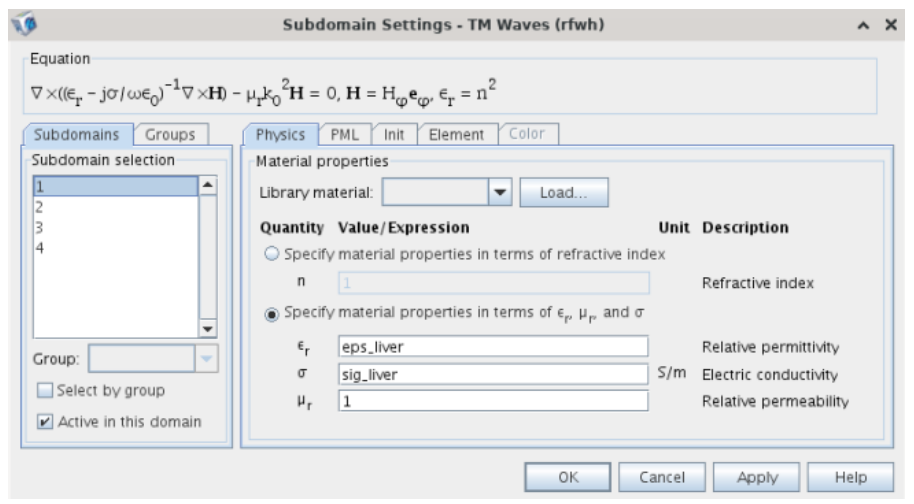


Fig. 1.7 | Example of the subdomain settings of the TM Waves part

The boundary conditions are defined according to the nature of each surface. On the metallic surfaces of the antenna (central conductor, outer conductor, and the short-circuited tip), the perfect conductor condition is imposed; that is, the tangential electric field is set to zero, simulating the real behavior of metals without the need to model their interior. At the input port, located at the base of the coaxial cable, a Port condition is applied with an input power of 10 W and coaxial mode specification, representing the actual feeding of the antenna.

For the outer boundaries of the domain, absorbing conditions (scattering boundary condition) are used to simulate wave propagation outside the tissue and to prevent artificial reflections that could affect the solution within the region of interest. Additionally, along the axis of symmetry (r = 0), an axial symmetry condition is applied, which takes advantage of the rotational geometry of the system and reduces the problem to two dimensions.

In the subdomain configuration, the corresponding electromagnetic properties are assigned to each region: hepatic tissue is assigned the experimentally defined permittivity and conductivity, while the inner dielectric and the catheter are assigned only the relative permittivity. The external air is modeled with a relative permittivity of one and zero conductivity.

1.3.4. Model Meshing

The mesh generation constitutes an essential step to ensure the accuracy and numerical stability of the simulation, especially due to the coexistence of very different geometric scales between the antenna and the surrounding tissue. Since the electromagnetic field presents very steep gradients near the antenna and the slot, while in the hepatic tissue and the external air the variations are much smoother, an adaptive meshing approach that combines local refinement and global efficiency is required.

Following the detailed procedure in the practice script, the mesh is manually adjusted through the free mesh parameter box. First, the custom mesh size option is selected, and a maximum global element size of 3×10^{-3} meters is set. This value is sufficient to adequately discretize most of the domain, including the hepatic tissue and the air, where the field variations are relatively smooth and excessively small elements are not required.

However, in the region of the antenna's inner dielectric (subdomain 3), where the energy

concentration and electromagnetic field gradients are much higher, a stricter local refinement is defined, setting the maximum element size to 1.5×10^{-4} meters. This refinement is essential to accurately capture the local field maxima and the distribution of absorbed energy in the vicinity of the antenna and the slot, which are the areas of greatest physical and clinical interest in the model.

Once these parameters are defined, the domain is remeshed to apply the new element sizes, and a visual inspection of the mesh is performed, verifying that the refinement in the antenna and the transition towards the hepatic tissue are adequate and that no distorted elements exist in the critical areas. This meshing strategy allows balancing precision in the regions of greatest interest with computational efficiency in the rest of the domain, ensuring that both the electromagnetic field and the resulting heat transfer are representative of the real phenomenon.

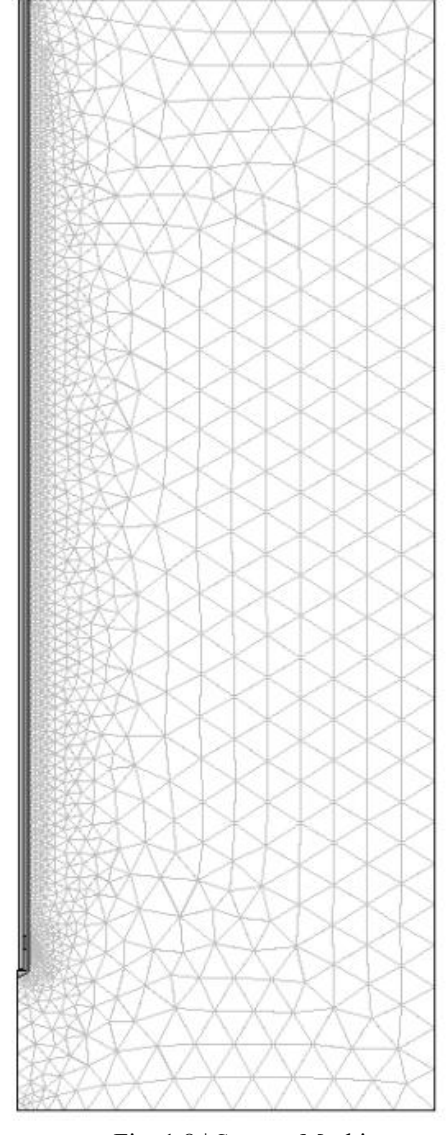


Fig. 1.8 | System Meshing

1.4. Results

The procedure for analyzing the effect of power and frequency in microwave liver therapy is structured in two distinct phases to isolate and understand the influence of each parameter on thermal distribution and treatment efficacy.

In the first phase, the frequency is kept constant, typically at the standard value of 2.45 GHz, which is widely used in microwave coagulation therapy due to its good balance between penetration and heating efficiency. With the frequency fixed, several simulations are performed by varying the input power at the antenna port (8 W, 10 W, 12 W, and 15 W). In each case, the coupled problem of electromagnetic waves and heat transfer is solved, analyzing how increasing power affects the extent and shape of the ablation zone, the maximum temperature reached in the tissue, and the spatial distribution of the SAR. This approach allows observation, for example, that higher powers produce more extensive ablation zones and faster heating, but may also increase the risk of damaging surrounding healthy tissue.

In the second phase, the strategy is reversed: the input power is fixed at a representative value (10 W), and the operating frequency of the antenna is varied, exploring values such as 2 GHZ, 2.45 GHz, 3 GHz and 3GHz. For each frequency, the simulation and analysis process is repeated, assessing how frequency variation modifies the penetration depth of the electromagnetic wave, the shape and size of the ablation zone, and the overall efficiency of the treatment. This analysis is fundamental because lower frequencies tend to penetrate more deeply, generating larger ablation zones, while higher frequencies can concentrate heating in more superficial or localized regions.

In both cases, after each simulation, key results are extracted and compared, such as the temperature profile, the extent of the ablated zone, the SAR distribution, and the total absorbed power in the tissue. This stepwise procedure enables a systematic and controlled evaluation of the impact of power and frequency on the efficacy and safety of microwave therapy, providing valuable information for the clinical optimization of the treatment.

1.4.1. Liver Temperature with Variable Potencies

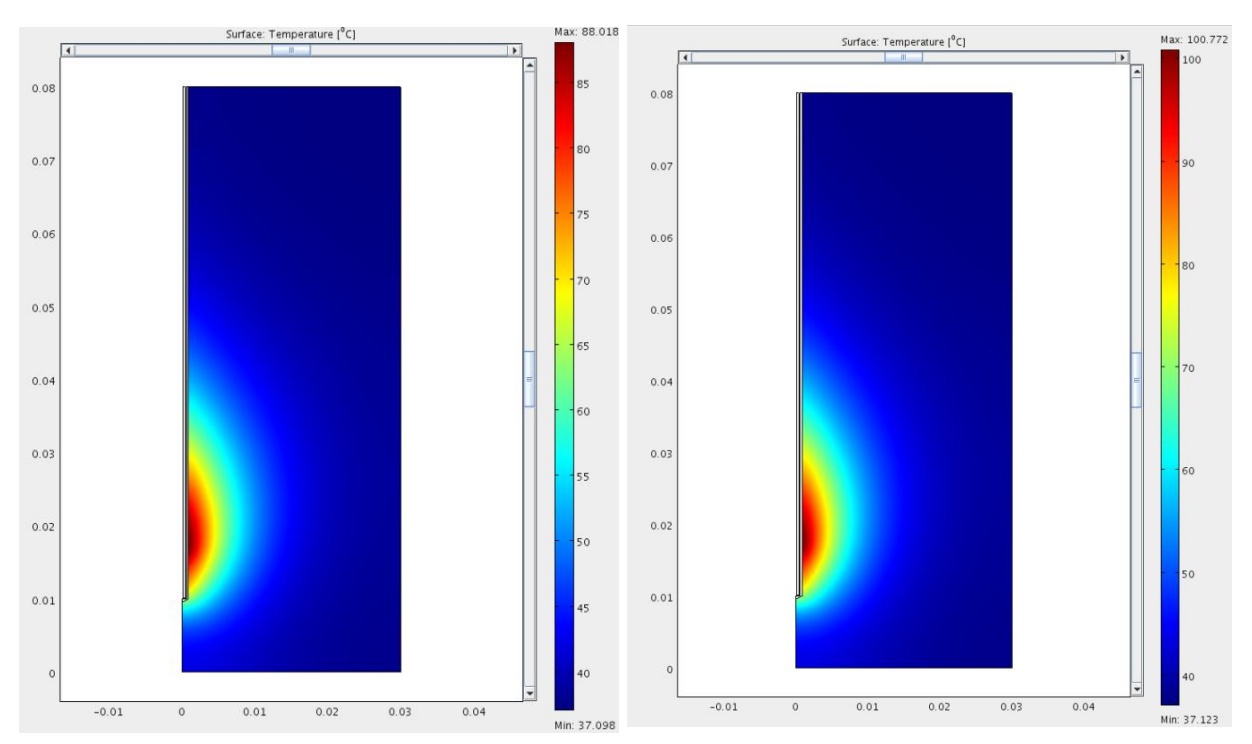
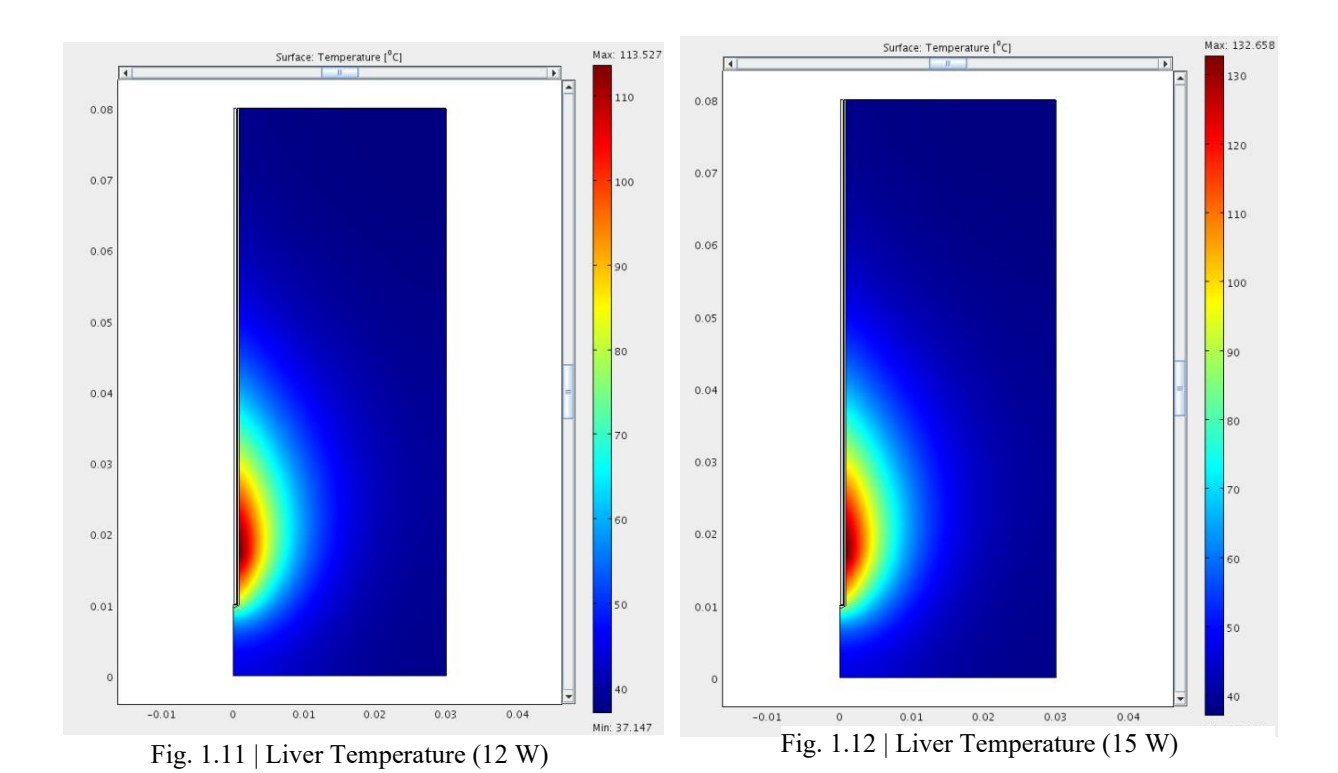


Fig. 1.9 | Liver Temperature (8 W)

Fig. 1.10 | Liver Temperature (10 W)



23

The attached images show the temperature distribution in hepatic tissue subjected to microwave ablation, with the frequency kept constant (2.45 GHz) and the input power of the antenna progressively increased (8 W, 10 W, 12 W, and 15 W). The analysis of these results allows several relevant conclusions to be drawn for the thesis:

As the supplied power increases, there is a significant rise both in the maximum temperature reached near the antenna and in the extent of the ablated zone. In the image corresponding to 8 W, the maximum temperature is around 88 °C, while for 10 W, 12 W, and 15 W, the maximum temperatures rise to approximately 101 °C, 114 °C, and 133 °C, respectively. This behavior is consistent with the physics of the process: resistive heating induced by microwave absorption is directly proportional to the applied power, resulting in a greater energy deposit per unit time in the surrounding tissue.

In addition to the increase in maximum temperature, it is observed that the region of tissue exceeding the critical thresholds for thermal necrosis (above 60 °C) expands notably with power. This means that higher power not only achieves faster ablation but also increases the volume of treated tissue, which can be beneficial for targeting larger tumors or ensuring wider safety margins. However, this effect also carries the risk of damaging adjacent healthy tissue if the spatial distribution of heat is not properly controlled.

The shape and symmetry of the heated region remain constant, indicating that the geometry of the antenna and the distribution of the electromagnetic field do not vary with power; rather, it is the level of deposited energy that determines the magnitude of the thermal effect.

In conclusion, increasing the input power in microwave therapy at constant frequency results in a rise in both the maximum temperature reached and the volume of ablated tissue. This direct relationship underscores the importance of carefully adjusting the applied power to achieve a balance between treatment efficacy and patient safety, avoiding overheating that could cause collateral damage to structures adjacent to the tumor.

1.4.2. The density of the microwave heat source with variable frequency

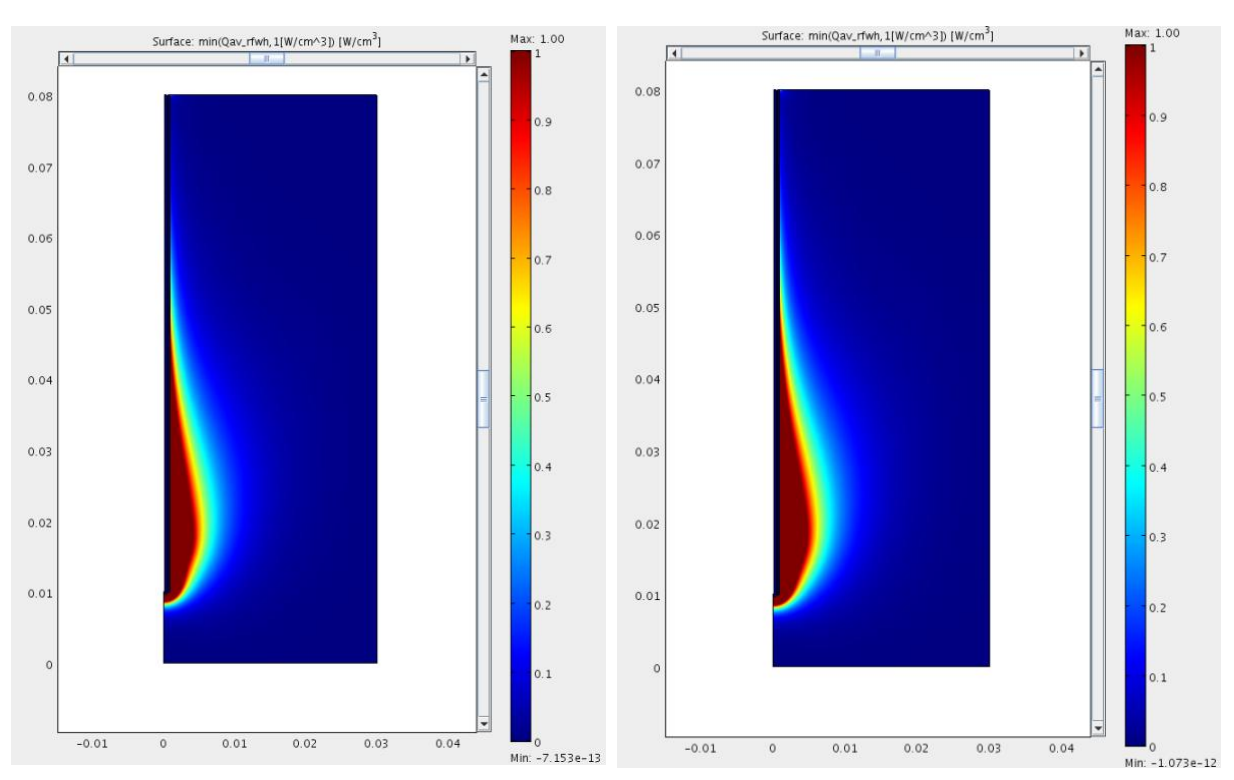


Fig. 1.13 | The density of the microwave heat source (8 W)

Fig. 1. 14 | The density of the microwave heat source (10 W)

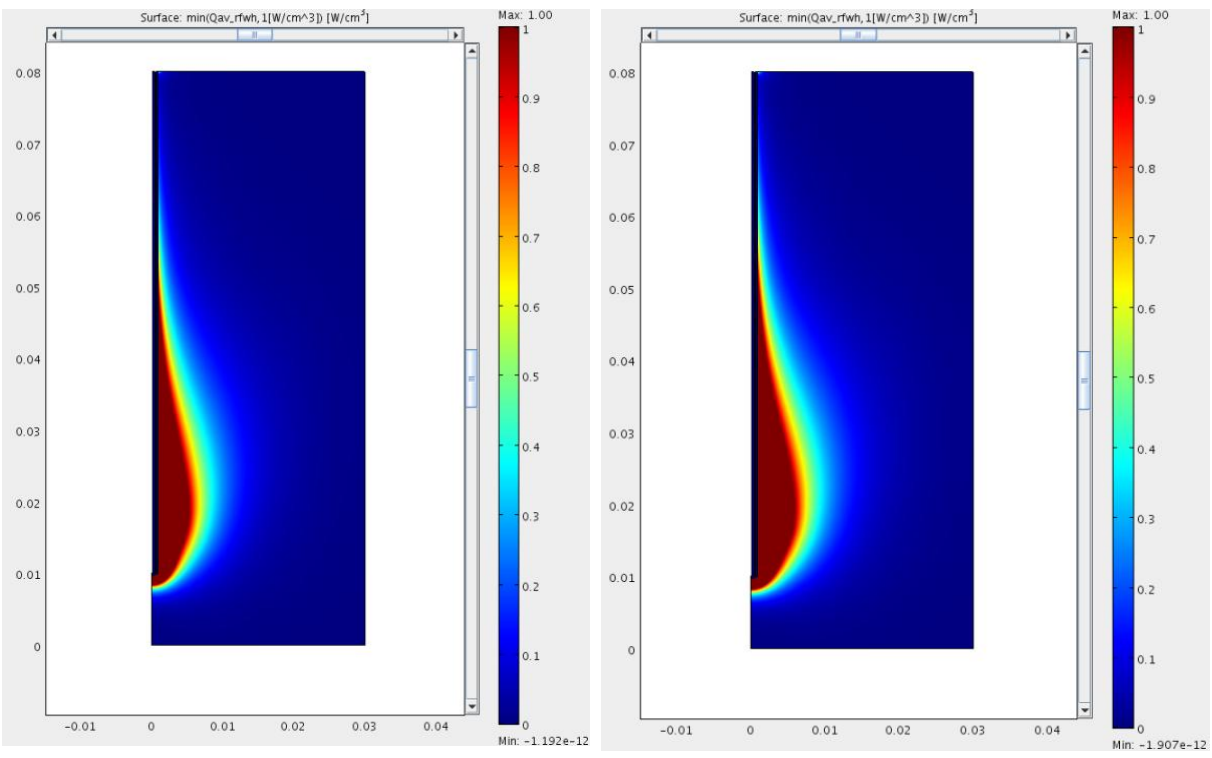


Fig. 1.15 | The density of the microwave heat source (12 W)

Fig. 1.16 | The density of the microwave heat source (15 W)

In all the images, the region of maximum absorption is located near the slot and the tip of the antenna, which is consistent with the physics of the problem: most of the electromagnetic energy is dissipated in the immediate vicinity of the source, generating localized heating that is fundamental to the effectiveness of tumor ablation. As the distance from the antenna increases, the absorbed power density decreases rapidly, resulting in a steep thermal gradient and relative protection of the more distant healthy tissue.

Comparing the images, it is observed that as the input power increases, the extent of the red and yellow colored region expands, indicating that not only does the maximum absorbed power increase, but also the volume of tissue exposed to significant heating levels. This behavior is consistent with experimental results: a greater energy supply leads to a larger ablation zone and a higher maximum temperature reached in the tissue.

The shape of the absorption region remains approximately constant, with an ellipsoidal and symmetric distribution relative to the antenna axis, highlighting that the geometry of the antenna and the configuration of the electromagnetic field determine the heating pattern, while the input power controls the magnitude and extent of the thermal effect. This is fundamental for clinical design: it allows the treated tissue volume to be predicted and controlled by adjusting the applied power, while maintaining spatial selectivity thanks to the applicator configuration.

In summary, these images illustrate how the absorbed power density, and therefore, the effectiveness of microwave ablation, depends directly on the supplied power, while the shape and location of the heating zone are determined by the antenna geometry and electromagnetic field distribution. This analysis supports the importance of precise power control to maximize tumor destruction and minimize damage to surrounding healthy tissue.

1.4.3. Normalized SAR value along a line parallel to the antenna Plot

0.01

0.02

0.03

Fig. 1.17 | Normalized SAR value along a line parallel to the antenna

0.05

0.06

0.07

0.08

0.04

The image shows the evolution of the normalized SAR (Specific Absorption Rate) along the depth of insertion in hepatic tissue, at a fixed distance of 2.5 mm from the axis of the microwave antenna. Each curve corresponds to a different input power value (8 W, 10 W, 12 W, and 15 W), allowing for a direct comparison of the effect of applied power on the spatial distribution of electromagnetic energy absorption.

All curves display a similar profile: the SAR progressively increases with depth until reaching a maximum, located near the antenna slot (around 0.06–0.07 m), and then drops sharply. This behavior reflects the localization of the most intense heating in the vicinity of the slot and the tip of the antenna, where the absorbed power density is highest, and the rapid attenuation of energy as the distance from the source increases.

The effect of input power is clearly visible: as the power increases, the maximum SAR value also increases and the curve rises, although the position of the maximum and the general shape of the profile remain constant. This indicates that the antenna geometry and the electromagnetic field distribution determine the location and extent of the maximum absorption zone, while the power controls the magnitude of the effect. Furthermore, the area under each curve increases with power, implying a greater volume of tissue exposed to significant absorption levels and, therefore, a more extensive ablation.

Overall, the figure clearly illustrates how the applied power is the main control parameter for adjusting the intensity and reach of microwave ablation, without altering the relative location of maximum heating. This result is fundamental for clinical planning, as it allows the treatment to be tailored to the size and position of the tumor, maximizing efficacy and minimizing damage to adjacent healthy tissue.

1.4.4. Liver Temperature with Variable Frecuencies

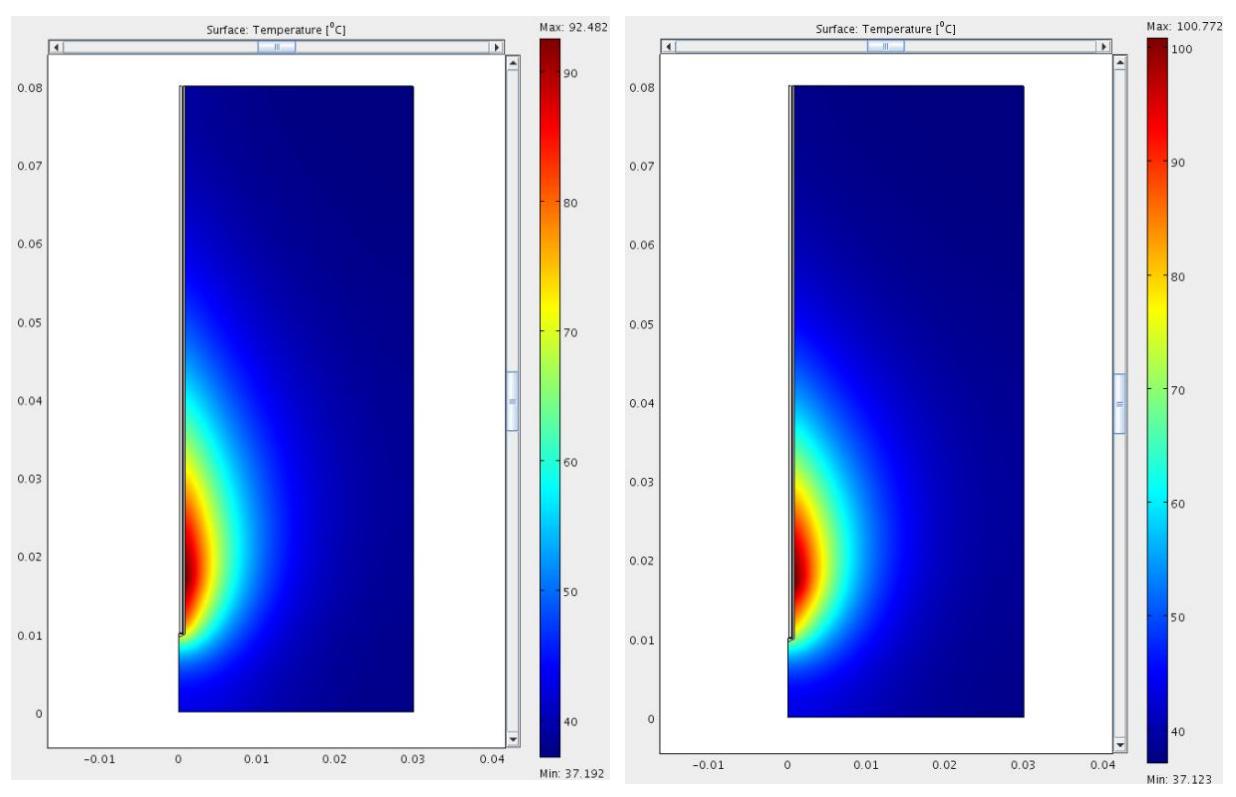


Fig. 1.18 | Liver Temperature (2 GHz)

Fig. 1.19 | Liver Temperature (2.45 GHz)

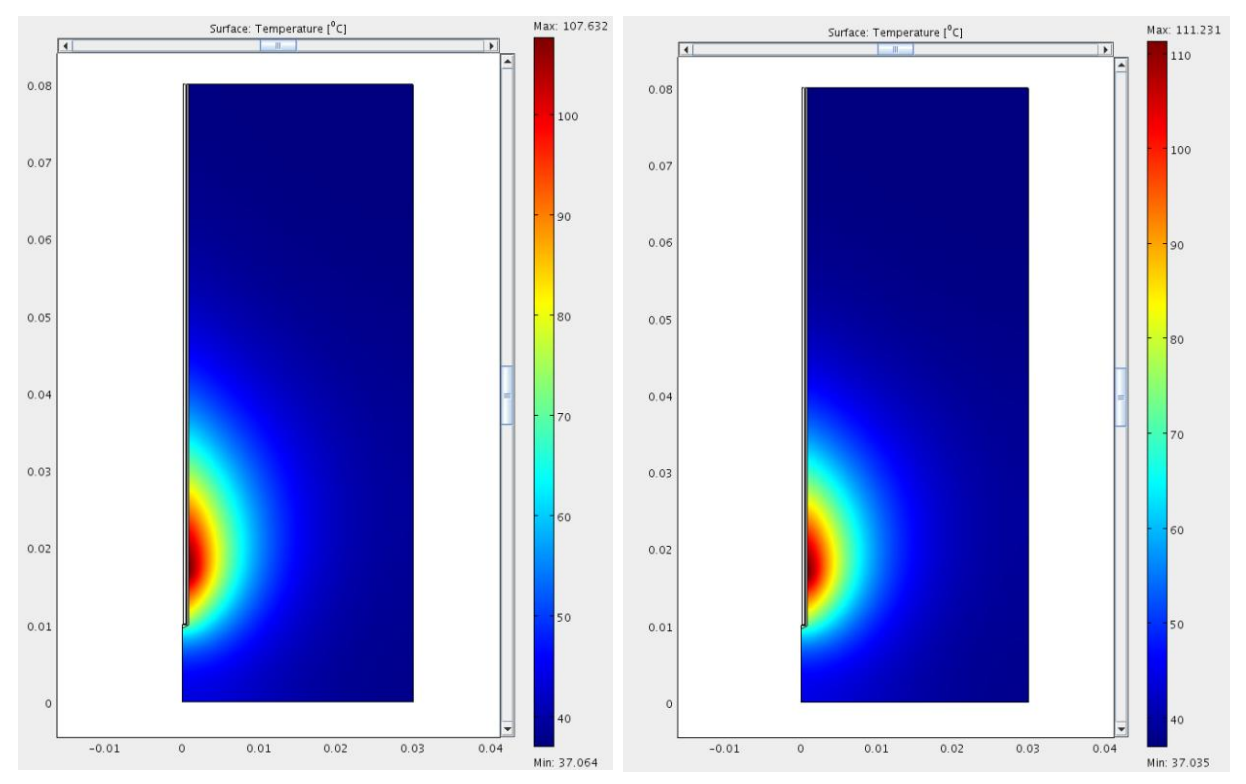


Fig. 1.20 | Liver Temperature (3 GHz)

Fig. 1.21 | Liver Temperature (3.5 GHz)

The previous images present a detailed analysis of the temperature evolution in hepatic tissue during microwave ablation, keeping the input power constant at 10 W and varying the frequency between 2.0, 2.45, 3.0, and 3.5 GHz, as shown in the attached images.

Firstly, it is observed that the maximum temperature reached increases progressively with frequency: at 2.0 GHz it reaches 92.5 °C, at 2.45 GHz 100.8 °C, at 3.0 GHz 107.6 °C, and at 3.5 GHz 111.2 °C. This increase is consistent with the physics of microwave ablation, since the electromagnetic absorption of tissue is higher at greater frequencies, resulting in more intense heating near the antenna.

However, the effective heating area clearly decreases as the frequency increases. This is visually evident in the images: the orange, yellow, and green zones, which correspond to regions with temperatures above 60 °C a typical threshold for tissue necrosis become smaller and more concentrated around the antenna as the frequency increases. Thus, although the maximum temperature is higher, the volume of tissue reaching therapeutic temperatures decreases and becomes more focused, implying a more precise and localized ablation.

Clinically, these results highlight the importance of selecting the operating frequency according to the therapeutic goal: lower frequencies allow treatment of larger volumes, while higher frequencies are ideal for small or localized lesions where maximum precision and minimal collateral damage are required. Moreover, the focusing of heating at high frequencies demands even stricter control of power and exposure time to avoid overheating and complications.

In summary, increasing the frequency in microwave ablation raises the maximum temperature achieved but reduces and focuses the effective heating area, which has direct implications for both the efficacy and safety of the treatment.

1.4.5. The density of the microwave heat source with variable frequency

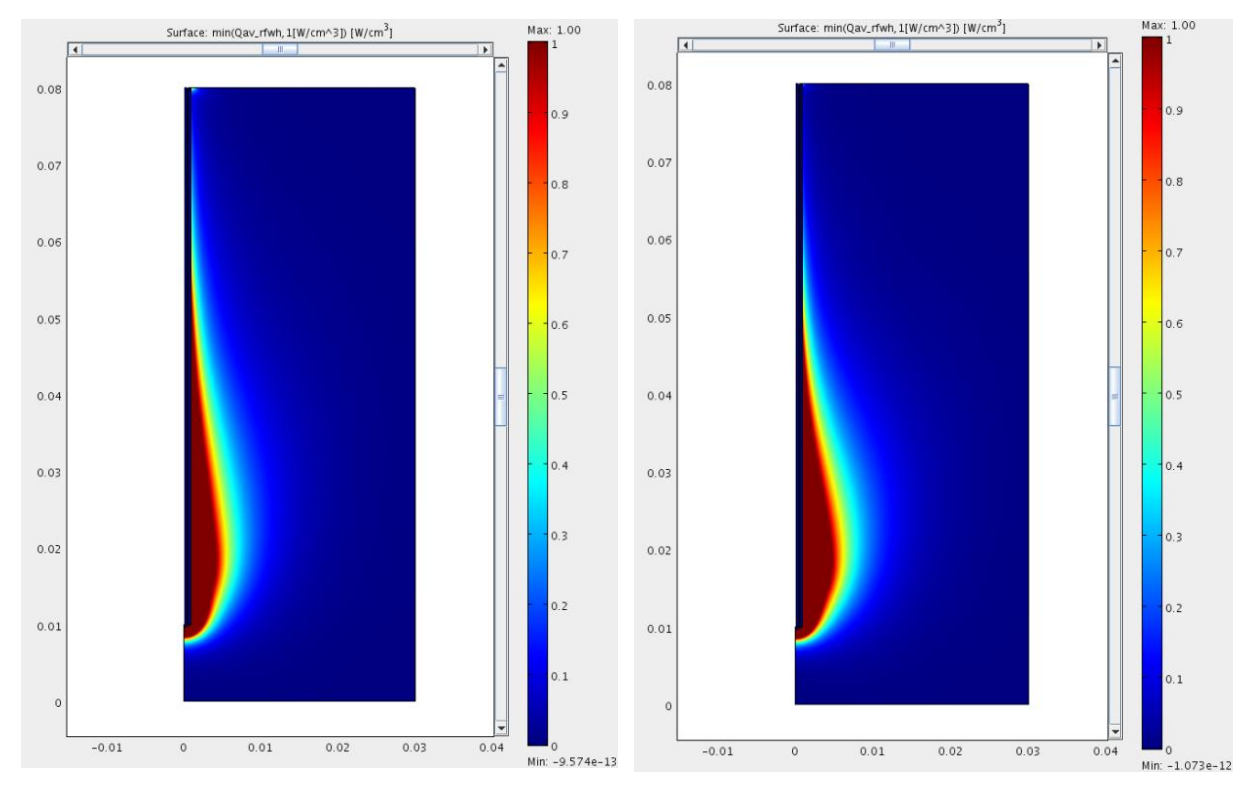


Fig.1.22 | The density of the microwave heat source (2 GHz)

Fig. 1.23 | The density of the microwave heat source (2.45 GHz)

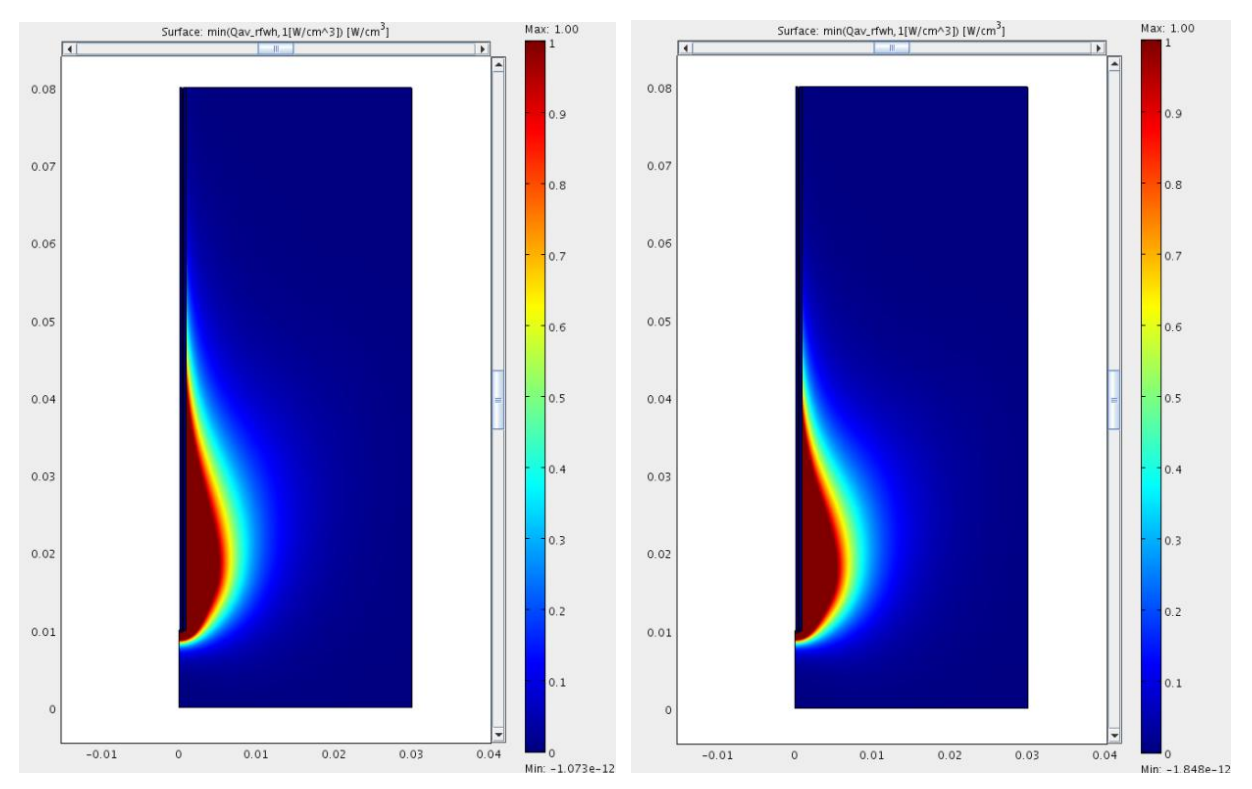


Fig. 1.24 | The density of the microwave heat source (3 GHz)

Fig. 1.25 | The density of the microwave heat source (3.5 GHz)

The presented images correspond to the spatial distribution of absorbed power density (resistive heating) in hepatic tissue during microwave ablation, evaluated for different operating frequencies of the antenna: 2.0 GHz, 2.45 GHz, 3.0 GHz, and 3.5 GHz. Each image uses a color scale to display the normalized absorbed power value within the domain, where red indicates areas of maximum absorption (up to 1 W/cm³) and blue represents regions with virtually no absorption.

In all figures, maximum power absorption is observed in the immediate vicinity of the slot and the tip of the antenna, which is consistent with the physics of the process and the applicator's geometry. The distribution pattern is very similar across all frequencies: the high-absorption region extends in an ellipsoidal and symmetric manner with respect to the antenna axis, and the power density decreases rapidly as one moves away from the source, revealing a strong spatial gradient.

When comparing the images, it is evident that, although the overall shape of the absorption region remains unchanged, both the intensity and the extent of the maximum absorption zone increase slightly with frequency. This effect is a consequence of the higher coupling efficiency and electromagnetic absorption of hepatic tissue at higher frequencies, resulting in a more localized energy deposition and potentially more intense heating near the antenna. However, the rapid attenuation of absorbed power towards the periphery is maintained in all cases, which helps limit thermal damage to regions distant from the applicator.

These results confirm that the frequency parameter not only influences the magnitude of heating but also the spatial selectivity of the treatment: higher frequencies tend to concentrate energy in volumes closer to the antenna, enabling more precise and localized ablation. Nevertheless, this same effect may increase the risk of overheating in the immediate region around the slot, so frequency adjustment must be carried out carefully according to the tumor's location and size.

In conclusion, the images demonstrate that the distribution of absorbed power in microwave ablation depends on the operating frequency, and that higher frequencies favor greater energy concentration in the target area, increasing treatment efficacy but requiring precise clinical control to avoid adverse effects on surrounding healthy tissue. These findings are consistent with the literature and highlight the importance of frequency as an optimization parameter in microwave therapy.

1.4.6. Normalized SAR value along a line parallel to the antenna Plot

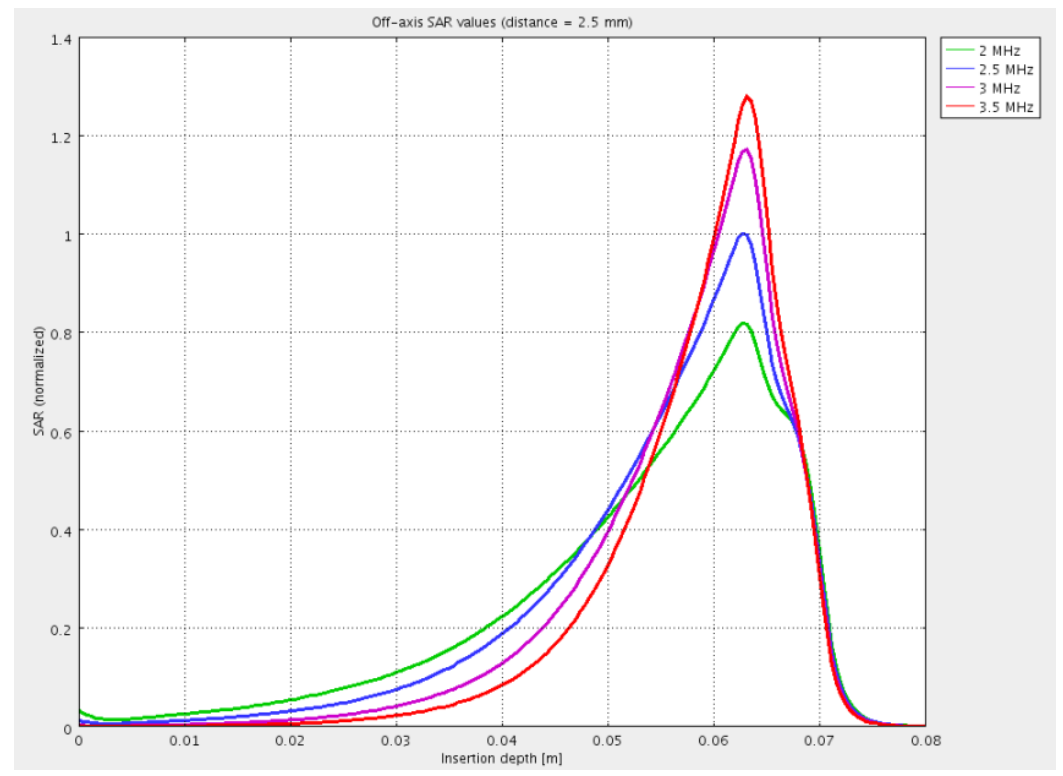


Fig. 1.26| Normalized SAR value along a line parallel to the antenna

The obtained graph shows the evolution of the normalized SAR (Specific Absorption Rate) along the depth of insertion in hepatic tissue, at a fixed distance of 2.5 mm from the axis of the microwave antenna, for four different frequencies: 2.0, 2.45, 3.0, and 3.5 GHz. Each curve represents the specific absorption profile of electromagnetic energy for a particular frequency, allowing a direct comparison of the effect of frequency on the spatial distribution of SAR in microwave ablation treatment.

All curves display a similar profile: the SAR progressively increases with depth until reaching a maximum, located around 60–65 mm of insertion, which corresponds to the area near the slot and tip of the antenna where energy absorption is greatest. Subsequently, the SAR drops sharply, reflecting the rapid attenuation of electromagnetic energy in the tissue as the distance from the source increases.

The effect of frequency is clearly visible: as the frequency increases, the maximum SAR value also increases, and the peak becomes sharper and more localized. The curve corresponding to 3.5 GHz (red) shows the highest and narrowest peak, while that of 2.0 GHz (green) presents a lower and broader peak. This indicates that, at higher frequencies, energy absorption in the tissue is more efficient and localized, which can result in more precise and controlled ablation. However, it also means that heating is concentrated in a smaller volume, which may increase the risk of overheating in the immediate vicinity of the antenna if treatment parameters are not properly adjusted.

.

1.5. Conclusion

The analysis of the results obtained in Chapter 1 clearly demonstrates the crucial influence exerted by both power and operating frequency on the efficacy and safety of microwave liver ablation therapy. Firstly, when the frequency is held constant and the power supplied to the antenna is increased, there is a significant rise in both the maximum temperature reached in the tissue and the ablation volume. This behavior confirms that the energy deposited is directly proportional to the applied power, which allows for the treatment of larger tumors or the assurance of wider safety margins, although it also increases the potential risk of damaging adjacent healthy tissue if not properly controlled.

On the other hand, varying the frequency while keeping the power fixed reveals that higher frequencies induce more intense and localized heating, but within smaller volumes, whereas lower frequencies allow for the treatment of larger areas, albeit with a lower concentration of energy. This finding underscores the importance of selecting the optimal frequency based on the size and location of the tumor, always seeking a balance between therapeutic precision and patient safety.

The spatial distribution of both temperature and SAR remains consistent with the geometry of the antenna and the configuration of the electromagnetic field, demonstrating that the applicator design is decisive for the heating pattern, while the operating parameters adjust the magnitude and extent of the thermal effect.

In summary, the results obtained allow us to conclude that microwave ablation therapy is highly dependent on the careful parameterization of power and frequency. An appropriate selection and control of these parameters, based on multiphysics simulation, is essential to maximize treatment efficacy, minimize risks, and advance towards more personalized and safer clinical protocols.

Chapter 2 – SAR of a Human Head Next to a Wi-Fi Antenna

2.1. Introduction

The rapid development of wireless technologies has led to an increasing integration of radiofrequency emitting devices into everyday life, making the human head one of the most exposed regions to artificial electromagnetic fields. Unlike clinical settings, where exposure is controlled and directed for therapeutic purposes, the interaction between telecommunications antennas and the human body occurs continuously and in unregulated environments, raising specific concerns about the safety and potential biological effects of non-ionizing radiation.

This chapter focuses on the study of the specific absorption rate (SAR) in the human head when it is near a Wi-Fi antenna, with particular attention to the most widely used frequency bands in current standards: 2.45 GHz, 5 GHz, and 6 GHz. The choice of these frequencies is based on their relevance in international standards such as IEEE 802.11ac (Wi-Fi 5) and IEEE 802.11ax (Wi-Fi 6/6E): the 2.45 GHz band has traditionally been used by Wi-Fi and other wireless services, the 5 GHz band was introduced to increase capacity and reduce spectrum congestion, and the 6 GHz band enables higher speeds and greater efficiency in environments with a high density of connected devices.

The analysis is carried out using numerical simulations that allow for the visualization and quantification of the spatial distribution of the electric field and SAR in a simplified anthropomorphic model, representative of cranial and brain anatomy. The main objective is to characterize how electromagnetic energy absorption varies depending on frequency and antenna geometry, identifying the areas of highest exposure and evaluating the penetration depth and location of the maximum SAR. This approach is essential for anticipating potential risks, validating international regulations, and contributing to the design of wireless devices that minimize unnecessary exposure in sensitive organs such as the brain.

2.2. Theorical basis

The specific absorption rate (SAR) is the parameter that quantifies how much electromagnetic energy human tissues absorb when exposed to radiofrequency fields, such as those emitted by Wi-Fi antennas. It is expressed in watts per kilogram (W/kg) and is fundamental for evaluating the safety of electronic devices near the user.

SAR is calculated using the formula:

$$SAR = \frac{\sigma |E|^2}{\rho}$$

where:

- σ is the electrical conductivity of the tissue (S/m),
- |E| is the magnitude of the electric field (V/m),
- ρ is the density of the tissue (kg/m³).

International organizations such as IEEE and the International Commission on Non-Ionizing Radiation Protection (ICNIRP) set maximum SAR limits to protect health, especially in sensitive areas like the head. For example, the typical limit is 1.6 W/kg averaged over 1 gram of tissue.

To analyze energy absorption, simplified models of the human head are commonly used, such as the specific anthropomorphic mannequin (SAM). This model replicates the anatomy of the head in a standardized way, which facilitates the comparison of results and ensures reproducibility in simulations. In this study, a version of the SAM model reduced to 60% of its original size is employed, and the brain is represented as a homogeneous ellipsoid to simplify the geometry. The dielectric properties assigned to the different tissues are as follows: for the brain, an electrical conductivity of 2.09 S/m and a relative permittivity of 54.7 are used, while for the cortical bone, the values are 0.4 S/m for conductivity and 11.35 for relative permittivity.

The behavior of electromagnetic radiation in tissues is described by the wave equation:

$$\nabla \times \frac{1}{u} \nabla \times E - \omega^2 \varepsilon E = 0$$

Where μ is the magnetic permeability and ϵ is the electrical permittivity of the material. This equation allows calculation of the spatial distribution of the electric field generated by the microstrip antenna.

The antenna used is of the microstrip type, consisting of a metallic sheet on a dielectric substrate (FR4) and a ground plane, powered by a 50 Ω port. This type of antenna is common due to its compact size and efficiency, and in the model it is placed near the simulated head. To simulate a realistic environment, the head-antenna assembly is placed inside an air domain surrounded by perfectly matched layers (PML), which act as barriers to prevent reflections and emulate free-space conditions, similar to an anechoic chamber.

In summary, the theoretical foundation integrates concepts from electromagnetism, properties of biological materials, and numerical simulation techniques. This allows quantifying and visualizing the distribution of energy absorbed in the human body when exposed to radiofrequency fields generated by Wi-Fi antennas.

2.3 Problem Modeling

2.3.1. Model Geometry

To begin the modeling process, the geometry of the human head is first imported into the COMSOL Multiphysics environment. This geometry corresponds to the specific anthropomorphic mannequin (SAM). Before importing, the head has been adjusted and reduced to 60% of its original size to facilitate handling and reduce the computational load of the model. The import is performed from an external file called "sar_wifi_antenna.mphbin".

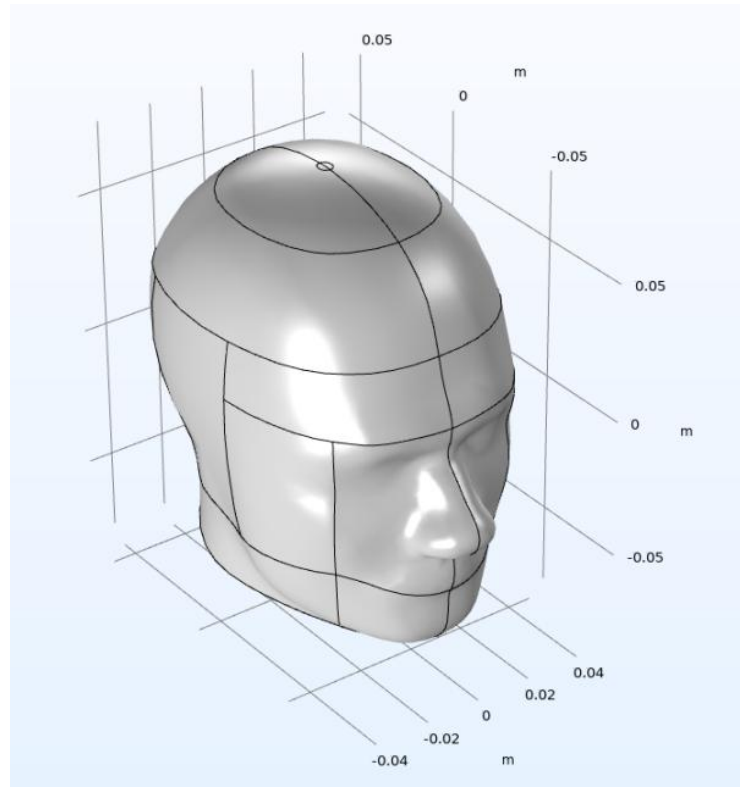


Fig. 2.1 | Result of importing "sar wifi antenna.mphbin"

Once the head has been imported, the next step is to create a simplified representation of the brain. To do this, an ellipsoid is added inside the head using COMSOL's geometry tools. The semi-axes and the position of the ellipsoid are defined so that it is correctly located within the head, thus representing the brain volume in a simple and homogeneous way.

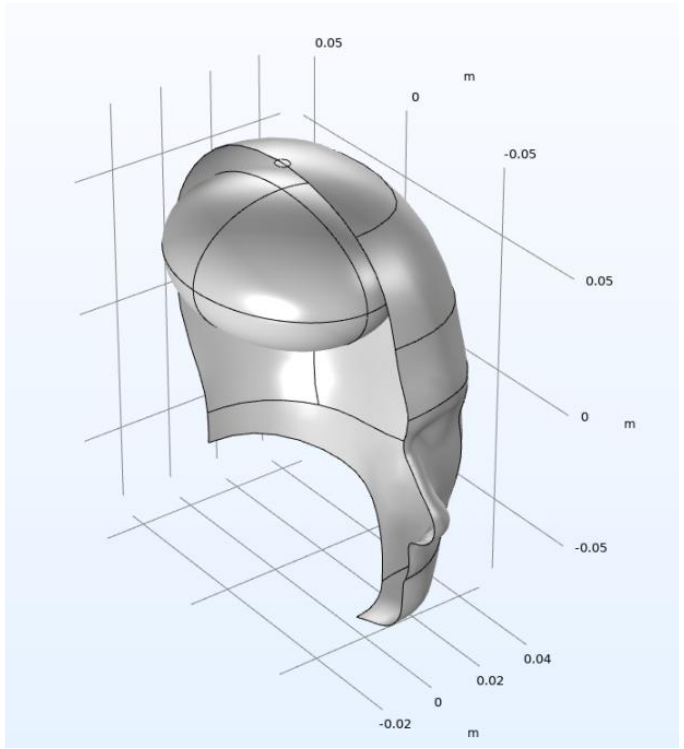
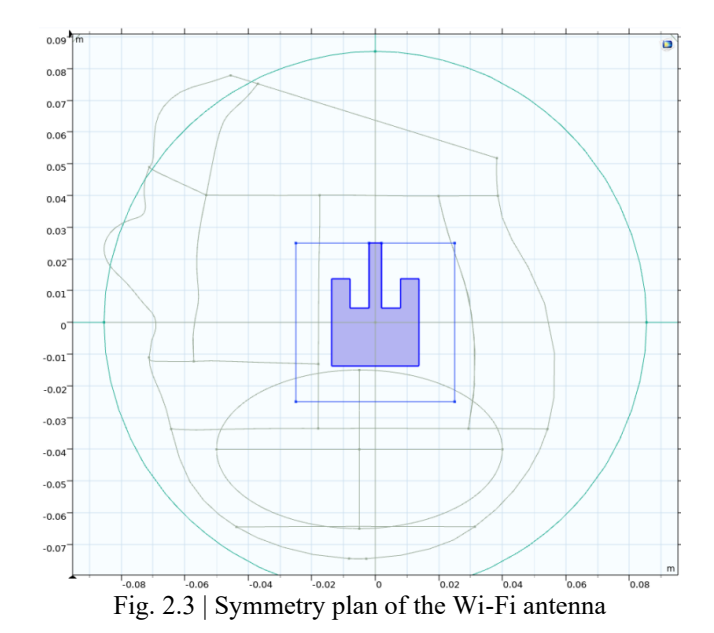


Fig. 2.2 | Illustration of the ellipsoid as a simulation of the brain

The following describes the construction of the Wi-Fi antenna, which in this case is a microstrip patch type. The antenna consists of three main elements: a rectangular block of FR4 dielectric material serving as the substrate, a thin rectangular metallic sheet placed on the upper face of the substrate functioning as the radiator, and a metallic ground plane on the lower face of the substrate. The substrate has dimensions of 4 mm in width, 50 mm in depth, and 5 mm in height. On the upper surface of the substrate, the metallic patch is defined as a square with sides of 27.5 mm, centered on the plane, while the ground plane covers the entire lower base of the block. This geometric arrangement allows the antenna to resonate within the Wi-Fi frequency band and maximizes energy transfer to the surrounding environment, facilitating the study of electromagnetic interaction with the human head.



After constructing the head, brain, and antenna, a sphere is added from the geometry menu ("Sphere"). This sphere serves an essential function in the simulation: it acts as the air domain surrounding the entire system, allowing electromagnetic waves to propagate freely around the head and the antenna, as would occur in a real environment. In the sphere configuration, a sufficiently large radius (0.18 m) is defined to ensure that both the head and the antenna are completely contained within it and are far from the domain boundaries, thus preventing artificial borders from affecting wave propagation.

Next, in the "Layers" section of the sphere configuration, an additional layer of 0.05 m thickness is specified. This layer will be used as a Perfectly Matched Layer (PML), which is a widely employed numerical technique to simulate free-space conditions. The PML absorbs electromagnetic waves that reach this region, preventing them from reflecting back into the domain of interest. This is fundamental for obtaining realistic results, since in practice, the waves radiated by the antenna do not encounter reflective boundaries in the environment.

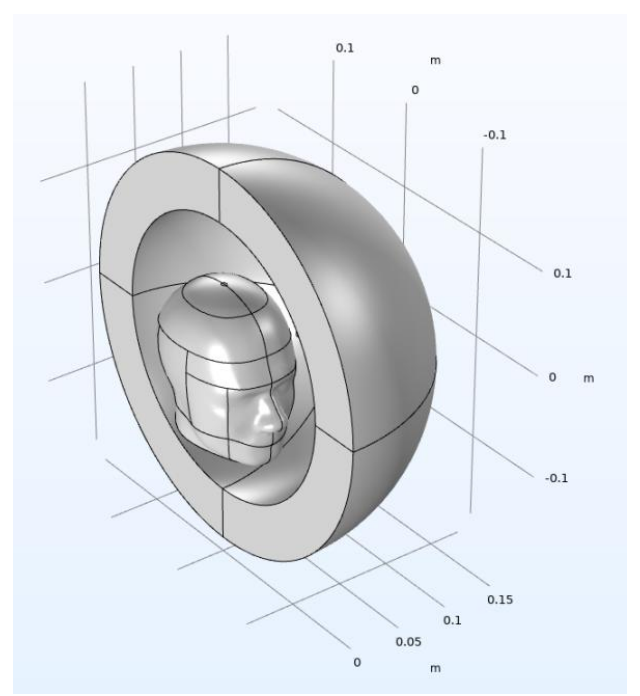


Fig. 2.4 | Model with the sphere implemented (half of the sphere has been hidden for better viewing)

2.3.2. Materials

The selection and assignment of materials is fundamental to ensure the physical fidelity of the model and the validity of the results obtained in the simulation. Each material has been chosen and parameterized based on its biological or technological relevance.



Fig. 2.5 | List of materials used for the system

The brain is modeled as a homogeneous material with an electrical conductivity of 2.09 S/m and a relative permittivity of 54.7, which are representative values for brain tissue at frequencies around 2.45 GHz. These properties determine the brain's capacity to absorb and store electromagnetic energy and are fundamental for the calculation of SAR.

	Property	Variable	Value	Unit	Property group
S	Relative permittivity	epsilonr_isc	54.7	1	Basic
\leq	Relative permeability	mur_iso ; n	1	1	Basic
\subseteq	Electric conductivity	sigma_iso ;	2.09	S/m	Basic
\leq	Density	rho	1000	kg/m³	Basic

Fig. 2.6 | Configuration of the "Brain" material

The cortical bone represents the rest of the head and is characterized by a conductivity of 0.4 S/m and a relative permittivity of 11.35. This reflects its lower capacity for absorption and transmission of energy compared to brain tissue, which affects the internal distribution of the electric field and the SAR.

	Property	Variable	Value	Unit	Property group
\subseteq	Relative permittivity	epsilonr_is	11.35	1	Basic
\leq	Relative permeability	mur_iso ; n	1	1	Basic
\leq	Electric conductivity	sigma_iso	0.4	S/m	Basic
\subseteq	Density	rho	2000	kg/m³	Basic

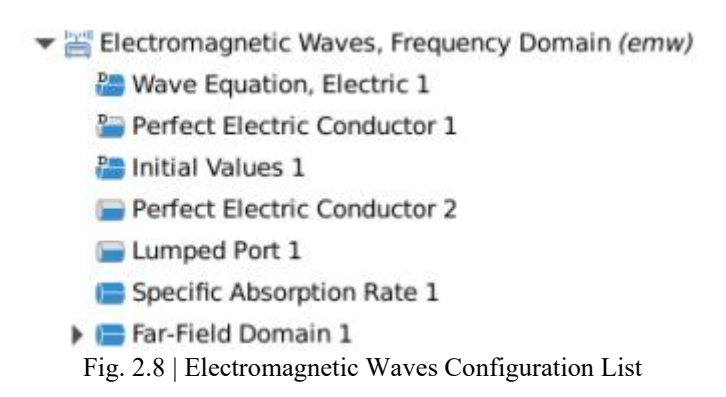
Fig. 2.7 | Configuration of the "Head" material

The dielectric substrate of the antenna is FR4, a material widely used in electronics due to its good dielectric and mechanical stability. It was selected from the COMSOL materials library.

The metallic parts of the antenna (radiator and ground plane) are modeled as perfect electric conductors (PEC), which implies that their conductivity is sufficiently high for losses to be negligible in the context of the simulation.

2.3.3. Electromagnetic Waves Configuration

In the Electromagnetic Waves, Frequency Domain (emw) section of this study, several fundamental nodes are employed to accurately and realistically model and analyze the interaction between the patch antenna and the human head.



The core of the simulation is the Wave Equation, Electric node, which solves the wave equation for the electric field throughout the entire domain. In this model, all domains are selected, including the head, brain, antenna, surrounding air, and the PML layer. This ensures that electromagnetic wave propagation is calculated considering both biological tissues and dielectric materials, as well as the air environment, allowing for the spatial distribution of the electric field necessary for subsequent SAR analysis.

The metallic surfaces of the antenna, namely the radiator and the ground plane, are defined using the Perfect Electric Conductor (PEC) node. In practice, this is specifically applied to boundaries 62 and 66, which correspond to the metallic surfaces in the model. This simulates the ideal behavior of a metal, ensuring that the tangential electric field is zero and that electromagnetic energy is correctly reflected by the antenna.

The antenna feed is implemented with the Lumped Port node. In this case, boundary 63 is selected, corresponding to the feed point of the patch. The lumped port is configured with an impedance of 50 Ω , representing the typical connection of a signal source in real microstrip applications. This setup allows the electromagnetic signal to be introduced into the system and the power supplied to the radiator to be controlled.

To evaluate energy absorption in the tissues, the Specific Absorption Rate (SAR) functionality is activated in domains 6 and 7, which correspond to the brain and the rest of the head, respectively. This node uses the previously obtained electric field distribution to calculate, point by point, the energy absorbed by the tissue according to the standard SAR formula. This calculation is fundamental for analyzing safety and regulatory compliance, as it allows results to be compared with international exposure limits for the human head.

The simulation environment is completed by applying a Scattering Boundary Condition to the outer boundaries of the air domain, just before the PML layer. This allows electromagnetic waves to exit the domain without reflection, emulating free-space conditions and avoiding numerical artifacts. Additionally, a Far-Field Domain is defined in domain 5 (air), which enables the calculation of far-field radiation parameters, such as the antenna's radiation pattern, and the analysis of directivity and efficiency in the presence of the head.

2.3.4 Model Meshing

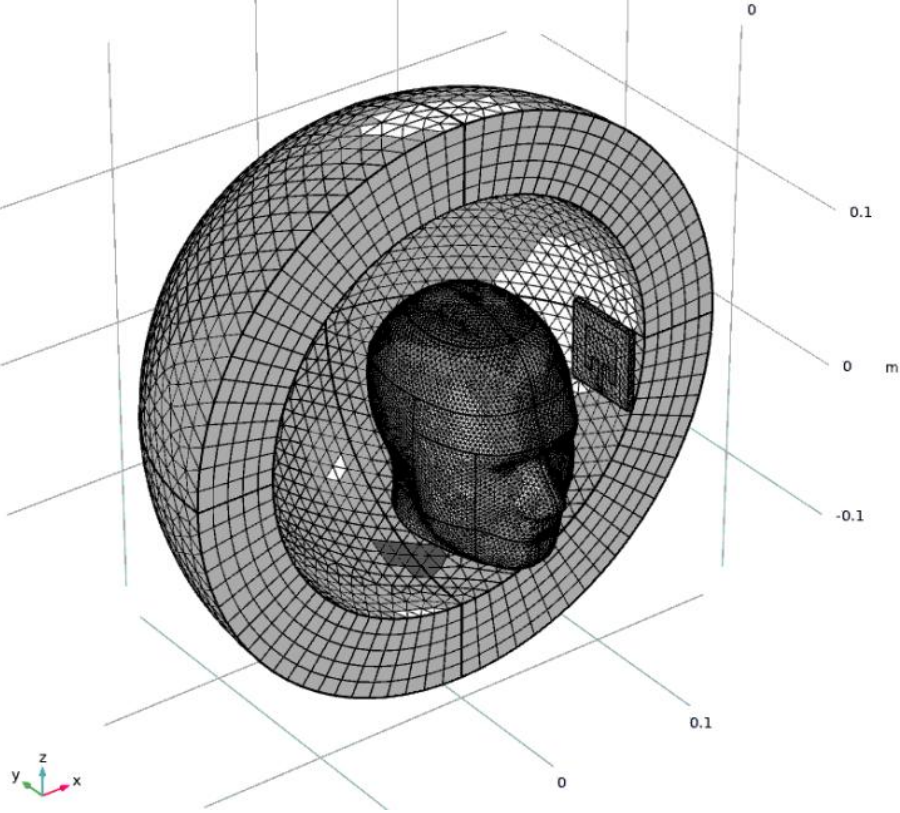


Fig. 2.9 | System Meshing

After defining the geometry and materials, meshing is carried out automatically using the Build All option in the Mesh 1 node. No manual refinement or specific element size selection is specified for any region of the model.

This means that COMSOL generates a mesh adapted to the physics and the defined operating frequency (2.45 GHz), adjusting the element size according to the geometric and material characteristics present. The automatic meshing ensures that the most critical areas, such as the interface between the antenna and the head or the interior of the brain, receive adequate resolution to capture the electric field gradients and the local SAR distribution, while in less sensitive regions, such as the air and the PML, larger elements can be used to optimize computational resources.

This approach, although simple, is sufficient to obtain reliable and reproducible results in the context of SAR studies in the human head next to a Wi-Fi antenna.

2.4. Results

$2.4.1.\ Bi-dimensional\ distribution\ of\ the\ electric\ field\ (V/m)\ in\ the\ human\ head\ exposed$

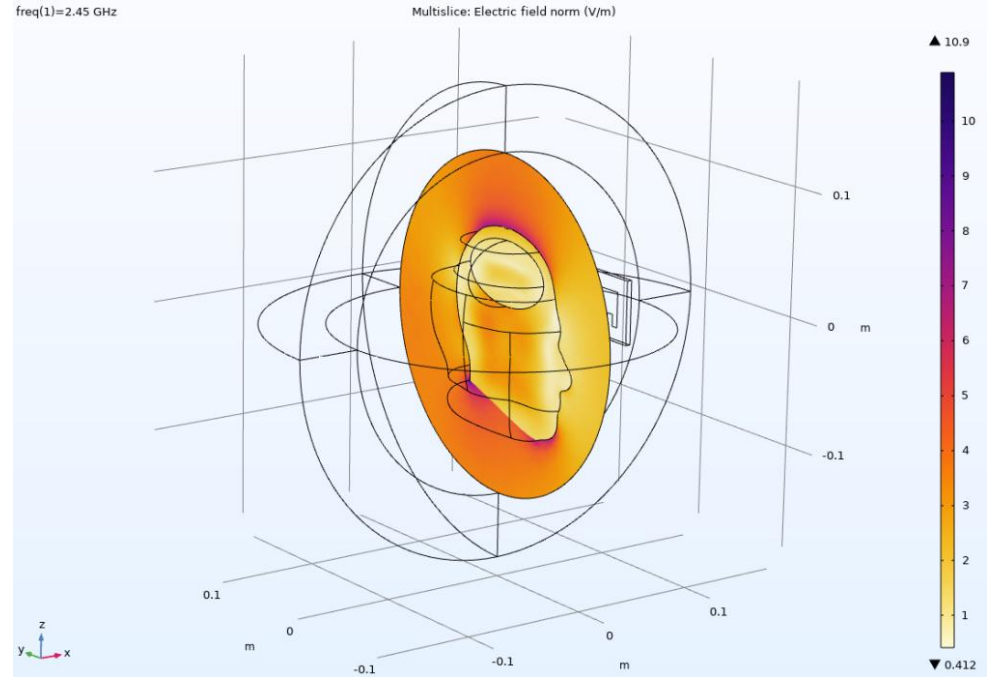


Fig. 2.10 | Bi-dimensional distribution of the electric field (2.45 GHz)

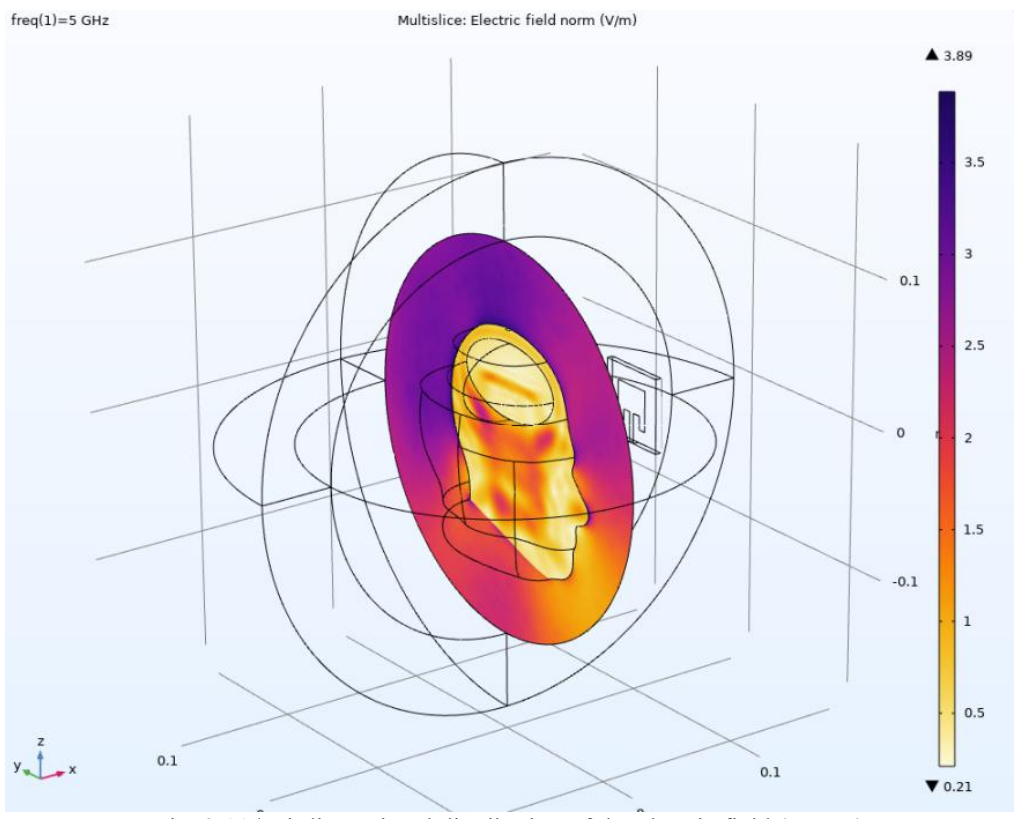


Fig. 2.11 | Bi-dimensional distribution of the electric field (5 GHz)

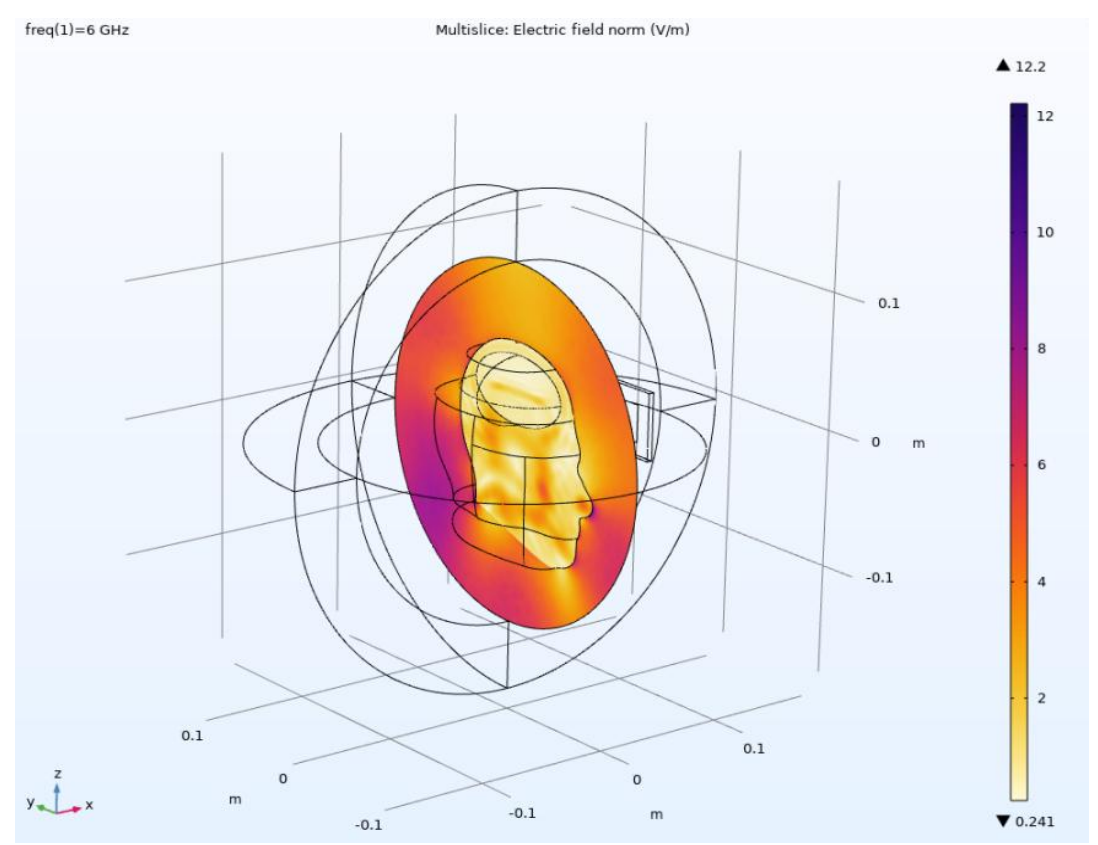


Fig. 2.12 | Bi-dimensional distribution of the electric field (6 GHz)

The presented images show the two-dimensional distribution of electric field intensity (V/m) inside the human head when a patch antenna operating at 2.45 GHz, 5 GHz, and 6 GHz is placed next to the lateral surface of the skull. In the image corresponding to 2.45 GHz, it can be observed that the maximum electric field values are concentrated in the area of direct contact between the antenna and the head, reaching intensities greater than 10 V/m near the surface and rapidly decreasing as the field penetrates the tissue. This reflects the natural attenuation of electromagnetic waves in biological media and the progressive absorption of energy by the tissues.

When analyzing the image for 5 GHz, it is evident that the electric field distribution is even more superficial. The maximum values are also located in the immediate vicinity of the antenna, but the attenuation is faster and the spatial extent of the significant field is smaller than at 2.45 GHz. This behavior is consistent with the physical phenomenon that, at higher frequencies, the penetration depth of the electric field decreases and the energy is concentrated in the outermost layers of cranial tissue, increasing superficial focusing.

In the image corresponding to 6 GHz, this trend is intensified: the maximum electric field intensity remains at the surface in contact with the antenna, but the area of influence is even more reduced and superficial. Electromagnetic energy is dissipated almost exclusively in the outer layers of the tissue, with minimal penetration into the interior of the head, implying that the risk of deep exposure decreases, but the concentration of surface energy may be higher.

It is essential to highlight that, although the effective penetration of the electric field decreases at higher frequencies, the density of transmitted and absorbed energy at the surface can also increase. This means that, while the risk of effects in deeper regions is lower, the probability of localized overexposure in the superficial zone increases, which must be carefully considered in risk assessment and in the design of modern wireless devices.

On the other hand, it is relevant to note that in the 2–3 GHz band, a local maximum in electric field intensity and, by extension, in tissue energy absorption can be observed. This phenomenon is due to the coincidence between the electromagnetic wavelength and the characteristic dimensions of the human head, which favors resonant coupling that maximizes energy transfer from the antenna to the tissue. Additionally, the dielectric properties of the tissues and the optimal penetration depth in this frequency range contribute to the combination of sufficient penetration and surface concentration, potentially resulting in a local maximum in electric field intensity. Some scientific literature supports the existence of these relative maxima in the 2–3 GHz region, both in electric field intensity and in specific absorption (SAR), due to the interaction between wavelength, tissue dielectric properties, and the geometry of the human head[12][13].

2.4.2. Local distribution of the specific absorption rate in the human head

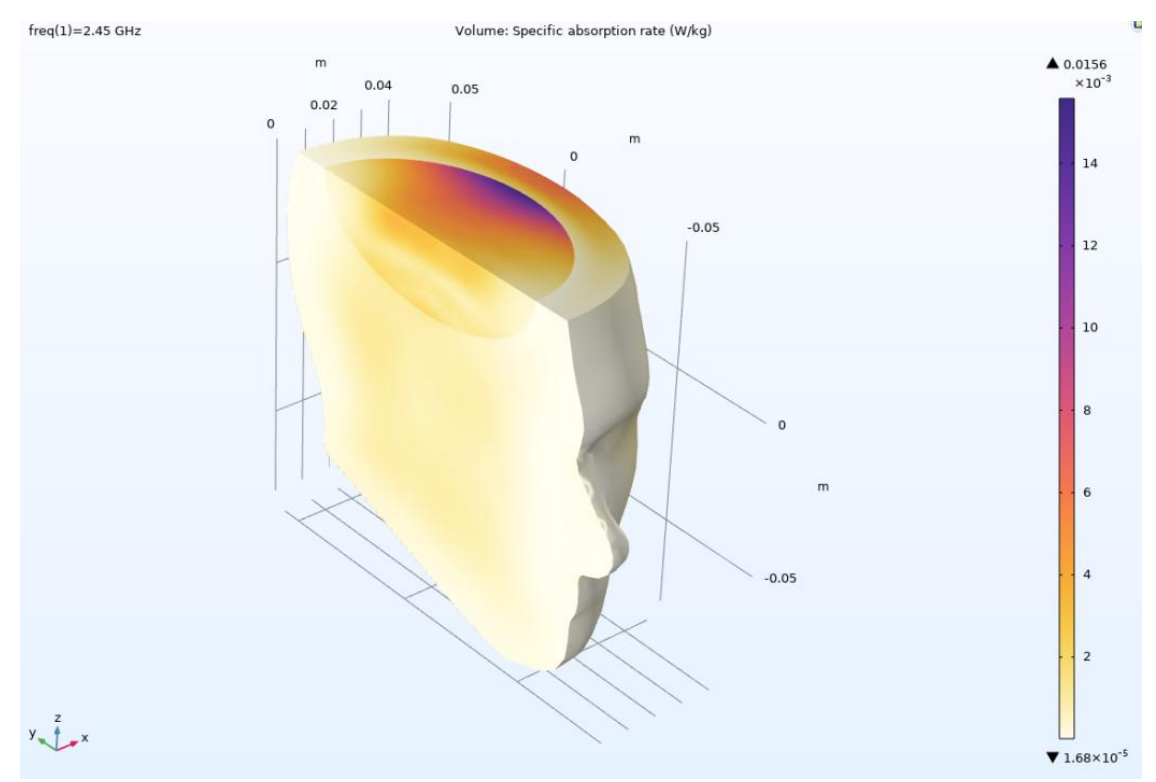


Fig. 2.13 \mid Local distribution of the specific absorption rate (2.45 GHz)

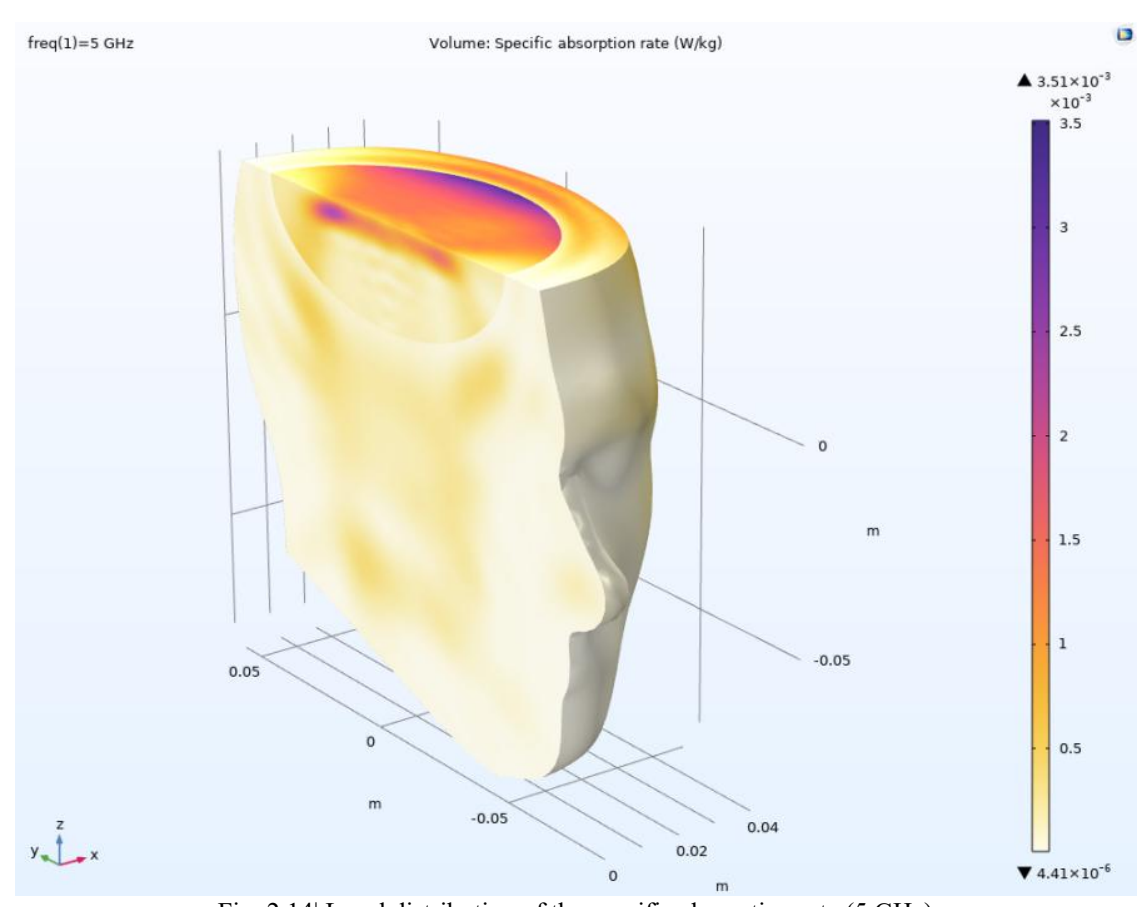


Fig. 2.14| Local distribution of the specific absorption rate (5 GHz)

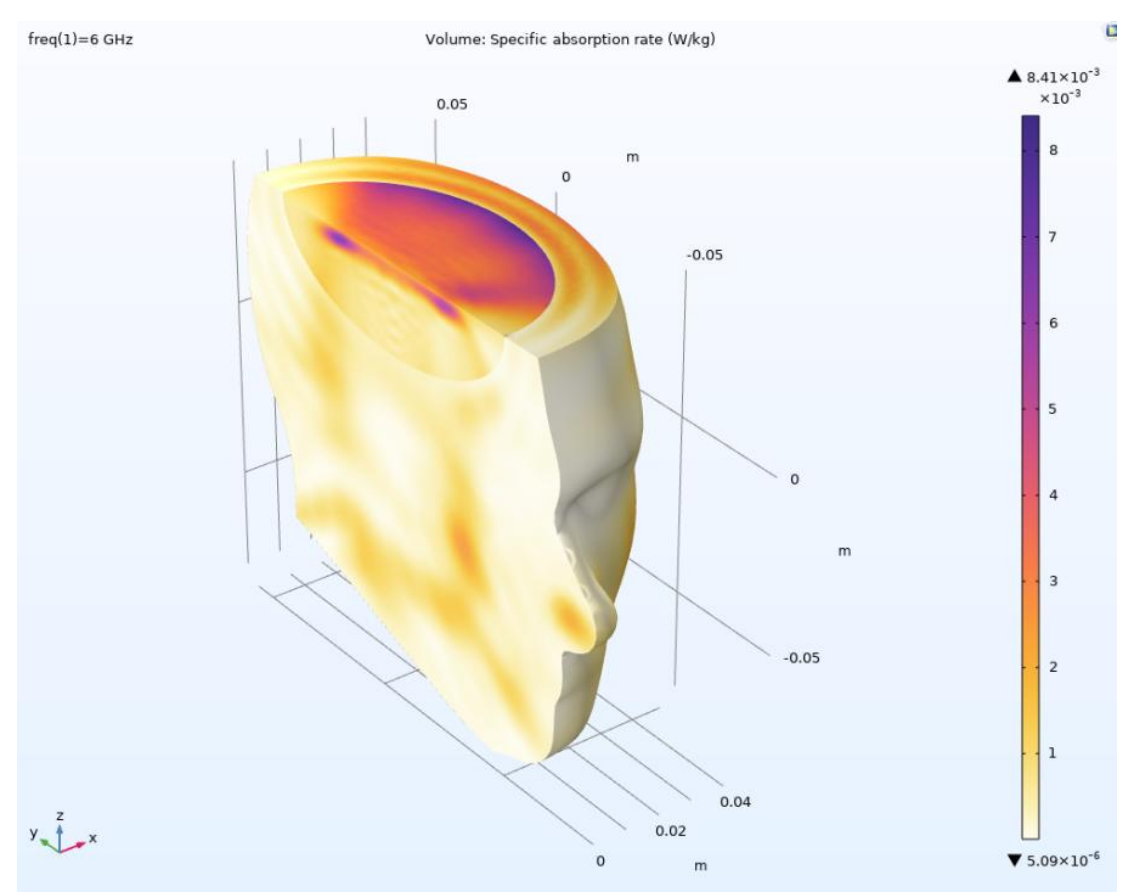


Fig. 2.15 Local distribution of the specific absorption rate (6 GHz)

The three images show the distribution of the Specific Absorption Rate (SAR) in the human head model exposed to a patch antenna at frequencies of 2.45 GHz, 5 GHz, and 6 GHz. Comparing these images allows for an analysis of how the specific absorption of electromagnetic energy varies as a function of frequency, a key aspect for safety assessment and the design of wireless devices.

In the first image, corresponding to 2.45 GHz, it can be observed that the region of highest SAR is located near the surface of the head, precisely at the point of field incidence, with maximum values reaching approximately 1.5×10^{-2} W/kg. The SAR penetrates relatively deep, showing a significant spatial extension within the cranial tissue. This is consistent with the literature, which reports that at frequencies in the 2–3 GHz band, electromagnetic field penetration is greater and absorption is not limited only to the surface[12][13].

In the second image, for 5 GHz, the SAR distribution is more superficial and localized, and the maximum values decrease to about 3.5×10^{-3} W/kg. The field attenuates more rapidly, and energy absorption is concentrated in the outer layers of the tissue, with less penetration into the interior of the head. This behavior is consistent with increasing frequency, as penetration depth decreases and superficial absorption increases.

In the third image, at 6 GHz, this trend becomes more pronounced: the region of highest SAR remains superficial, the maximum values decrease further (around 8.4×10^{-3} W/kg), and the absorption is distributed in a more reduced area close to the surface. This reflects the well-known effect of high frequencies, where electromagnetic energy is dissipated almost exclusively in the outer layers of the tissue and effective penetration is minimal.

It is essential to highlight that the color scale varies in each image, which can be misleading if one only looks at the visual pattern without considering the numerical values. For example, although the area of intense color may appear similar in extent, the absolute SAR values decrease significantly as frequency increases. Therefore, to properly compare absorption and biological risk, it is crucial to pay attention to the scale bar in each graph.

In conclusion, the images reflect a logical and expected physical behavior: as frequency increases, the maximum SAR decreases and absorption becomes more superficial, while at intermediate frequencies such as 2.45 GHz, the penetration and spatial extension of SAR in the tissue are greater. This pattern is consistent with electromagnetic theory and with experimental and numerical results reported in the scientific literature [12][13].

2.4.4. SAR averaged over 1 gram of tissue (SAR1g) on the simulated human

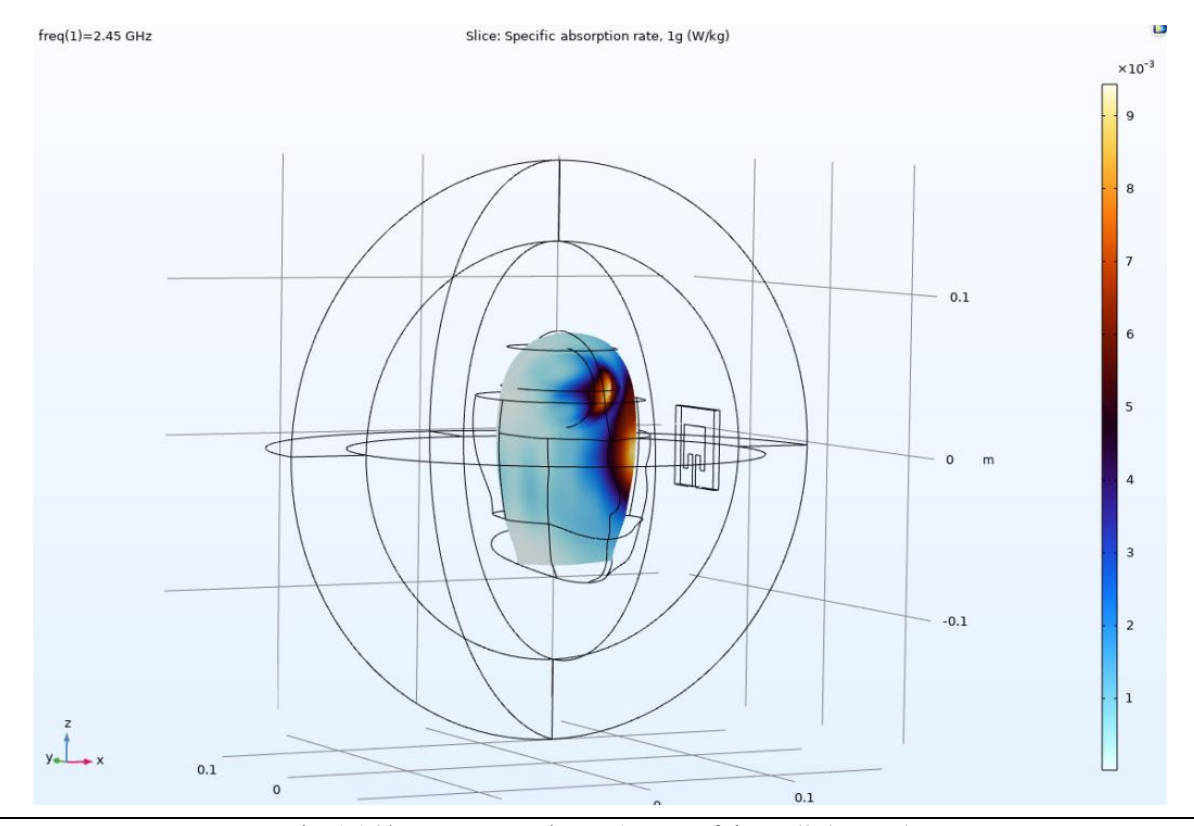


Fig. 1.16 | SAR averaged over 1 gram of tissue (2.45 GHz)

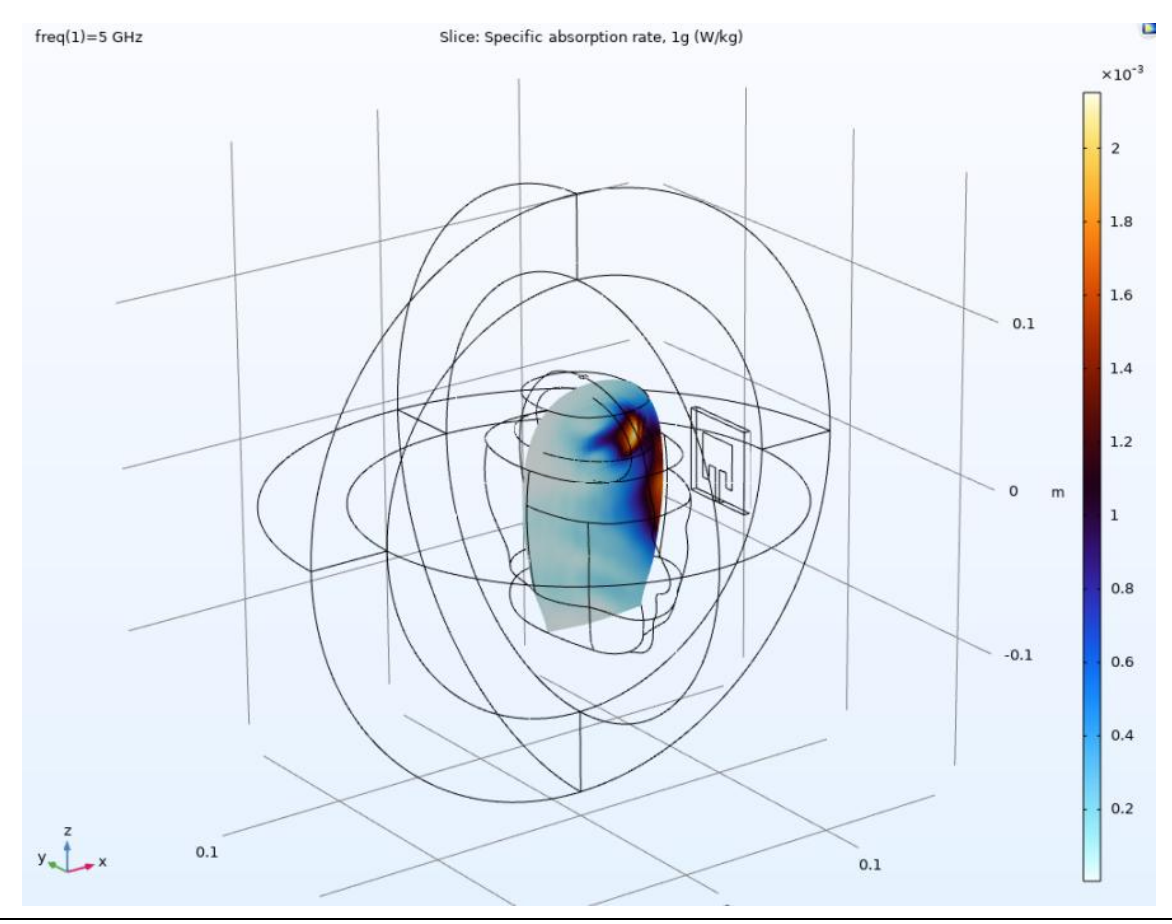


Fig. 1.17 | SAR averaged over 1 gram of tissue (5 GHz)

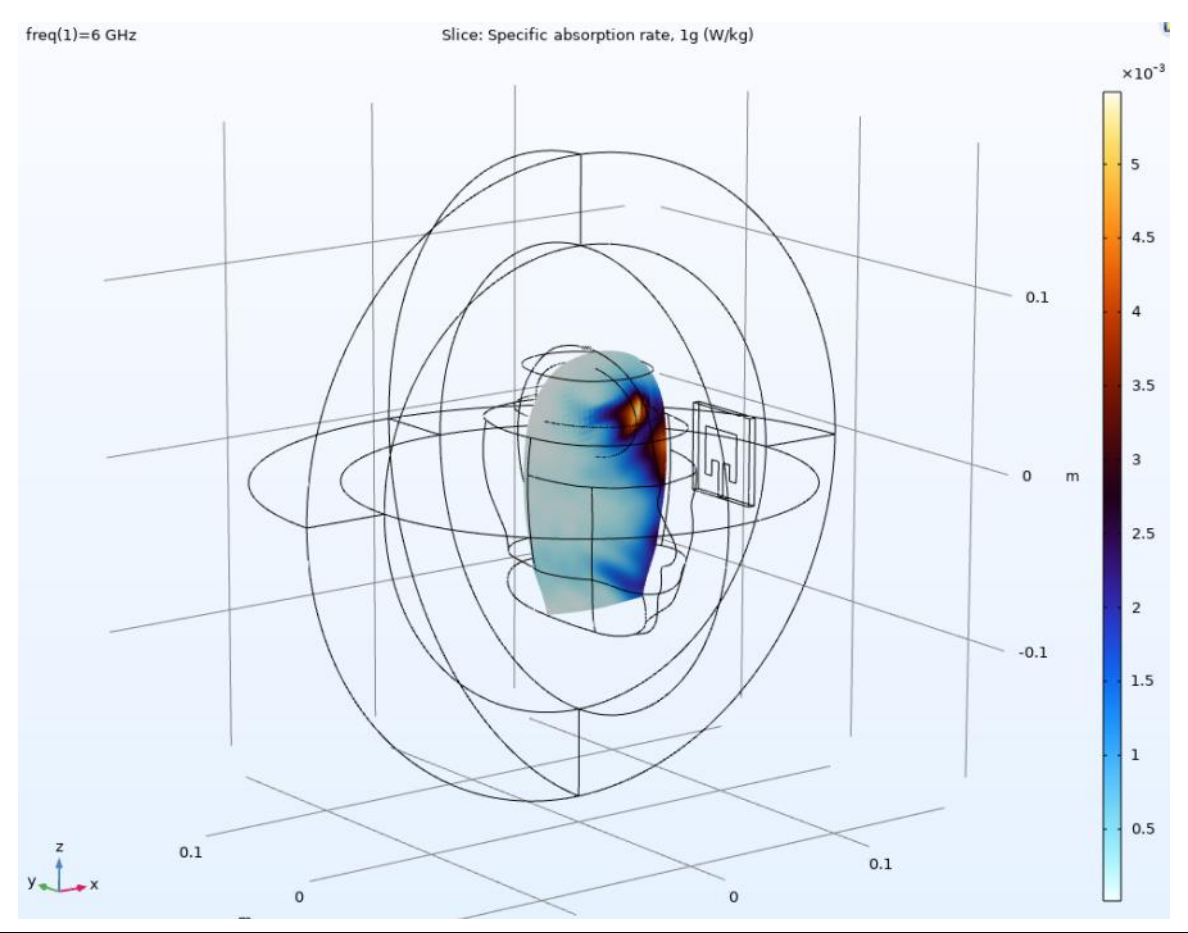


Fig. 1.18 | SAR averaged over 1 gram of tissue (6 GHz)

The three images show the spatial distribution of the Specific Absorption Rate (SAR) per gram of tissue in the human head model exposed to a patch antenna at frequencies of 2.45 GHz, 5 GHz, and 6 GHz, respectively. Comparing these images allows for the analysis of how the specific absorption of electromagnetic energy varies as a function of frequency, a key aspect for safety assessment and the design of wireless devices.

In the first image, corresponding to 2.45 GHz, it can be observed that the region of highest SAR is located near the lateral surface of the head, precisely in the area of field incidence, with maximum values reaching approximately 9×10^{-3} W/kg. The SAR penetrates relatively deep, showing a significant spatial extension within the cranial tissue. This is consistent with the literature, which reports that at frequencies in the 2–3 GHz band, electromagnetic field penetration is greater, and absorption is not limited only to the surface [12][13].

In the second image, for 5 GHz, the SAR distribution is more superficial and localized, and the maximum values decrease to about 2×10^{-3} W/kg. The field attenuates more rapidly, and energy absorption is concentrated in the outer layers of the tissue, with less penetration into the interior of the head. This behavior is consistent with increasing frequency, as penetration depth decreases and superficial absorption increases.

In the third image, at 6 GHz, this trend becomes more pronounced: the region of highest SAR remains superficial, the maximum values decrease further (around 5×10^{-3} W/kg), and the absorption is distributed in a more reduced area close to the surface. This reflects the well-known effect of high frequencies, where electromagnetic energy is dissipated almost exclusively in the outer layers of the tissue and effective penetration is minimal.

In conclusion, the images reflect a logical and expected physical behavior: as frequency increases, the maximum SAR decreases and absorption becomes more superficial, while at intermediate frequencies such as 2.45 GHz, the penetration and spatial extension of SAR in the tissue are greater. This pattern is consistent with electromagnetic theory and with experimental and numerical results reported in the scientific literature [12][13].

2.4. Conclusion

The developed practice has made it possible, through numerical simulation in COMSOL, to carry out a detailed analysis of the interaction between electromagnetic radiation and human cranial tissue in the frequency range of 2.45 GHz, 5 GHz, and 6 GHz. The main objective was to study the distribution of the electric field and the SAR (Specific Absorption Rate) in the human head exposed to a patch antenna, evaluating how the operating frequency influences the penetration, absorption, and localization of electromagnetic energy in biological tissues.

Throughout the simulation, it was confirmed that the general trend predicted by electromagnetic theory holds: as frequency increases, the penetration depth of the electric field decreases and absorption becomes concentrated in the most superficial layers of the tissue. Thus, at 2.45 GHz, the electric field and SAR show greater spatial extension and penetrate more deeply into the cranial tissue, implying a larger volume of potentially affected tissue. However, at 5 GHz and especially at 6 GHz, absorption becomes much more superficial and localized, with a rapid drop in intensity inside the tissue. This behavior is consistent with the scientific literature, which describes the decrease in penetration depth and the increase in superficial absorption as frequency increases in the microwave range.

Nevertheless, the results obtained also highlight the existence of non-linear variations and relative minima in electric field intensity and SAR, particularly at the intermediate frequency of 5 GHz. This phenomenon can be explained by the complex dielectric response of biological tissues in the gamma dispersion region, the influence of geometry and coupling between the antenna and the head, and the appearance of resonant modes or partial field cancellations within the model. The specialized literature indicates that the permittivity and conductivity of tissue do not vary linearly with frequency, but rather present dispersion regions where absorption and attenuation can show relative minima and maxima. Moreover, the interaction between the wavelength and the dimensions of the head can favor or hinder energy coupling at certain frequencies, thus generating these local minima.

On the other hand, this work has highlighted the usefulness and power of multiphysics simulation in COMSOL for the study of complex electromagnetic phenomena in biological systems. The ability to parameterize materials, geometry, and boundary conditions, as well as to analyze the influence of frequency and antenna configuration, makes it possible to obtain detailed and relevant information for risk assessment, the safe design of wireless devices, and the protection of public health against exposure to non-ionizing radiation.

.

Chapter 3 – SAR in Human Head

3.1. Introduction

The advancement and proliferation of wireless devices have significantly increased the population's exposure to electromagnetic fields, especially in the head region, where particularly sensitive organs such as the brain are located. Unlike the previous section, which focused on modeling microwave therapy for medical applications, this section addresses a daily and preventive issue: the evaluation of electromagnetic energy absorption in the human head due to the proximity of radiation sources such as telecommunications antennas.

For this analysis, the Specific Absorption Rate (SAR) is used, a widely recognized parameter in the literature and international standards, which quantifies the energy absorbed by biological tissues when exposed to radiofrequency fields. The use of simplified models, such as the Standard Anthropomorphic Mannequin (SAM), facilitates the comparison of results and the reproducibility of simulations, also allowing the model to be adapted to different scales and study conditions.

In this work, the head model is reduced to 60% of its original size to optimize computation, and the brain morphology is simplified using a homogeneous ellipsoid. The dielectric properties of the tissues are assigned according to representative values from the literature for each frequency considered. Unlike conventional approaches that usually analyze a single frequency, here four key frequencies (500, 835, 1000, and 1500 MHz) are explored, selected for their relevance in telecommunications standards and their use in commercial devices. This approach allows for comparing how the SAR distribution and local heating vary as a function of frequency, providing a broader and more realistic view of the potential impact of everyday exposure to electromagnetic fields.

Thus, this section complements the previous analysis, shifting the focus from the therapeutic and controlled application of electromagnetic energy to risk assessment and health protection in common exposure scenarios, aiming to contribute both to the validation of regulations and the design of safer devices.

3.2. Theorical Basis

The analysis of electromagnetic energy absorption in the human head, as addressed in Chapter 3, builds upon the physical and methodological foundations established in Chapters 1 and 2, but adapts them to the context of environmental and preventive exposure rather than therapeutic intervention. While Chapter 1 focused on the controlled and localized application of microwaves for cancer therapy(where the primary concern is maximizing thermal efficacy within a tumor while protecting healthy tissue)Chapter 2 introduced the concept of Specific Absorption Rate (SAR) as a key parameter for quantifying energy absorption in the head when exposed to Wi-Fi antennas, emphasizing the importance of frequency, geometry, and tissue properties in determining exposure patterns.

In this chapter, the focus shifts to a more comprehensive evaluation of SAR and local temperature increase in the cranial tissue when the head is exposed to telecommunications antennas operating at frequencies commonly encountered in daily life. Unlike the high-power, short-duration exposures in medical applications, environmental exposures are characterized by lower intensity but longer duration, and involve more complex anatomical geometries.

To achieve a realistic representation of electromagnetic interactions, the standard SAM Phantom geometry is employed, as recommended by international guidelines for SAR assessment in devices used near the head. This model incorporates spatial heterogeneity in the dielectric and thermal properties of brain tissue, using volumetric interpolation functions derived from MRI data. This approach allows for a more accurate simulation of internal tissue variability and a more precise mapping of SAR distribution, which is essential for identifying regions of heightened susceptibility.

The propagation of electromagnetic waves from the antenna is resolved using the vector Helmholtz equation, with local electrical properties assigned to each point in the domain. The model also integrates heat dissipation mechanisms, such as blood perfusion and thermal conduction, by applying the Pennes bioheat equation to estimate the temperature increase resulting from electromagnetic absorption. This multiphysics coupling is crucial for predicting not only the energy absorbed but also the realistic thermal impact under prolonged exposure conditions.

A key methodological distinction from previous chapters is the multifrequency analysis: several frequencies (500, 835, 1000, and 1500 MHz) are explored to assess how absorption and heating vary with frequency and penetration depth in brain tissue. This is particularly relevant for evaluating the safety of mobile devices and other radiofrequency emitters that operate outside the Wi-Fi bands analyzed in Chapter 2.

In summary, the theoretical basis of Chapter 3 extends the electromagnetic and thermal principles introduced earlier, adapting them to the context of environmental exposure by incorporating tissue heterogeneity, multifrequency simulation, and advanced multiphysics modeling. This approach enables a more realistic and comprehensive assessment of the risks associated with everyday exposure to radiofrequency fields near the human head, complementing the clinical and device-focused analyses of the previous chapters.

3.3. Poblem Modeling

3.3.1. Definitions and Geometry

The first step in the modeling process is to define the constants and global parameters that characterize the physical system to be simulated. These parameters include the electrical and thermal properties of the materials involved, such as the relative permittivity and electrical conductivity of brain tissue, density, and specific heat capacity, as well as the corresponding values for blood and other materials present in the model. Operational parameters are also established, such as the antenna's operating frequency, along with auxiliary variables for the spatial interpolation of properties, which are necessary to reflect the real variability of biological tissues.

Name	Expression	Value	Description
epsilonr_pcb	5.23	5.23	
epsilonr0_brain	58.13	58.13	
sigma0_brain	1.15[S/m]	1.15 S/m	
rho_brain	1.03e3[kg/m^3]	1030 kg/m ³	
sdamping	2e-4	2E-4	
edamping	4e-4	4E-4	
soffset	-1.0[S/m]	-1 S/m	
eoffset	-50	-50	
c_blood	3639[J/(kg*K)]	3639 J/(kg·K)
rho_blood	1000[kg/m^3]	1000 kg/m ³	
odamping	1.08e-6[1/s]	1.08E-6 1/s	
ooffset	7.8e-4[1/s]	7.8E-4 1/s	
f0	500[MHz]	5E8 Hz	
f1	835[MHz]	8.35E8 Hz	
f2	1000[MHz]	1E9 Hz	
f3	1500[MHz]	1.5E9 Hz	

Fig. 3.1 | Definition of constants

The constant epsilonr_pcb (5.23) represents the relative permittivity of the FR4 substrate used in the patch antenna, which determines the electromagnetic behavior and resonance characteristics of the antenna. The constants epsilonr0_brain (58.13) and sigma0_brain (1.15 S/m) define the base relative permittivity and electrical conductivity of brain tissue at the reference frequency, crucial for accurately modeling wave propagation and energy absorption in the head.

The parameter rho_brain (1030 kg/m³) is the density of brain tissue and is essential for calculating the local SAR (specific absorption rate), as SAR depends on the absorbed power per unit mass. The auxiliary constants sdamping, edamping, soffset, eoffset, odamping, and ooffset are used in the interpolation functions that spatially modulate conductivity, permittivity, and blood perfusion rate within the head, based on MRI-derived data. These allow the model to realistically represent the heterogeneous nature of biological tissues.

For thermal modeling, c_blood (3639 J/(kg·K)) and rho_blood (1000 kg/m³) specify the specific heat capacity and density of blood, respectively, both of which are necessary for the bioheat equation that describes heat transfer and dissipation due to blood perfusion.

Finally, the constants f0, f1, f2, and f3 correspond to the different operating frequencies used in the simulations: 500 MHz, 835 MHz, 1000 MHz, and 1500 MHz. These allow for a parametric analysis of how frequency affects electromagnetic absorption and heating within the head.

After defining the constants, the three-dimensional geometry representing the physical environment of the problem is constructed. The main element is the human head, whose shape is imported from a file called "sar_in_human_head.mphbin." In addition to the head, a patch antenna is modeled near the lateral surface of the head, which will serve as the source of the frequencies to be absorbed by the head.

The antenna used in the SAR in Human Head model is a rectangular patch antenna placed near the lateral surface of the head. Its geometry consists of a rectangular metallic patch with a side length of 6 cm, deposited on a square dielectric substrate (FR4) of the same dimensions and 1.6 mm thickness. Beneath the substrate, there is a metallic ground plane, also square and 6 cm on each side, which acts as an electrical reference and defines the radiation pattern of the antenna.

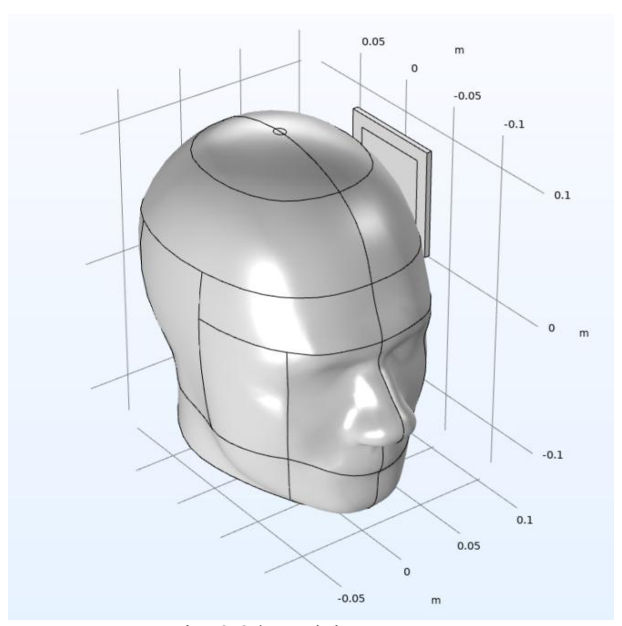


Fig. 3.2 | Model Geometry

Once the main elements have been created, an air domain is designed to surround the entire system, along with an outer layer of absorbing material (PML, Perfectly Matched Layer), which simulates open boundary conditions and prevents artificial reflections of electromagnetic waves. The geometry is completed by adding details such as the antenna substrate and the precise position of each component, ensuring that the spatial arrangement of the elements accurately reflects the experimental situation to be analyzed.

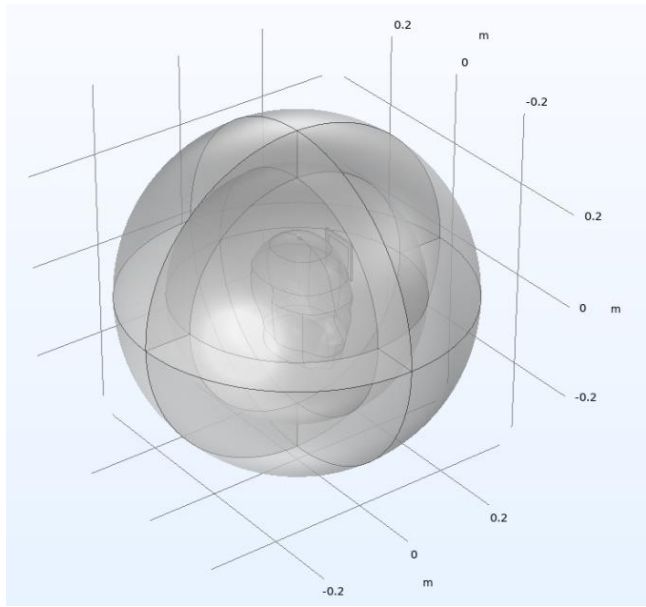
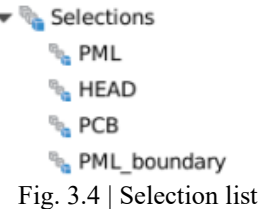


Fig. 3.3| Geometry of PML

To facilitate the assignment of materials and the configuration of the physics, explicit selections are created for the different domains ("Head" for the head, "PCB" for the antenna, "PML" for the absorbing layer). In addition, specific views are set up with transparency and by hiding certain entities, which simplifies the selection of domains and the visualization of the geometry during the modeling process.



A volumetric data file (sar_in_human_head_interp.txt) is imported, containing spatial information about the variation of properties within the head, derived from magnetic resonance imaging. This interpolation function ("fbrain") is used to assign variable properties (permittivity, conductivity, and perfusion rate) based on the position within the head domain.

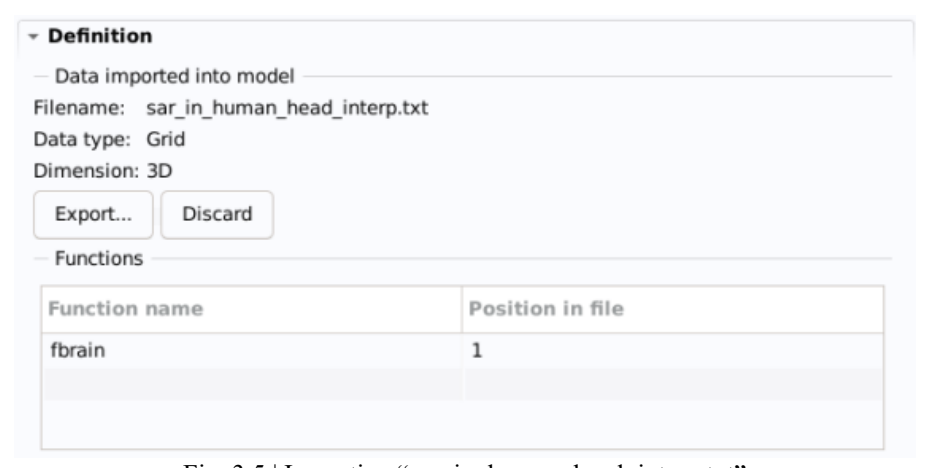


Fig. 3.5 | Importing "sar_in_human_head_interp.txt"

.

Additionally, local variables are defined that depend on the interpolation function, allowing the relative permittivity, conductivity, and blood perfusion rate to vary spatially in a realistic manner.

Name	Expression	Unit	Description
epsilonr_brain	<pre>epsilonr0_brain* (1+fbrain(x[1/m], y[1/m],z[1/m])* edamping)+eoffset</pre>		Relative permittivity of the brain
sigma_brain	<pre>sigma0_brain*(1+ fbrain(x[1/m],y[1/ m],z[1/m])* sdamping)+soffset</pre>	S/m	Conductivity of the brain
omega_head	<pre>odamping* fbrain(x[1/m],y[1/ m],z[1/m])+ooffset</pre>	1/s	Blood perfusion rate

Fig. 3.6 | Definition of variables

3.3.2. Materials

After defining the geometry and interpolation functions, materials are assigned to each domain of the model:



- Head: A custom material is created for the head, assigning it thermal properties (conductivity, density, specific heat capacity) and variable electrical properties (relative permittivity and conductivity). The latter are defined using local variables that depend on the interpolation function, so the head has properties that vary spatially in a realistic way.

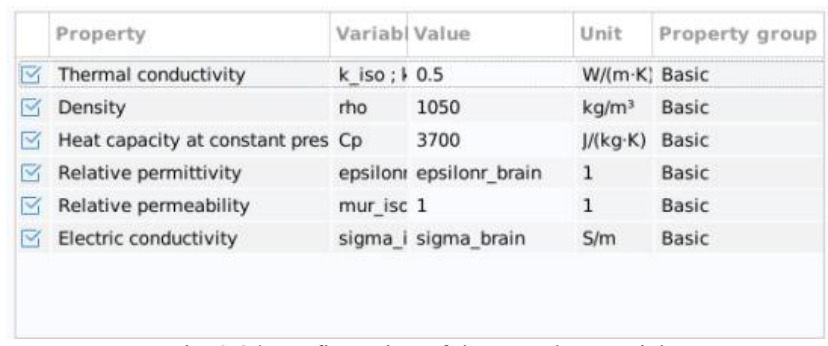


Fig. 3.8 | Configuration of the "Head" material

- Antenna (PCB): Another material is defined for the antenna plate, specifying its relative permittivity, conductivity, and other dielectric properties characteristic of the patch material.

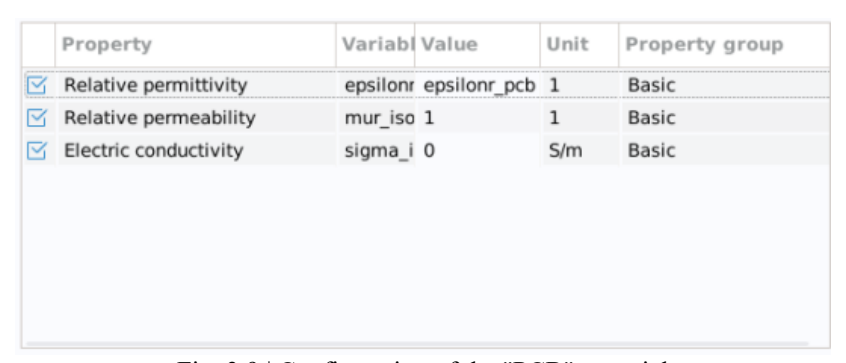


Fig. 3.9 | Configuration of the "PCB" material

- Air: The air domain surrounding the head and the antenna is assigned by selecting the "Air" material from COMSOL's built-in material library.

3.3.3. Electromagnetic Waves Configuration

The configuration of the nodes in the Electromagnetic Waves, Frequency Domain (emw) module for the SAR in human head practice is very similar to that used in the Wi-Fi antenna study, although adapted to the geometry and specific materials of this model.

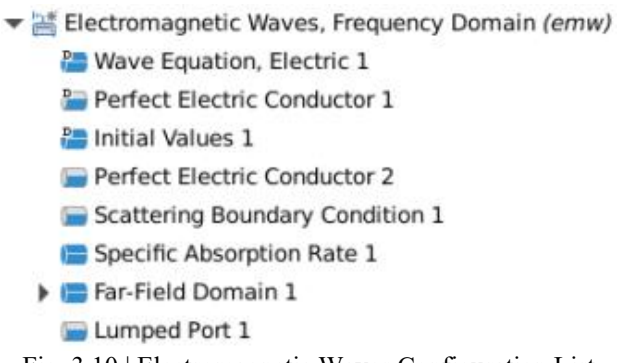


Fig. 3.10 | Electromagnetic Waves Configuration List

The Wave Equation, Electric node is applied to all relevant domains, including the head, brain, surrounding air, antenna, and the PML layer. This ensures that the propagation of the electromagnetic wave is correctly calculated in all present materials.

The metallic surfaces of the antenna, such as the radiator and the ground plane, are defined as Perfect Electric Conductor (PEC), assigning this condition to the corresponding boundaries.

The antenna is fed through a Lumped Port on boundary 55, configured with a reference impedance of 75 Ω and an excitation of 45.5 V, following the parameters from the COMSOL example. This port introduces the electromagnetic signal and allows control of the power supplied to the system.

For SAR calculation, the Specific Absorption Rate node is activated in domain 6, which corresponds to the brain. This allows for obtaining the local distribution of energy absorbed in the brain tissue, serving as the basis for the safety analysis.

The Scattering Boundary Condition is applied to the outer limits of the air domain (boundaries 5–8, 33, 34, 39, and 44), just before the PML, allowing electromagnetic waves to exit the domain without reflection, thus simulating free-space conditions.

Finally, a Far-Field Domain is defined in the air domain to calculate far-field radiation parameters if necessary.

3.3.4. Model Meshing

The mesh generation in the SAR model of the human head is a critical process to achieve precise and physically realistic results, especially due to the variety of scales present in the geometry and the sensitivity of the simulation to the spatial resolution of the electromagnetic field and the SAR.

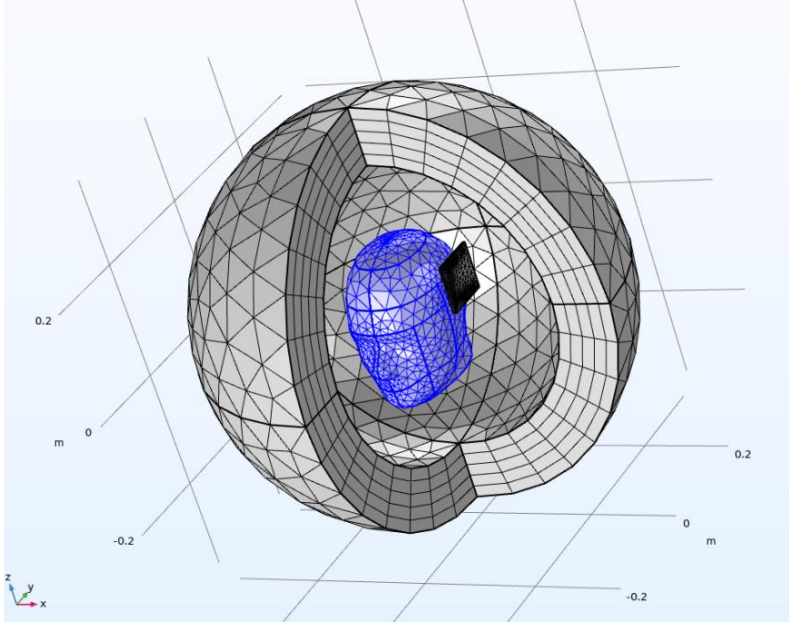


Fig. 3.11 | Model meshing

In this case, a tetrahedral mesh is used for the head, the antenna, and the air domain, while a swept mesh is applied in the PML region. This approach allows for more precise control in the absorption direction and improves the convergence of iterative solvers.

For critical regions such as the metallic patch of the antenna and the feed line, especially small element sizes are defined. On edges 81–84, 86, 87, and 89–91, a maximum element size of 0.0015 m is set, ensuring adequate resolution of the high gradients of the electric field and the surface currents in the antenna. In the domain corresponding to the brain (Domain 6), the "Extra fine" mesh is selected, following the recommendation of having at least five elements per effective wavelength in the tissue, which is essential to avoid dispersion errors and to accurately capture the maximum SAR values.

In the PML, the swept mesh relies on a user-controlled distribution, assigning the external faces of the air domain (PML_boundary) as reference surfaces for element generation. This allows the element size to be adapted along the radial direction, optimizing the absorption of outgoing waves without unnecessarily increasing the total number of elements.

The air domain and regions far from the antenna and the head can be meshed with larger elements, since the field variation is smoother in these areas and the main interest is the efficient absorption of waves by the PML. However, a gradual transition in element size is maintained to avoid discontinuities that could affect numerical convergence.

With the mesh defined, the next step is to establish the multiphysics coupling between the two main physics of the model, electromagnetic wave propagation and heat transfer. This coupling is implemented using the "Electromagnetic Heating" node, which transfers the power absorbed by the tissues (calculated from the local SAR) as a heat source in the bioheat equation. It is important to note that this coupling is applied only to the head domain, since it is in this tissue that the radiation-induced heating is studied. The next step is to configure the study, and for this, a direct solver is used, as the system size allows it.

3.3.5 Solver configuration

In this model, the simulation is solved in two coupled steps: first, the electromagnetic field generated by the antenna is calculated in the frequency domain, considering the spatial dielectric properties of brain tissue. Then, the obtained SAR value is used as a thermal source to calculate the stationary temperature in the tissue using the bioheat equation.

The electromagnetic solver is configured to ensure adequate field resolution, adjusting the mesh to the wavelength of the frequency of interest. For heat transfer, a stationary solver is used, solving for the thermal increase from the transferred SAR. Coupling between modules is performed using the "Electromagnetic Heating" operator, and intermediate solutions are stored to facilitate analysis and debugging. Numerical tolerances are adjusted to ensure stability in areas with high field or temperature gradients.

3.4. Results

3.4.1. Local increase temperature in the head

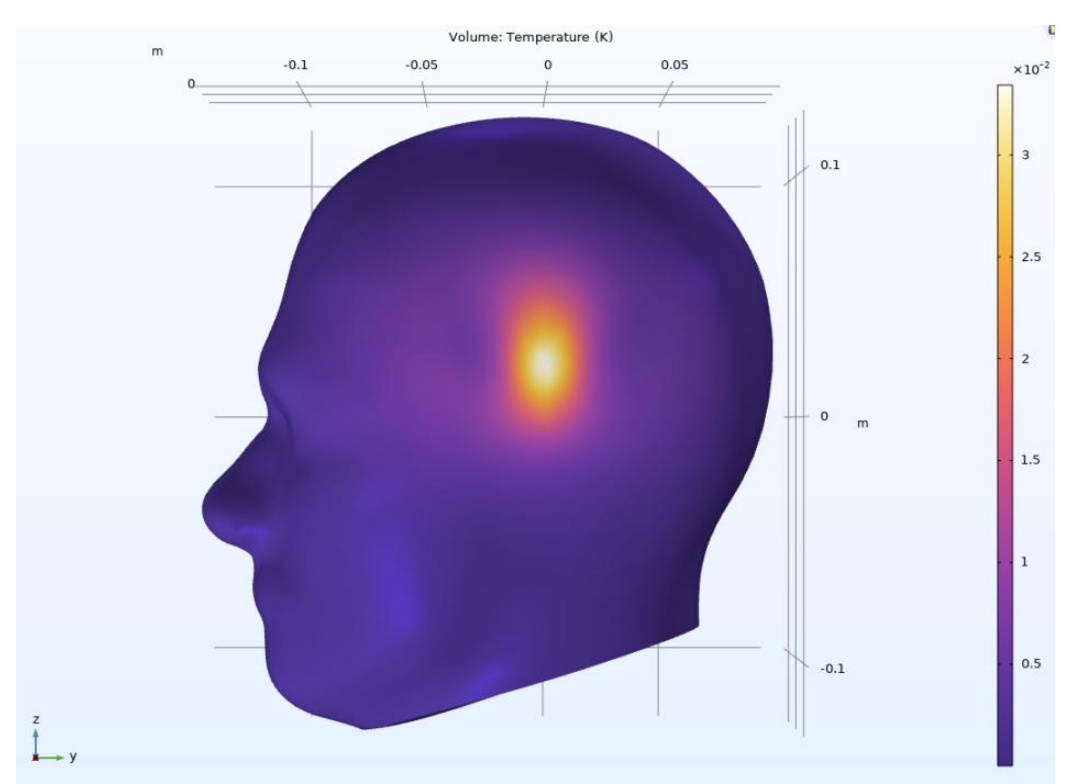


Fig. 3.12 | Local increase temperature in the head (500 MHz)

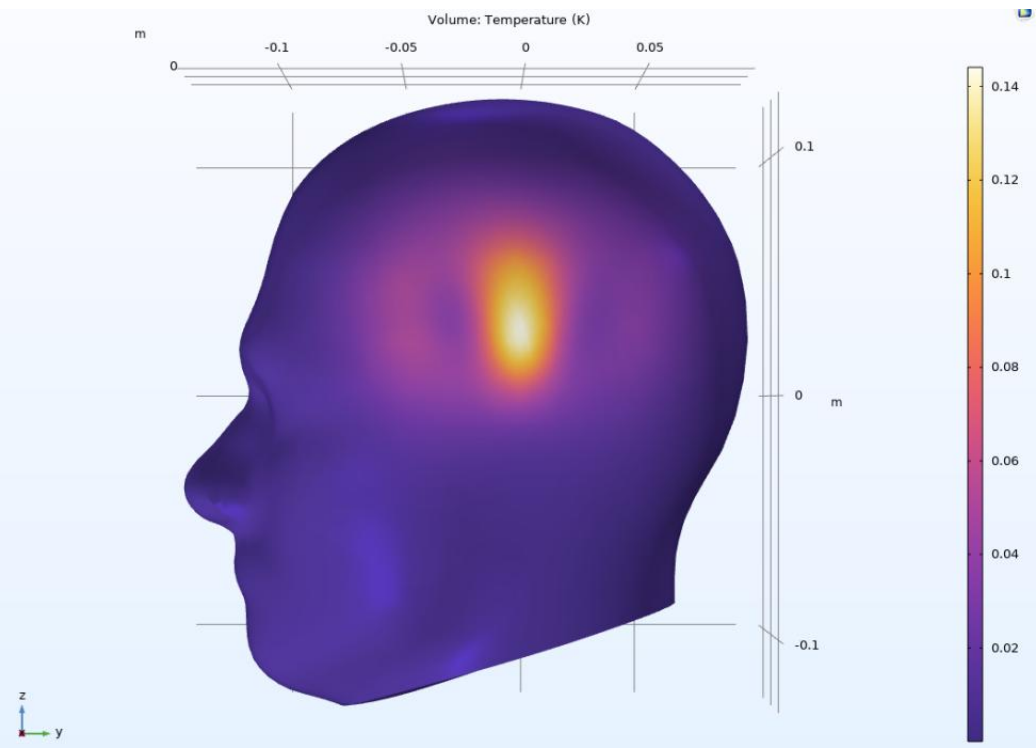


Fig. 3.13 | Local increase temperature in the head (835 MHz)

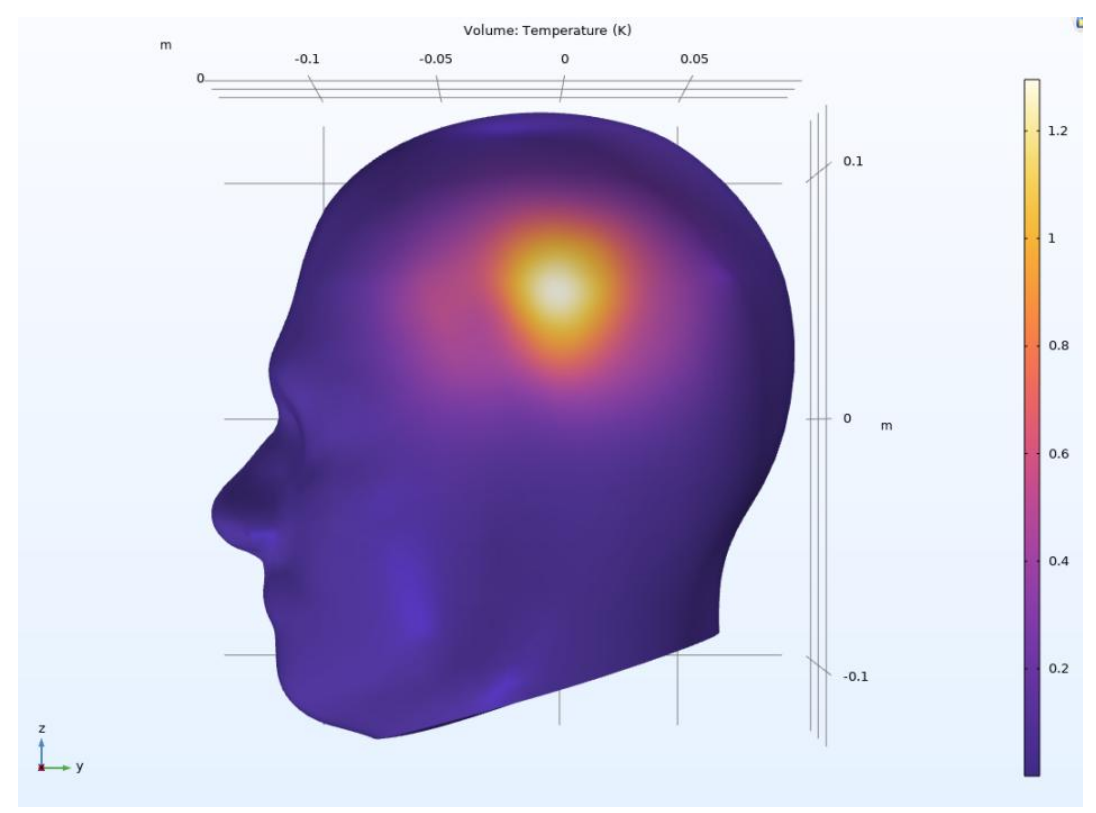


Fig. 3.14 | Local increase temperature in the head (1000 MHz)

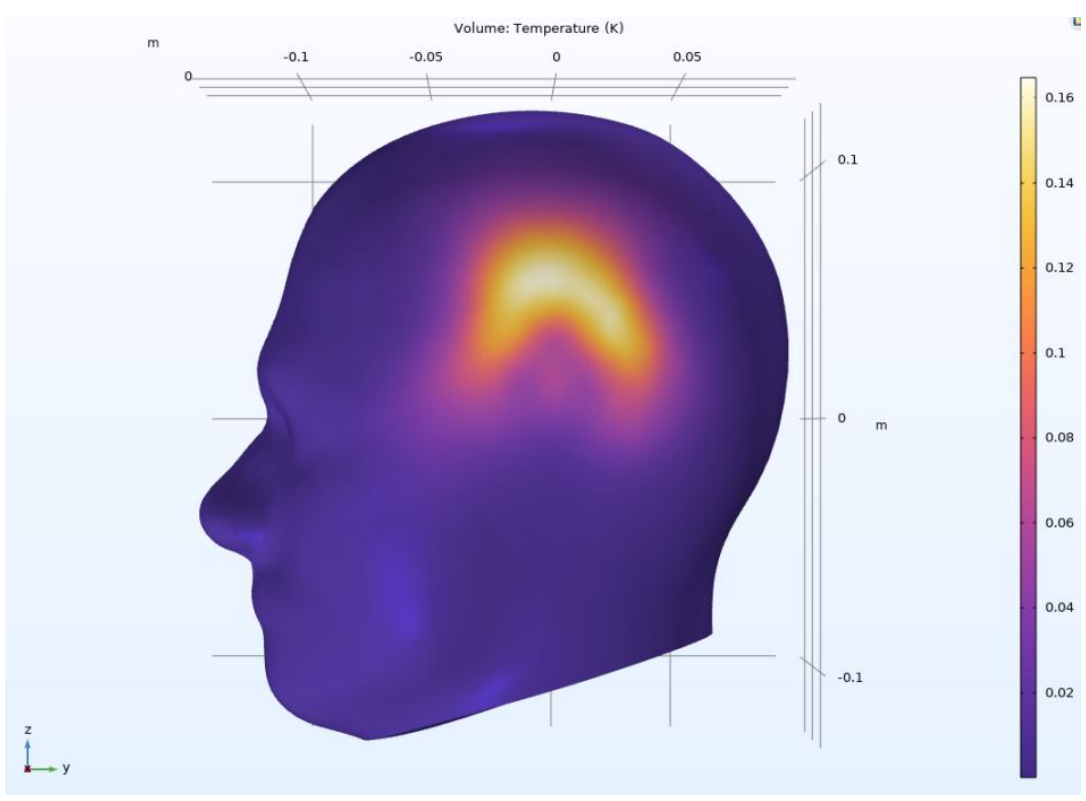


Fig. 3.15| Local increase temperature in the head (1500 MHz)

The analysis of the simulation images for frequencies of 500, 835, 1000, and 1500 MHz clearly shows how the frequency of electromagnetic radiation affects both the magnitude and the surface extension of heating in cranial tissue. As the frequency increases, it can be seen that the area of surface heating becomes larger and the maximum recorded temperature also increases notably.

In the image corresponding to 500 MHz, the maximum surface temperature is approximately $2.8 \times 10^{-2} \text{ K}$. The heating area is relatively small, and the thermal distribution is more diffuse. At 835 MHz, the maximum temperature reaches about 0.14 K, and a significant expansion of the affected area is already observed, with a greater concentration of energy on the surface.

The simulation for 1000 MHz shows the most prominent phenomenon: the maximum surface temperature rises to 1.2 K, which represents a much greater increase compared to the previous and subsequent frequencies. Additionally, the heating area is the largest among all simulations, covering a considerable region of the cranial surface. This behavior, which breaks the expected upward proportionality, can be explained by the appearance of geometric resonance phenomena in the human head around frequencies of 900–1200 MHz, where the electromagnetic wavelength couples efficiently with the anatomical dimensions of the head, generating local maxima in absorption and temperature[5]. The coupling efficiency and the SAR distribution can favor greater thermal accumulation at intermediate frequencies, while at 1500 MHz the energy dissipates rapidly in a very thin superficial layer, limiting the maximum thermal increase at the surface.

Finally, at 1500 MHz, the maximum surface temperature decreases to approximately 0.16 K. Although the heating area remains considerable, the energy is distributed in an even more superficial layer and the magnitude of the heating does not reach the maximum observed at 1000 MHz.

3.4.2. Local distribution of SAR (logarithmic) in head sections

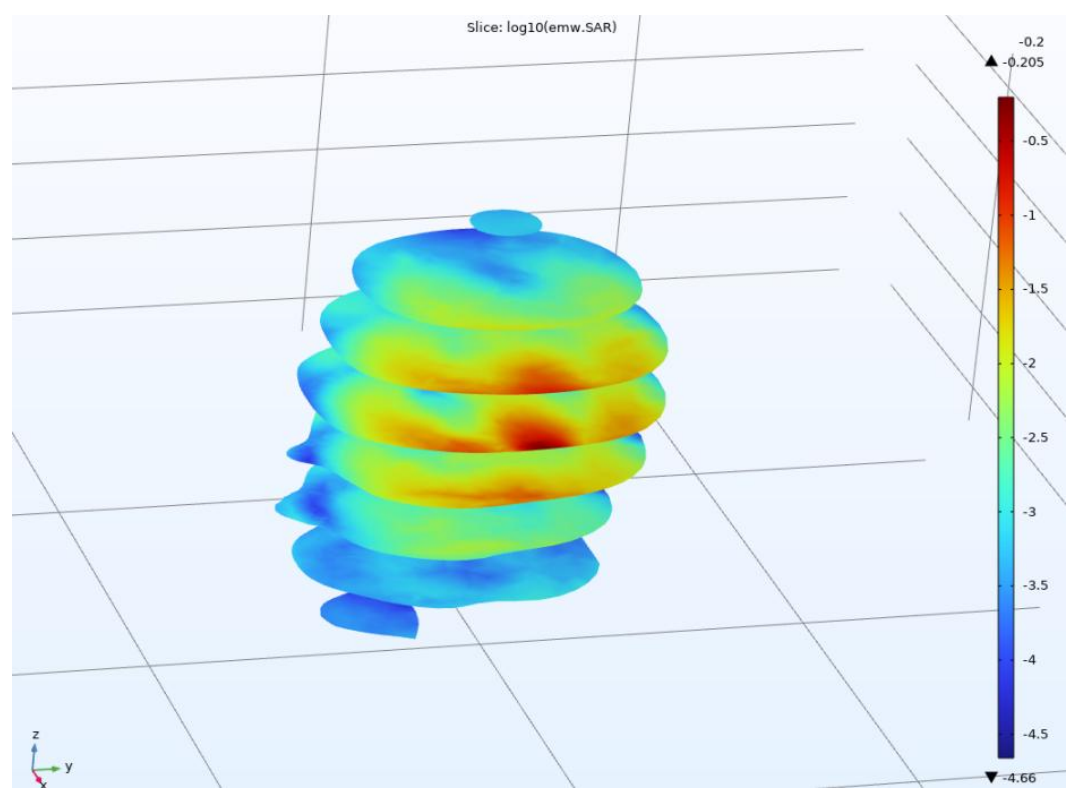


Fig. 3.16 | Local distribution of SAR (500 MHz)

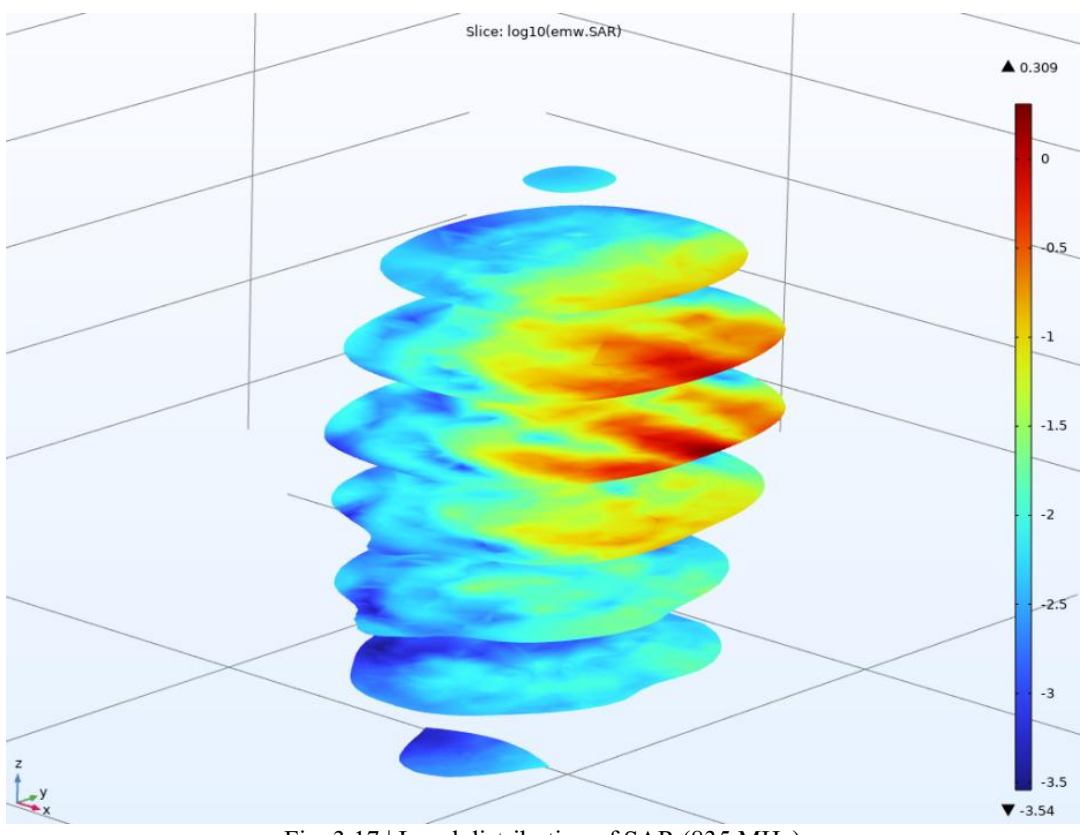


Fig. 3.17 | Local distribution of SAR (835 MHz)

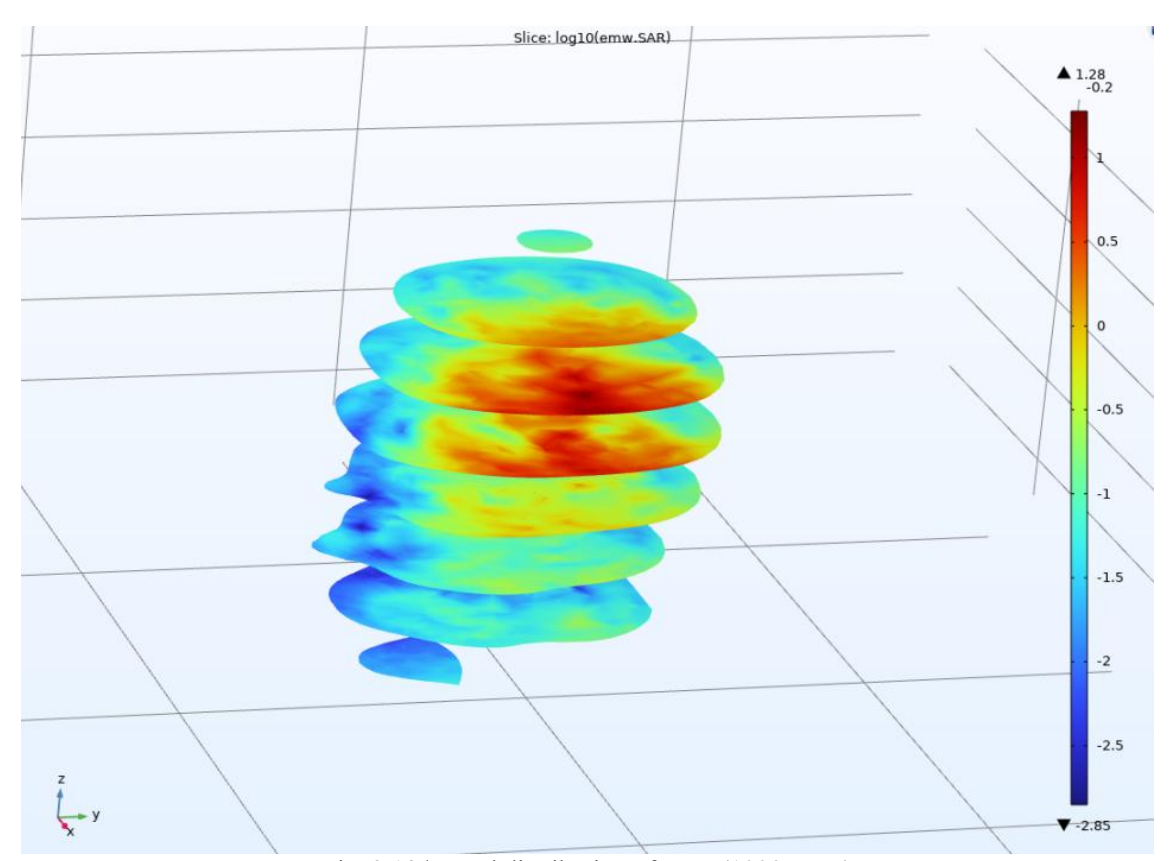


Fig. 3.18 | Local distribution of SAR (1000 MHz)

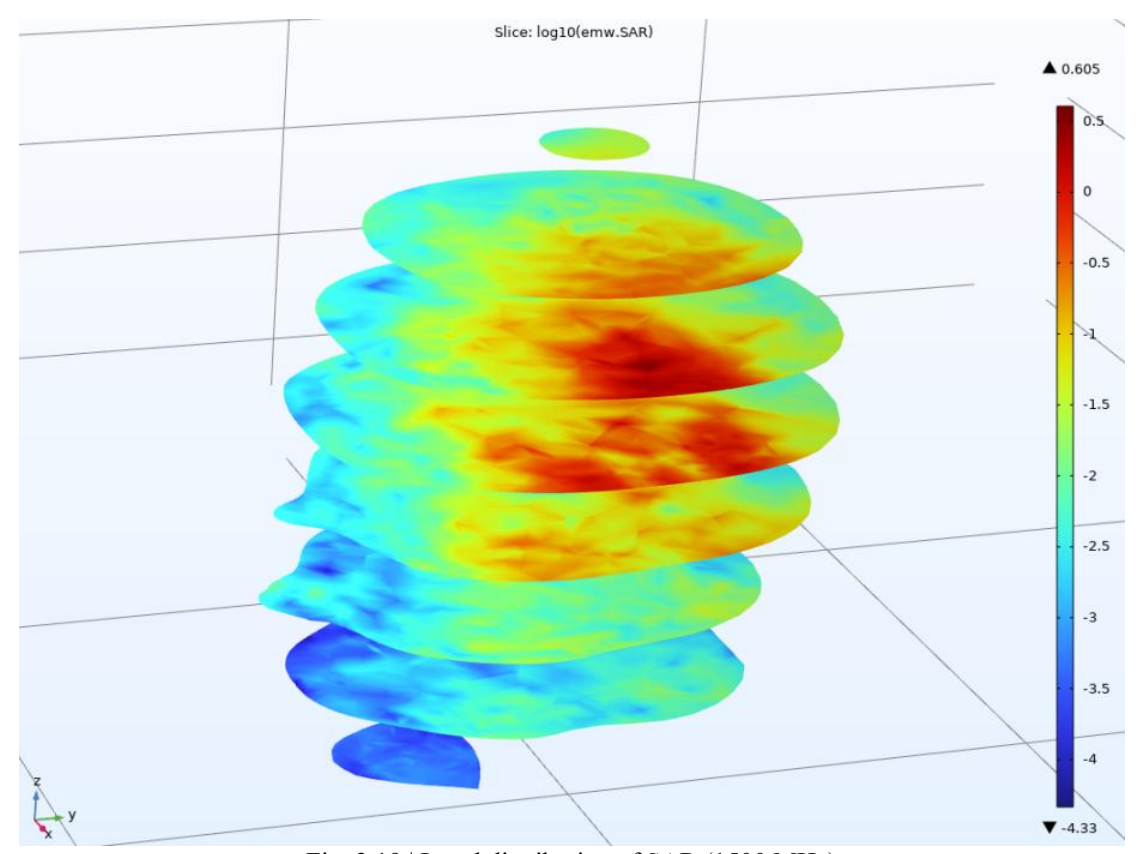


Fig. 3.19 | Local distribution of SAR (1500 MHz)

The images show the logarithmic distribution of the Specific Absorption Rate (SAR) in cross-sections of the human head model for different exposure frequencies. The analysis of these simulations allows for a comparison of how the depth and localization of electromagnetic energy absorption in cranial tissue vary as a function of the incident wave frequency.

Contrary to the general trend observed in the microwave and radiofrequency range, where an increase in frequency is usually associated with more superficial absorption, in this specific case it can be seen that at 1500 MHz the area of maximum absorption penetrates more deeply into the tissue than at 500 MHz. This phenomenon can be explained by the interaction between the wavelength, the dimensions of the cranial model, and the dielectric properties of the tissue, which may favor energy coupling and the appearance of absorption maxima at intermediate frequencies.

As previously mentioned, this behavior is not unusual in complex biological models: various studies have reported that the penetration depth does not decrease strictly monotonically with frequency, but may present relative maxima in certain ranges, especially between 900 and 1200 MHz, due to resonance effects and the multilayer structure of cranial tissue. Moreover, at higher frequencies, although absorption tends to be more superficial in terms of affected volume, the locally deposited energy can be higher, implying that maximum SAR values may increase in specific regions close to the antenna[5].

Therefore, these images illustrate that the relationship between frequency and penetration depth is complex and depends both on the electrical properties of the tissue and on the geometry and coupling between the source and the biological model. This result underscores the importance of performing multi-frequency simulations and of interpreting SAR maps considering not only frequency, but also the geometric configuration and specific characteristics of the model used. In this way, a more realistic and precise view is provided of the potential risks associated with exposure to electromagnetic fields in the human head.

3.4.3. Volumetric distribution of the specific absorption rate (SAR) in W/kg

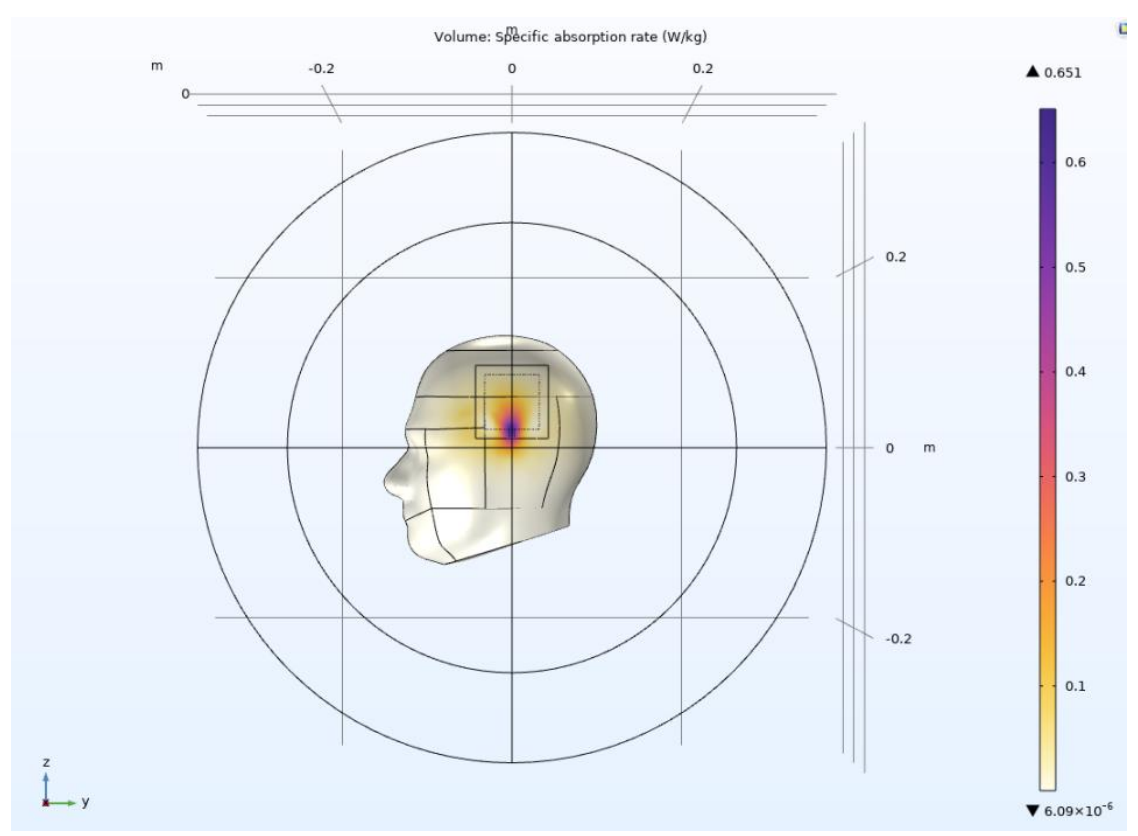


Fig. 3.20 | Volumetric distribution of SAR (500 MHz)

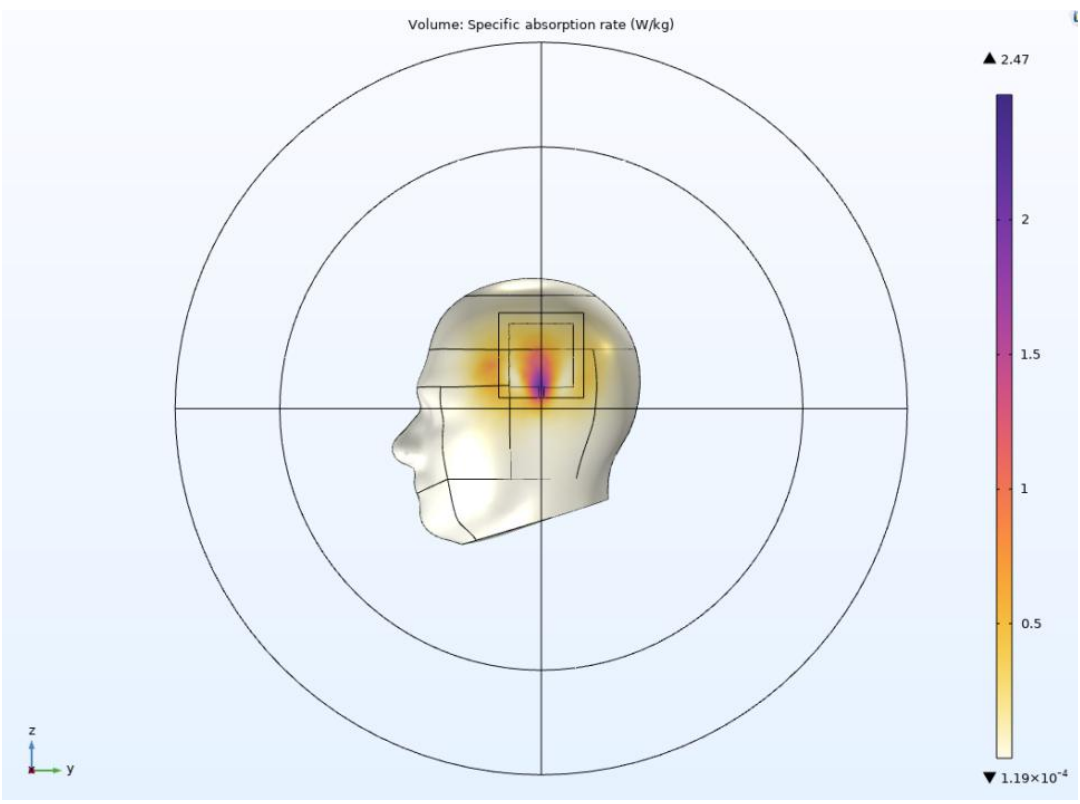


Fig. 3.21 | Volumetric distribution of SAR (835 MHz)

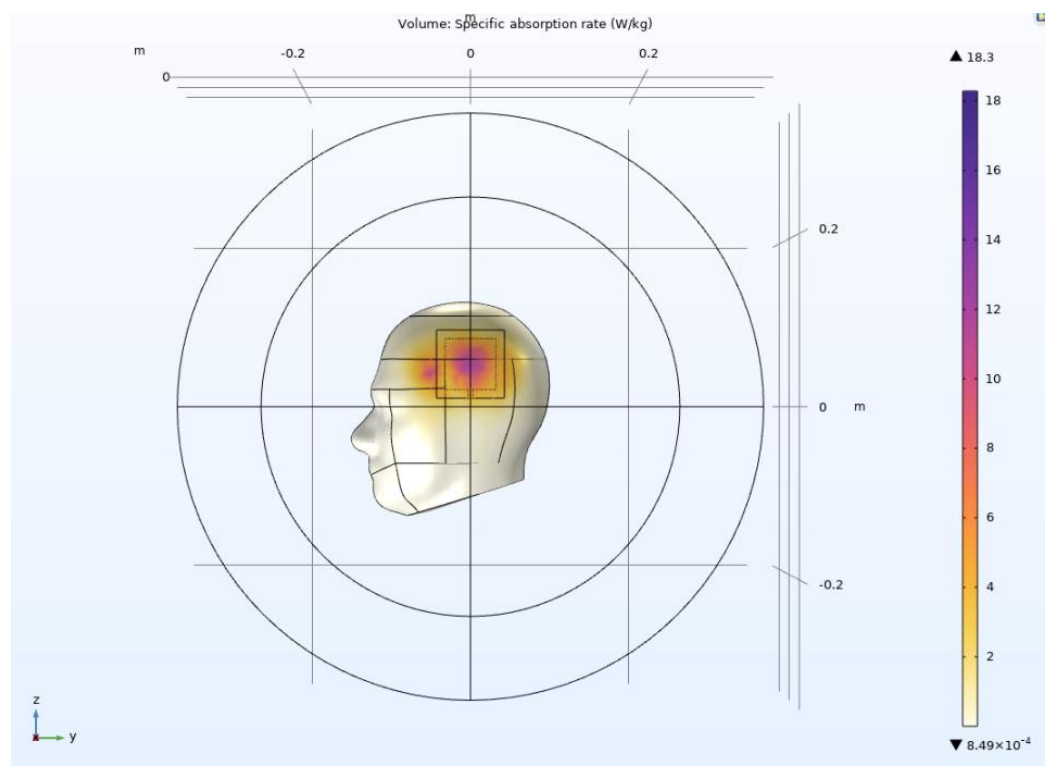


Fig. 3.22 | Volumetric distribution of SAR (1000 MHz)

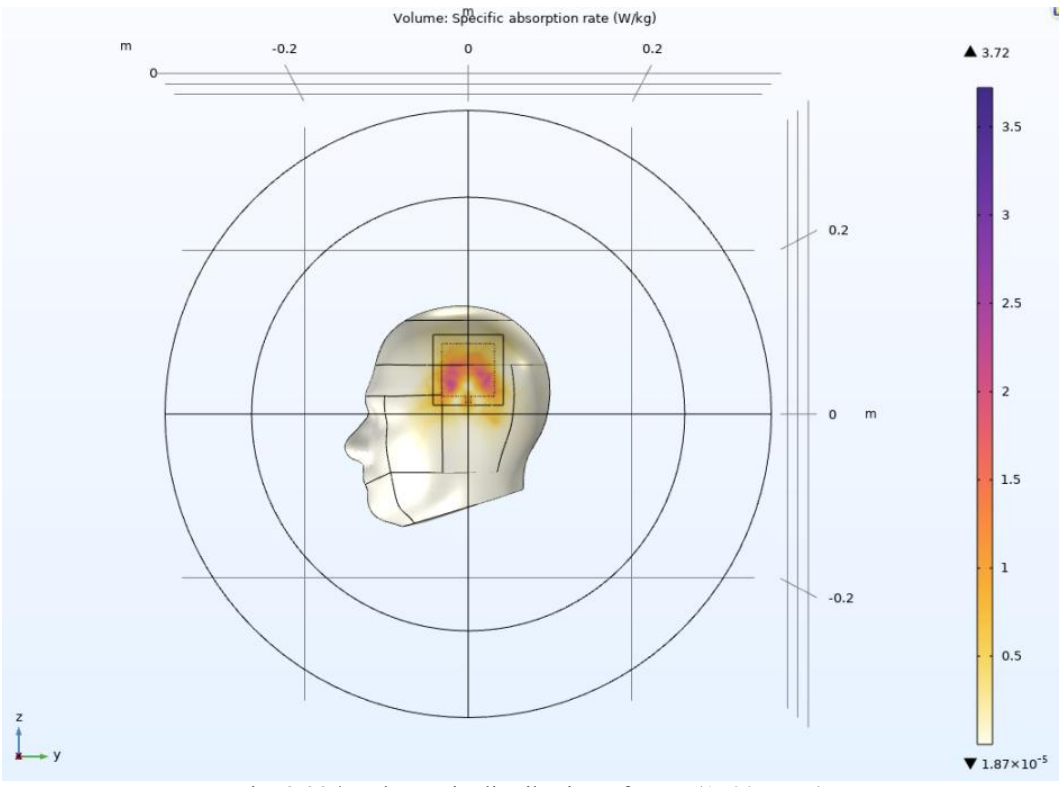


Fig. 3.23 | Volumetric distribution of SAR (1500 MHz)

The previous images show the volumetric distribution of SAR in the human head for increasing frequencies. In all of them, it can be observed that both the extent of the affected area and the maximum SAR value (W/kg) tend to increase with frequency, except in the case of 1000 MHz, where a relative maximum occurs due to the previously explained effects of geometric resonance.

In the first image (500 MHz), the absorption area is relatively limited and the maximum SAR value reaches approximately 0.65 W/kg. Moving to the second image, corresponding to a higher frequency, there is a notable increase in both the extent of the affected area and the maximum SAR value, which rises to 2.47 W/kg. This increase reflects how higher frequency promotes a more efficient transmission of energy to the surface, expanding the absorption zone and raising the local intensity.

The third image, corresponding to 1000 MHz, shows the relative maximum SAR, with a value reaching 18.3 W/kg and an even greater extent of the affected area. This result is interpreted as a consequence of geometric coupling and resonance phenomena, where the electromagnetic wavelength matches particularly well with the anatomical dimensions of the head, enhancing absorption and energy accumulation on the surface[5].

Finally, in the highest frequency image, the maximum SAR value is 3.72 W/kg and the absorption area remains considerably large, although smaller than that observed at 1000 MHz. This behavior confirms that, although the general trend is for SAR and the area of surface heating to increase with frequency, around 1000 MHz a relative maximum occurs due to geometric resonance, while at even higher frequencies the energy is distributed more superficially and the maximum accumulation decreases.

3.4.4. Increased temperature inside the human head as a result of the absorption of electromagnetic radiation

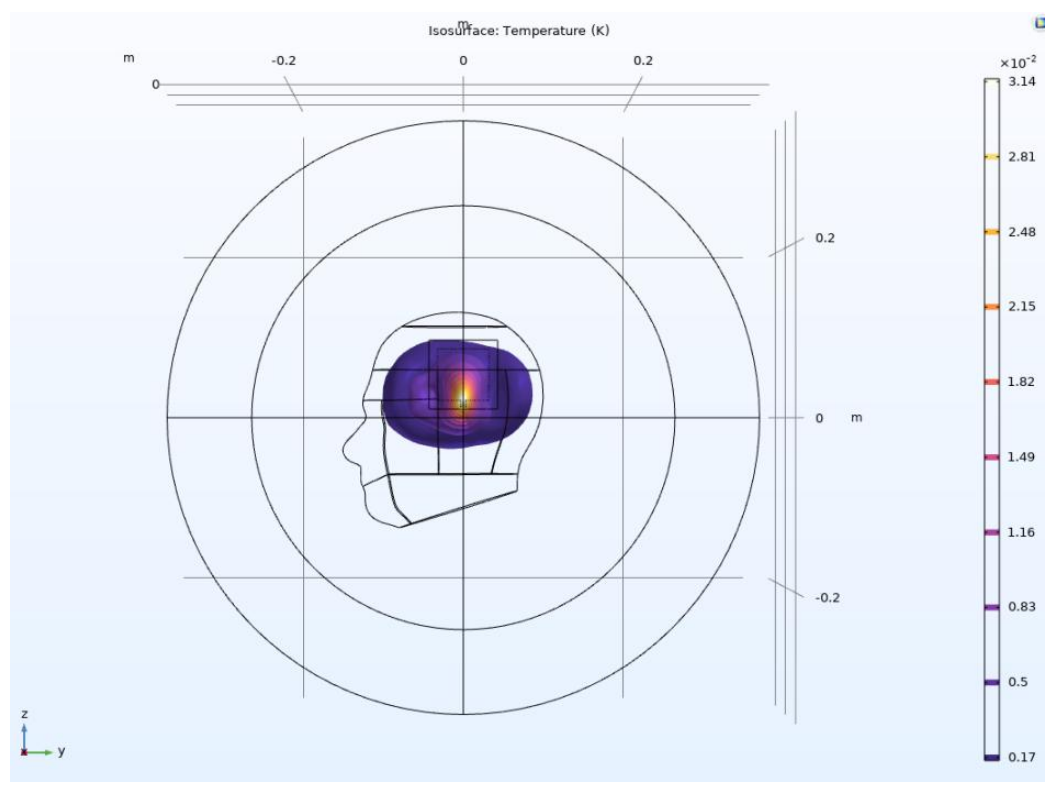


Fig. 3.24 | Increased temperature inside the human head (500 MHz)

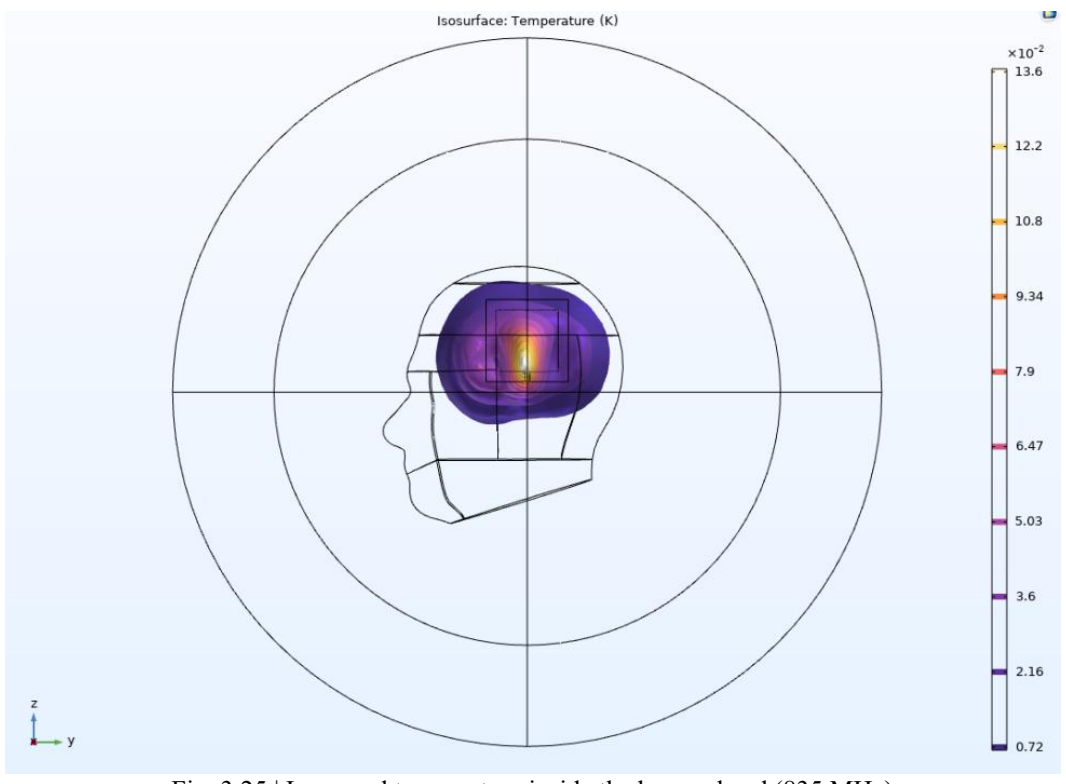


Fig. 3.25 | Increased temperature inside the human head (835 MHz)

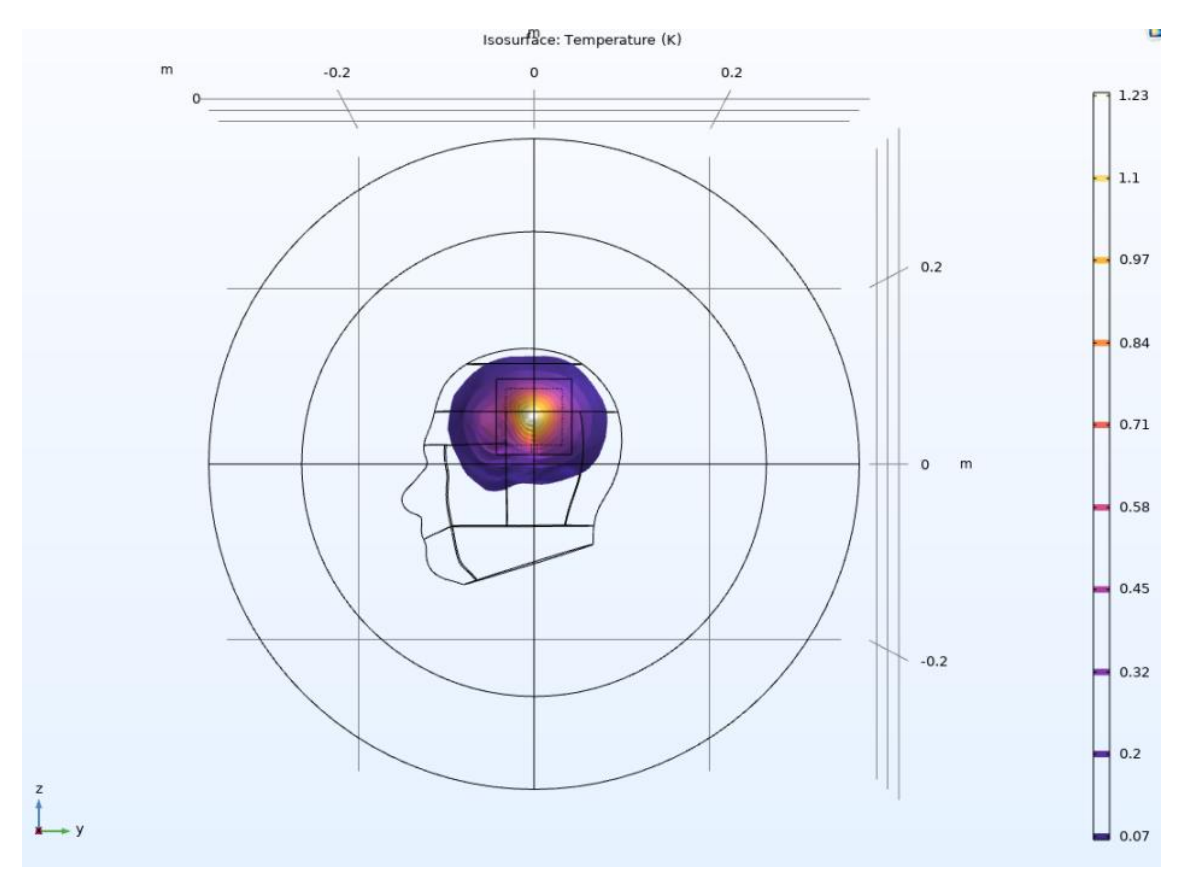


Fig. 3.26 | Increased temperature inside the human head (1000MHz)

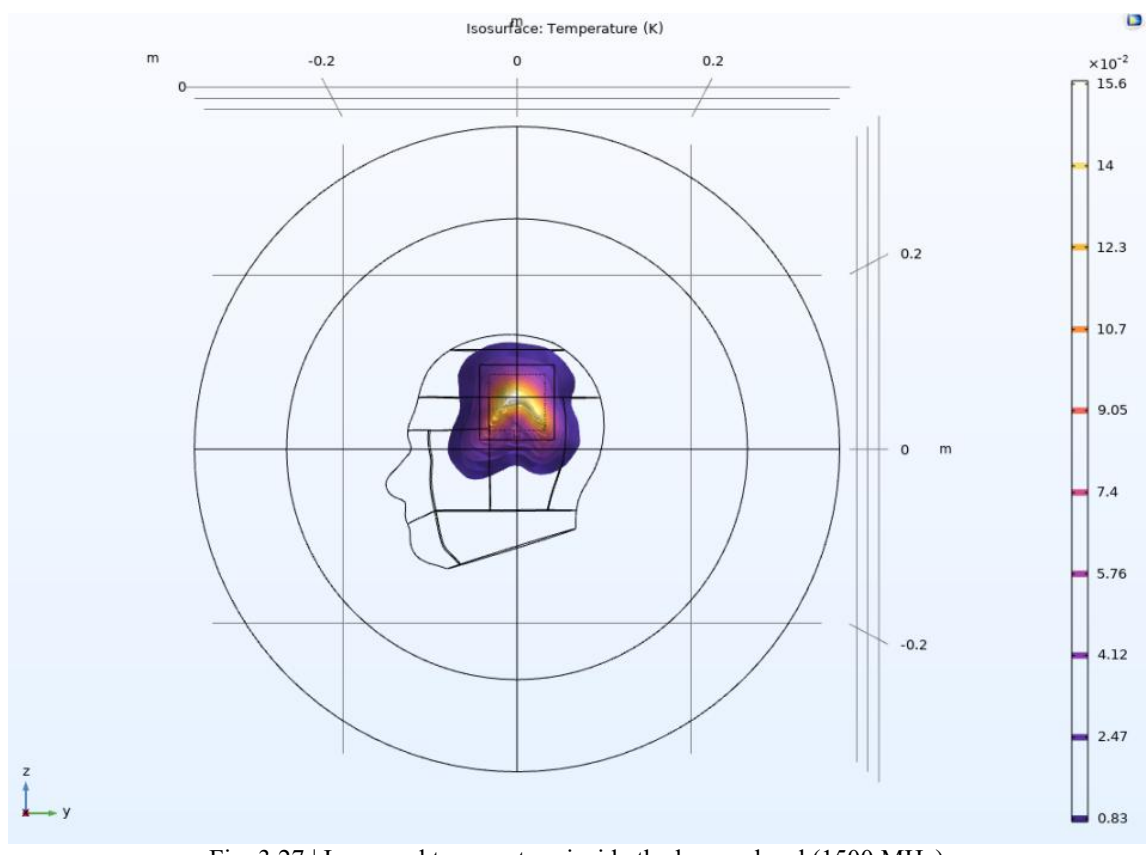


Fig. $3.27\ |$ Increased temperature inside the human head (1500 MHz)

Confirming what was presented in previous sections of the report, the analysis of these images clearly demonstrates the relationship between the frequency of electromagnetic radiation and the surface thermal behavior in the human head. In the first image, corresponding to the lowest frequency, both the heated area and the maximum temperature reached are relatively small, with the latter around 3.14×10^{-2} . The heating appears concentrated and limited to a compact region, indicating moderate and localized energy absorption.

In the second image, as the frequency increases, there is a rise in both the extent of the heated area and the maximum temperature, which reaches 13.6×10^{-2} K. The heating is more widely distributed over the cranial surface, reflecting greater efficiency in energy transfer, consistent with the trend observed at higher frequencies.

The third image presents the most prominent phenomenon: the maximum surface temperature reaches 1.23 K, and the heated area is the largest among all the simulations. This relative maximum at an intermediate frequency can be explained, as previously argued, by geometric resonance effects, in which the electromagnetic wavelength matches especially well with the anatomical dimensions of the head, favoring energy accumulation and the appearance of local temperature maxima.

In the fourth image, corresponding to the highest frequency, the maximum surface temperature decreases to $15.6\times10^{-2}\,\mathrm{K}$. Although the heated area remains appreciable, the energy is concentrated in an even more superficial layer and the magnitude of the heating does not reach the maximum observed at intermediate frequencies, probably due to rapid thermal dissipation and limited surface accumulation.

3.4.5. Distribution of relative permittivity in the head

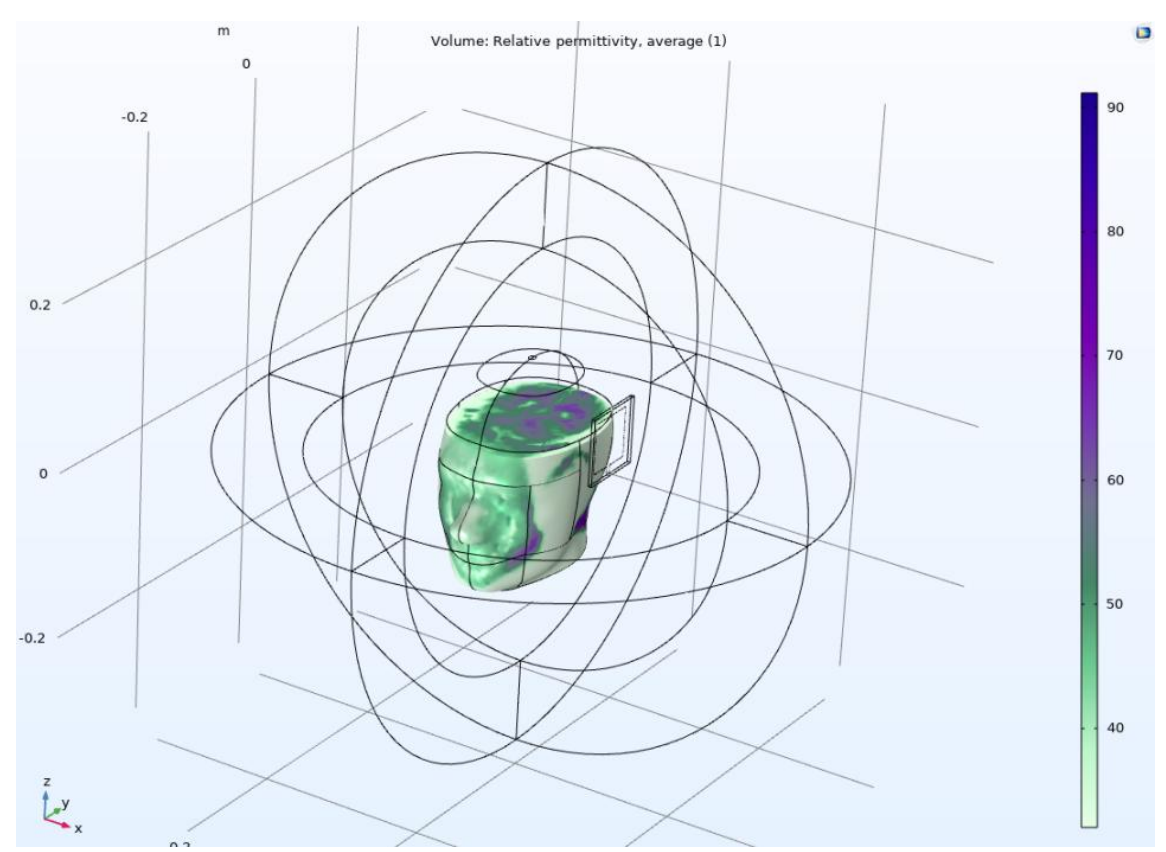


Fig. 3.28 | Distribution of relative permittivity in the head (500 MHz)

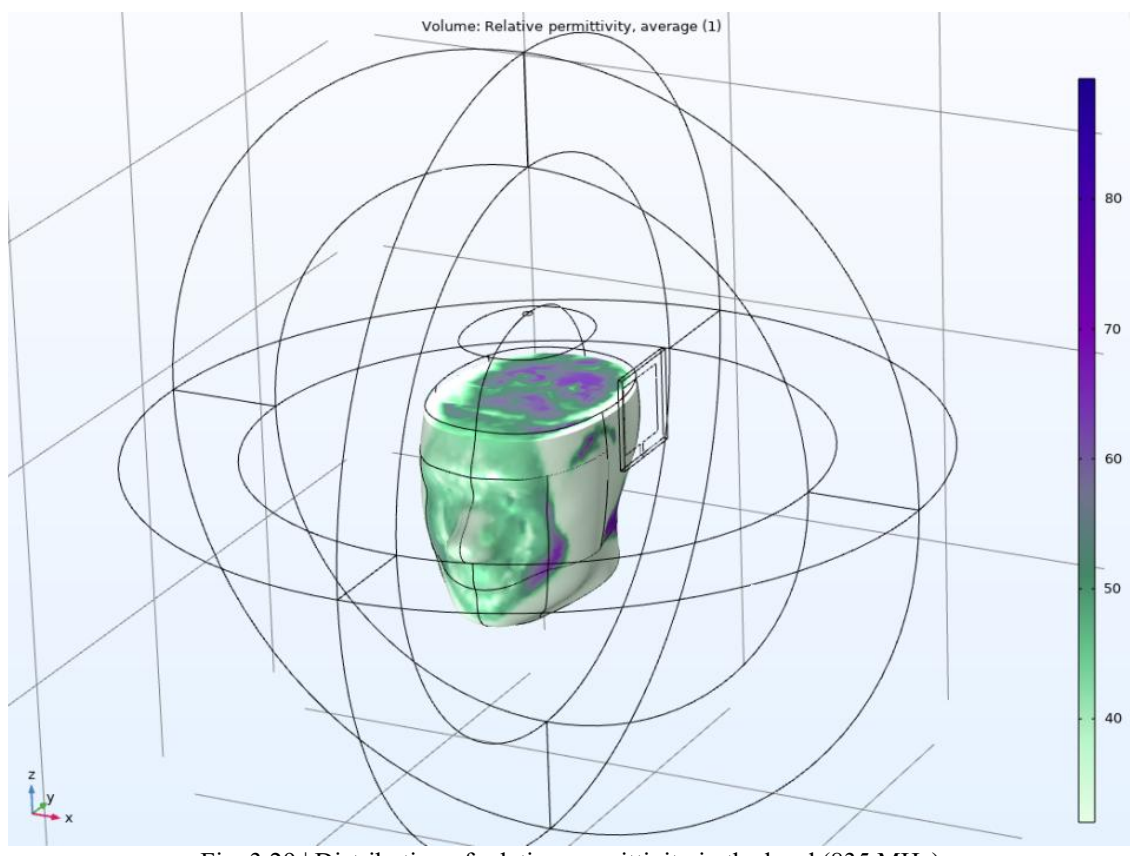


Fig. 3.29 | Distribution of relative permittivity in the head (835 MHz)

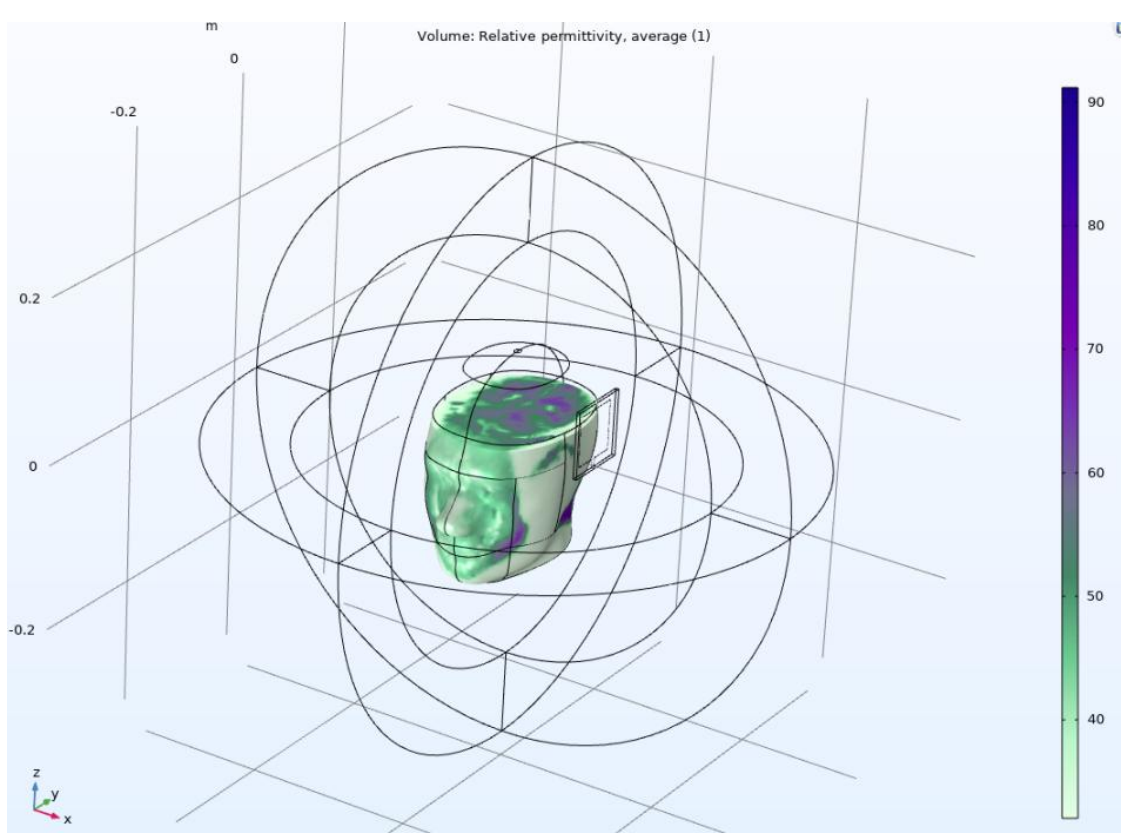


Fig. 3.30 | Distribution of relative permittivity in the head (1000 MHz)

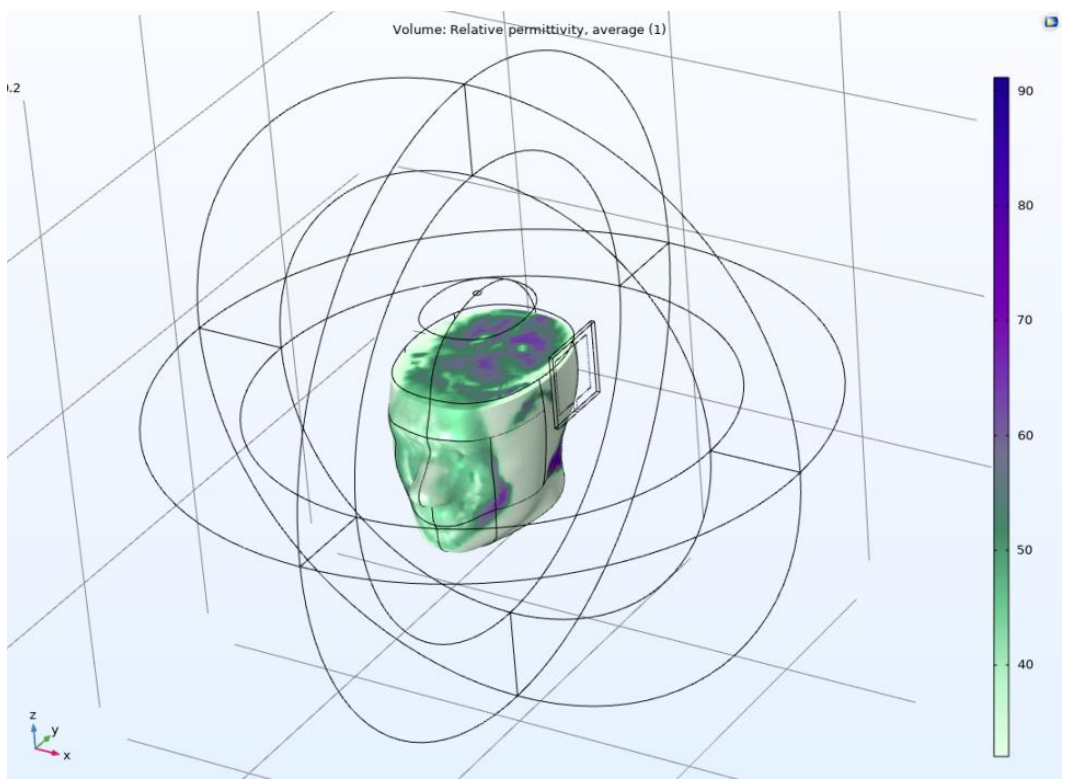


Fig. 3.31 | Distribution of relative permittivity in the head (1500 MHz)

The presented images show the spatial distribution of the average relative permittivity (ϵr) inside the human head model used in the SAR in Human Head simulation. This parameter is fundamental in electromagnetic simulation, as it determines how radiofrequency energy propagates and is absorbed in biological tissues.

Relative permittivity is an electrical property that indicates the ability of a material to store electrical energy in the presence of an electromagnetic field. In the biological context, tissues with a high water content, such as the brain, exhibit high values of relative permittivity, which directly influences the wave propagation speed, attenuation, and the distribution of absorbed energy. In SAR simulations, the spatial variability of relative permittivity is crucial to realistically represent the heterogeneity of tissues and to obtain accurate results regarding local absorption and heating.

In the images, it can be observed that relative permittivity is not uniform throughout the cranial volume, but rather presents areas with higher and lower values, reflecting the composition and internal structure of brain tissue, bone, and skin. The darker or bluish areas correspond to higher relative permittivity values (close to 90), typical of brain regions rich in water, while the lighter or greenish areas indicate lower values, associated with bone tissue or regions with lower water content.

When analyzing the images corresponding to the distribution of average relative permittivity in the SAR in Human Head model for different frequencies, it is observed that there is no significant change in the spatial pattern of relative permittivity when the frequency is modified. This is because the relative permittivity used in the model is mainly based on the structure and composition of the tissue, derived from MRI data, and not on the operating frequency selected for the simulation.

Relative permittivity is an intrinsic electrical property of biological materials and, although it can vary slightly with frequency over very wide ranges, in the context of these simulations and for the frequency range analyzed (500, 835, 1000, and 1500 MHz), the spatial distribution remains practically constant. The areas with high and low relative permittivity values reflect the natural heterogeneity of cranial tissue, but do not show appreciable changes when the frequency of the incident wave is altered.

Therefore, when modifying the frequency in this model, the main changes are observed in the distribution and magnitude of the SAR and the thermal increase, but not in the distribution of relative permittivity. This stability in permittivity is fundamental to ensure that the observed differences in absorption and heating are truly due to the effect of frequency on wave propagation and attenuation, and not to an artificial variation of the tissue's electrical properties.

3.5. Conclusion

The overall conclusion of Chapter 3 is that the frequency of electromagnetic radiation significantly determines both the magnitude and the surface extension of heating and energy absorption (SAR) in the human head. Throughout all the simulations and analyses performed, it is observed that increasing frequency tends to raise both the area of affected tissue and the maximum values of temperature and SAR, although this relationship is not strictly linear or uniform across the entire range studied.

In particular, the results show that at low frequencies the heating is more contained and localized, with relatively low maximum values of temperature and SAR. As the frequency increases, both the affected surface area and the magnitude of thermal and absorption effects increase, reaching a relative maximum at intermediate frequencies (around 1000 MHz). This maximum is explained by geometric resonance phenomena, where the electromagnetic wavelength couples efficiently with the anatomical dimensions of the head, favoring energy accumulation and the appearance of local maxima in heating and absorption.

At higher frequencies, although the energy is mainly absorbed at the surface, thermal dissipation and blood perfusion limit the maximum temperature increase, but the heating area can remain considerable. This pattern confirms that the thermal response and energy absorption do not depend solely on frequency, but also on cranial geometry, the dielectric properties of the tissue, and resonance effects that may arise in certain ranges.

Overall, the study highlights that risk assessment and the safe design of radiofrequency-emitting devices near the human head require a multifactorial and realistic analysis. It is not enough to consider only the exposure frequency; it is essential to integrate the interaction between the electromagnetic wave and anatomy, as well as the specific numerical values obtained in each simulation. Only in this way is it possible to anticipate possible biological effects and guide the development of wireless technologies toward maximum safety and efficiency.

Bibliography

[COMSOL1] COMSOL Multiphysics® Application Library, "Specific Absorption Rate (SAR) in the Human Brain," COMSOL AB, Stockholm, Sweden, 2023. [Online]. Available: https://www.comsol.com/model/specific-absorption-rate-sar-in-the-human-brain-2190

[COMSOL2] COMSOL Multiphysics® Application Library, "SAR of a Human Head Next to a Wi-Fi Antenna," COMSOL AB, Stockholm, Sweden, 2023. [Online]. Available: https://www.comsol.com/model/sar-of-a-human-head-next-to-a-wi-fi-antenna-71721

[COMSOL3] COMSOL Multiphysics® Application Library, "Microwave Cancer Therapy" COMSOL AB, Stockholm, Sweden, 2023. [Online]. Available: https://www.comsol.com/model/microwave-heating-of-a-cancer-tumor-30

- [1] "Microwave Frequency Bands: Applications and Advantages," RF Page, 2024. [Online]. Available: https://www.rfpage.com/microwave-frequency-bands/.
- [2] "Industrial Microwave Applications," IMS, 2021. [Online]. Available: https://industrialmicrowave.com/industrial-microwave-applications/
- [3] M. A. Khan et al., "Applications of Microwave Energy in Medicine," Frontiers in Medical Technology, vol. 3, 2021. [Online]. Available: https://pmc.ncbi.nlm.nih.gov/articles/PMC8065940/
- [4] "Military Applications of Microwave Technology," EITC, 2022. [Online]. Available: https://www.eitc.org/research-opportunities/military-applications-of-microwave-technology
- [5] A. Bamba, W. Joseph, J. B. Andersen, E. Tanghe, G. Vermeeren, D. Plets, J. Ø. Nielsen, and L. Martens, "Experimental Assessment of Specific Absorption Rate Using Room Electromagnetics," IEEE Transactions on Electromagnetic Compatibility, vol. 54, no. 4, pp. 747-757, 2012. Available: https://vbn.aau.dk/ws/files/61436249/EMC_journal_paper_Aliou_Bamba.pdf
- [6] GoConqr, "Embriología Clase 14 Sistema Nervioso," GoConqr, 2019. [Online]. Available: https://www.goconqr.com/ficha/16816150/embriologia-clase-14-sistema-nervioso.
- [7] Cadence PCB Design Blog, "Joule's Mechanical Equivalent of Heat: A Conversion Factor," 2022. [Online]. Available:

https://resources.pcb.cadence.com/rf-microwave-design/2022-joules-mechanical-equivalent-of-heat-a-conversion-factor.

[8] S. Fallahi and P. Prakash, "FIGURE 6. Microwave ablation antenna configurations; (a) monopole coaxial antenna, (b) single slot coaxial antenna, (c) dual slot coaxial antenna, (d) floating sleeve dipole antenna," in *Antenna Designs for Microwave Tissue Ablation*, 2018. [Online]. Available: https://www.researchgate.net/figure/Microwave-ablation-antenna-configurations-a-monopole-coaxial-antenna-b-single-slot_fig1_339703774

[9] M. F. Mosleh, "Wideband Fractal Circular-Shaped Microstrip Patch Antenna for Recent Wireless Applications," Conference Paper, 2020. [Online].

Available: https://www.researchgate.net/figure/The-components-of-MSA fig1 344418567

[10] S. Huss, et al., "Occupational exposure to radiofrequency electromagnetic fields," PMC, 2021.

Available: https://pmc.ncbi.nlm.nih.gov/articles/PMC9171125/

[11] R. J. Erwin, "Radiofrequency/Microwave Radiation Biological Effects and Safety Standards," DTIC, 1994.

Available: https://apps.dtic.mil/sti/citations/ADA282886

- [12] Joshi, M. S., & Joshi, G. R. (2017). "Analysis of SAR induced in Human Head due to the exposure of Non-ionizing Radiation.
- [13] Bamba, A. et al., "Experimental Assessment of Specific Absorption Rate Using Room Electromagnetics," IEEE Trans. EMC, 2012.

https://vbn.aau.dk/ws/files/61436249/EMC journal paper Aliou Bamba.pdf